

**STABILITY OPTIMIZATION INSTALLING DISTRIBUTED
GENERATION IN THE ELECTRICAL SYSTEM OF PUERTO RICO**

by

Damián Galarza-Torres

A thesis submitted in partial fulfillment
of the requirements for the degree of

MASTER OF SCIENCE

in

ELECTRICAL ENGINEERING
(Power System)

UNIVERSITY OF PUERTO RICO
MAYAGÜEZ CAMPUS

2009

Approved by:

Lionel R. Orama, D.Eng.
Member, Graduate Committee

Date

Efraín O'Neill Carrillo, Ph.D.
Member, Graduate Committee

Date

Erick E. Aponte, D.Eng..
Chairperson, Graduate Committee

Date

Juan Ortiz Navarro, Ph.D.
Representative of Graduate Study

Date

Benjamín Colucci, Ph.D.
Interim Dean of Engineering and Acting
Chairman of the Department

Date

Table of Contents

LIST OF FIGURES	V
LIST OF TABLES	VIII
LIST OF SYMBOLS.....	IX
ABSTRACT.....	XIII
RESUMEN	XIV
ACKNOWLEDGMENT	XV
DEDICATION	XVI
1 INTRODUCTION.....	1
1.1 JUSTIFICATION	1
1.2 OBJECTIVES.....	2
2 LITERATURE REVIEW	3
2.1 DISTRIBUTED GENERATION.....	3
2.1.1 <i>Introduction</i>	3
2.1.2 <i>Technologies</i>	5
2.1.3 <i>Applications and Advantages</i>	6
2.1.4 <i>Standards to Interconnect Distributed Resources with Power Systems</i>	8
2.2 POWER SYSTEM STABILITY	9
2.2.1 <i>Introduction</i>	9
2.2.2 <i>Rotor Angle Stability</i>	9

2.2.3	<i>Voltage Stability</i>	11
2.3	TRANSIENT STABILITY	12
2.3.1	<i>Introduction</i>	12
2.3.2	<i>Swing Equation and Power Angle Equation</i>	14
3	POWER SYSTEM MODELS	18
3.1	INTRODUCTION	18
3.2	SYNCHRONOUS GENERATOR MODEL.....	18
3.3	EXCITER SYSTEM MODEL	21
3.4	GOVERNOR MODEL	23
3.5	LOAD MODEL	24
4	ELECTRICAL SYSTEM OF PUERTO RICO	26
4.1	HISTORY	26
4.2	GENERATION	27
4.3	TRANSMISSION AND DISTRIBUTION SYSTEMS	29
4.4	PUERTO RICO CASE STUDY SCOPE AND DESCRIPTION	30
4.4.1	<i>Scope</i>	30
4.4.2	<i>Description</i>	31
5	OPTIMAL CAPACITY OF DISTRIBUTED GENERATION	33
5.1	INTRODUCTION	33
5.2	OCDG MODEL.....	34
6	RESULTS AND ANALYSIS	43

6.1	IEEE 14-BUS TEST SYSTEM	44
6.1.1	<i>Case 1: Synchronous DG Connected at Bus 4 (One Dimension)</i>	45
6.1.2	<i>Case 2: Synchronous DG Connected at Buses 4 and 5 (Two Dimensions)</i>	46
6.1.3	<i>Rotor Speed and Voltage Response</i>	47
6.1.4	<i>Critical Disturbance</i>	51
6.1.5	<i>Critical Clearing Time (CCT)</i>	55
6.1.6	<i>Goal Function Weights</i>	56
6.1.7	<i>Step Size</i>	57
6.2	SIMULATIONS OF THE ELECTRICAL SYSTEM OF PUERTO RICO	59
6.2.1	<i>Case #1: Fault at Bus 41, then open breaker between buses 35 and 41</i>	62
6.2.2	<i>Case #2: Fault at bus 39, then open breakers between buses 36 and 39</i>	67
6.2.3	<i>Case #3: Fault at bus 44, then open breaker between buses 35 and 44</i>	71
6.2.4	<i>Summary of the Electrical System of PR</i>	75
7	CONCLUSION AND FUTURE WORK	79
7.1	CONCLUSION	79
7.2	FUTURE WORK	81
	BIBLIOGRAPHY	82
	SELECTED BIBLIOGRAPHY	87
	APPENDIX A: IEEE 14-BUS TEST SYSTEM DATA	90
	APPENDIX B: PUERTO RICO ELECTRICAL SYSTEM DATA	93
	APPENDIX C: DISTRIBUTED GENERATION DATA	98

List of Figures

FIGURE 1: CENTRALIZED GENERATION VS. DISTRIBUTED GENERATION	4
FIGURE 2: SYNCHRONOUS GENERATOR REPRESENTATION	10
FIGURE 3: ABSOLUTE ANGLE STABLE TRANSIENT	12
FIGURE 4: ABSOLUTE ANGLE UNSTABLE TRANSIENT.....	13
FIGURE 5: SYNCHRONOUS MACHINE INFINITE BUS REPRESENTATION.....	15
FIGURE 6: POWER ANGLE CURVE - STABLE CASE.....	16
FIGURE 7: POWER ANGLE CURVE - UNSTABLE CASE.....	16
FIGURE 8: GENERATOR EQUIVALENT CIRCUIT DIRECT AXIS.....	19
FIGURE 9: GENERATOR EQUIVALENT CIRCUIT QUADRATIC AXIS.....	19
FIGURE 10: EXCITER CONTROL SYSTEM	21
FIGURE 11: AVR SYSTEM	22
FIGURE 12: GOVERNOR CONTROL SYSTEM	23
FIGURE 13: GOVERNOR TRANSFER FUNCTION	23
FIGURE 14: GEOGRAPHIC LOCATION OF GENERATIONS UNITS	27
FIGURE 15: TRANSMISSION SYSTEM	29
FIGURE 16: ELECTRICAL SYSTEM OF PUERTO RICO.....	32
FIGURE 17: OCDG FLOWCHART.....	38
FIGURE 18: IEEE 14-BUS TEST SYSTEM WITH DISTRIBUTED GENERATION	44
FIGURE 19: OPTIMAL PENETRATION OF P_{DG4} GOAL FUNCTION CURVE	45
FIGURE 20: OPTIMAL PENETRATION OF P_{DG4} AND P_{DG5} , TWO DIMENSION CONTOUR PLOT.....	46

FIGURE 21: ROTOR SPEED RESPONSE – IEEE 14-BUS TEST SYSTEM	49
FIGURE 22: VOLTAGE RESPONSE – IEEE 14-BUS TEST SYSTEM	50
FIGURE 23: ROTOR SPEED RESPONSE - UNSTABLE AND STABLE CASES.....	51
FIGURE 24: BUS VOLTAGE – UNSTABLE AND STABLE CASES	52
FIGURE 25: OPTIMAL PENETRATION OF DISTRIBUTED GENERATION	53
FIGURE 26: GOAL FUNCTION	54
FIGURE 27: CRITICAL CLEARING TIME	55
FIGURE 28: GOAL FUNCTION WEIGHTS.....	57
FIGURE 29: STEP SIZE	58
FIGURE 30: PUERTO RICO POWER FLOW SOLUTION - VOLTAGE MAGNITUDE	61
FIGURE 31: PUERTO RICO POWER FLOW SOLUTION - VOLTAGE ANGLE	61
FIGURE 32: PUERTO RICO POWER FLOW SOLUTION - REAL POWER.....	62
FIGURE 33: PUERTO RICO POWER FLOW SOLUTION - REACTIVE POWER.....	62
FIGURE 34: CASE 1 - ROTOR SPEED RESPONSE	63
FIGURE 35: CASE 1 – BUS VOLTAGE RESPONSE	64
FIGURE 36: CASE 1 – REAL POWER	65
FIGURE 37: CASE 1 – REACTIVE POWER	66
FIGURE 38: CASE 2 – ROTOR SPEED RESPONSE	67
FIGURE 39: CASE 2 – BUS VOLTAGE RESPONSE	68
FIGURE 40: CASE 2 - REAL POWER	69
FIGURE 41: CASE 2 – REACTIVE POWER	70
FIGURE 42: CASE 3 – ROTOR SPEED RESPONSE	71

FIGURE 43: CASE 3 – BUS VOLTAGE RESPONSE	72
FIGURE 44: CASE 3 – REAL POWER	73
FIGURE 45: CASE 3 – REACTIVE POWER	74
FIGURE 46: REAL POWER SUMMARY	76
FIGURE 47: REACTIVE POWER SUMMARY	77
FIGURE 48: REAL AND REACTIVE POWER LOSSES.....	78

List of Tables

TABLE 1: DISTRIBUTED GENERATION TECHNOLOGIES 5

TABLE 2: PRINCIPAL GENERATION UNITS 27

TABLE 3: GENERATION IN THE ELECTRICAL SYSTEM OF PUERTO RICO 28

TABLE 4: LOCATION OF THE DG CONNECTED 59

TABLE 5: COMPONENTS IN THE ELECTRICAL SYSTEM OF PUERTO RICO 60

List of Symbols

DG	Distributed Generation
P_{DG}	Real Power of Distributed Generation
Q_{DG}	Reactive Power of Distributed Generation
p_m	Mechanical Power
P_e	Electric Power
P_a	Acceleration Power
H	Inertia
δ	Power Angle
ω_r	Rotor Speed
X_T	Equivalent Reactance
x	Optimization State Variables Vector
y	Optimization Algebraic Variables Vector
$g(x, y, u)$	Algebraic Equations
$f(x, y, u)$	Differential Equations
$C(x, y, u)$	Objective Function
$C_1(x)$	Cost Associated with the State Variables
$C_2(y)$	Cost Associated with the Algebraic Variables
$C_3(u)$	Cost Associated with the Control Variable

x^*	Initial Optimization State Variables Vector
y^*	Initial Optimization Algebraic Variables Vector
Δt	Time Step
u	Control Variable
L	Augmented Goal Function
λ	Lagrange Multiplier Associated with the State Variables
β	Lagrange Multiplier Associated with the Algebraic Variables
ϵ	Tolerance Value
α	Control Multiplier
N_T	Number of Time Step
N_x	Number of Optimization State Variables
N_y	Number of Optimization Algebraic Variables
PR	Puerto Rico
PSAT	Power System Analysis Toolbox
OCDG	Optimal Capacity of Distributed Generation
T_m	Mechanical Torque
T_e	Electric Torque
P_{CG}	Real Power Central Generation
r_a	Stator Resistance

L_L	Stator Leakage Inductance
L_{ad} , L_{aq}	Mutual Inductance between the Stator and Rotor
v_d , v_q	Direct and Quadratic Axes Voltages
P	Real Power
Q	Reactive Power
V	Voltage Magnitude
θ	Voltage Angle
v_f	Field Voltage
e'_d , e'_q	Direct and Quadratic Axes Transient Voltages
x_d , x_q	Direct and Quadratic Axes Synchronous Reactance
x'_d , x'_q	Direct and Quadratic Axes Transient Reactance
T'_{d0} , T'_{q0}	Direct and Quadratic Axes Open Circuit Transient Time Constant
M	Mechanical Starting Time
D	Damping Coefficient
x_L	Stator Leakage Reactance
R	Droop
ω_{ref0}	Reference Speed
T_{max}	Maximum Turbine Output
T_{min}	Minimum Turbine Output

T_1	Transient Gain Time Constant
T_2	Governor Time Constant
p_m^{syn}	Synchronous Generator Mechanical Power
$T_{mech 0}$	Reference Turbine Output
AVR	Automatic Voltage Regulator
v_f^{syn}	Synchronous Generator Field Voltage
v_{ref}	Reference Voltage
v_0	Initial Reference Voltage
$V_{r max}$	Maximum Regulator Voltage
$V_{r min}$	Minimum Regulator Voltage
K_a	Amplifier Gain
T_a	Amplifier Time Constant
K_f	Stabilizer Gain
T_f	Stabilizer Time Constant
T_e	Field Circuit Time Constant
T_r	Measurement Time Constant
A_e	1 st Ceiling Coefficient
B_e	2 nd Ceiling Coefficient
Pu	Per Unit

Abstract

This thesis presented an optimization technique to determine the optimal capacity and location of distributed generation (DG), to improve system stability during and after a disturbance in the electrical system. The optimization algorithm employed discretized power systems dynamic equations as equality constraints in a non linear programming framework. The IEEE 14 Bus Test System and the Electrical System of Puerto Rico were used as models for the simulations. Several cases were analyzed and presented to determine the stability improvement by DG. Simulation results were presented through several plots and figures in order to appreciate the convergence and dynamic response of the electrical system. The Optimal Capacity of Distributed Generation (OCDG) algorithm was able to reach the optimal solution, accurately for each case. Simulations of the electrical system of Puerto Rico show that the main DG penetration was in the north and east of the island. Optimal DG penetration supports the network, improving the rotor angle stability and voltage stability during and after a disturbance. Results demonstrated the advantages of DG in the electrical system of Puerto Rico. The methodology presented could be further developed to optimally incorporate alternative energy technologies in the production of electrical energy.

Resumen

Esta tesis presenta una técnica de optimización que determina la capacidad y localización óptima de generación distribuida para mejorar la estabilidad durante y luego que ocurre un disturbio en el sistema eléctrico. El algoritmo de optimización emplea la discretización de las ecuaciones dinámicas del sistema de potencia como restricciones de igualdad en un sistema de programación no lineal. El sistema de 14 Barras de la IEEE y el sistema eléctrico de Puerto Rico fueron usados como modelos para las simulaciones. Varios casos son presentados para determinar el mejoramiento en la estabilidad del sistema eléctrico por medio de generación distribuida. Los resultados de las simulaciones son presentados mediante graficas y figuras con el propósito de apreciar la convergencia y la respuesta dinámica del sistema eléctrico. El algoritmo para determinar la Óptima Capacidad de Generación Distribuida fue capaz de alcanzar la solución óptima de manera precisa para cada caso. Las simulaciones del sistema eléctrico de Puerto Rico muestran que la mayor penetración de generación distribuida ocurrió en el norte y este de la isla. La óptima penetración de generación distribuida ayudo el sistema eléctrico, mejorando la respuesta de estabilidad del voltaje y ángulo de rotor, durante y luego del disturbio. Los resultados del estudio demostraron las ventajas de la generación distribuida en el sistema eléctrico de Puerto Rico. La metodología presentada podría desarrollarse de forma óptima con el propósito de implementar tecnologías alternas en la producción de energía eléctrica.

Acknowledgment

I would like to thank God for giving me the strength, wisdom and health to continue developing the study during the difficult moments. He has blessed me with the opportunity to complete my dream finalizing this work.

I am deeply indebted to Dr. Erick E. Aponte, president of my graduate committee, for giving me the opportunity to work under his guidance. His support and valuable comments motivate me to finalize this work. Thanks, Dr. Erick for your time and patience during this research.

I also want to acknowledge my graduate committee, Dr. Lionel R. Orama and Dr. Efraín O'Neill for serving as members of my graduate committee and for their valuable advice during the course of Master Program.

I would like to thank Joel D. Sefarin, Gary Soto and Hector G. Mendez for helping me obtain the necessary information to complete this work. Without their help this work could not be completed.

I wish to express my deepest gratitude to my fiancée Meliany Quintana for understanding me and her continued support during this period.

Finally, I would like to thank the graduate students of the Electrical and Computer Department, for their sincere friendship and support during the Master Program. I will never forget all the good moments that we passed in the university.

Dedication

This thesis is dedicated to my parents Carmen L. Torres Mercado (mother) and Roberto Galarza Valentín (father) for motivating me to continue fighting and teaching me never give up during hard times. They have made everything possible for me and I am eternally grateful. Thanks for supporting me during my professional career...

1 Introduction

1.1 Justification

Engineers around the world are developing different methods to improve the reliability and security of the electrical system. Newer technologies permit the production of electrical energy in an efficient, reliable and secure way, causing fewer damages for the environment. One solution is to build generation closer to the consumption areas. This is known as distributed generation (DG).

Increased electrical demand in the Northeast presents generation problems to the Puerto Rico electrical power system. Puerto Rico, like other countries around the world, has supply and demand problems. The main concentration of generation is in the south, while most of the load is in the north. If a fault occurs in the transmission system interconnecting these zones, it might cause serious damage to network security and eventually lead to system collapse. The installation of distributed generation will support the electrical system before, during and after a disturbance improving its dynamic response. Many studies and investigations show that distributed generation improves the stability of electric power systems [1] [2] [3] [4].

The overall goal of this investigation is to obtain the optimal conditions necessary, through dynamic simulation, to improve the stability of a power system after severe disturbances. The electrical system will be simulated for different faults in order to obtain the optimal conditions necessary to implement distributed generation and improve the stability response of the electrical system.

The vision of the study is to demonstrate the advantages of distributed generation, with a principal focus on system stability, in order to develop technology alternatives in the production

of electrical energy. This work could produce favorable results to the reliability of the electrical system of Puerto Rico. Consequently, the main contribution of this work will be the development of a planning tool to determine the optimal location and capacity of distributed generation, in order to improve the dynamic response to severe disturbances of the Puerto Rico electrical system.

1.2 Objectives

The principal objective of this investigation is to study the implementation of DG to improve system stability during and after the occurrence of severe disturbances in the electrical system. Stability simulations will be performed on a model similar to the Puerto Rico grid in order to identify the following important variables:

- DG sizing and location to avoid general system failure.
- Critical network areas during and after a disturbance.
- Optimal location and capacity for DG installation based on stability criteria.
- Network stability improvements after DG implementation.

The methods to obtain the objectives are discussed in the following section.

2 Literature Review

2.1 Distributed Generation

2.1.1 Introduction

Electrical power systems are complex networks and devices interacting to reliably generate transmit and distribute electrical energy to its customers. Centralized generation (CG) supplies large amounts of electrical energy from generators through transmission lines and distribution lines to the consumption area.

The electrical demand around the world is growing continuously and presents some limitations to the CG model. Costly and wasteful energy production, transmission congestion and environmental concerns are some problems exhibited by the centralized model [5]. Each mile of transmission line costs about one (1) million dollars to construct and approximately seven (7) percent of electricity is lost during the transmission as heat [6] [7]. To provide reliable and less expensive electrical energy to customers, new emphasis is being placed on DG.

Different technologies are being developed to generate electrical energy close to the consumption areas (load centers). This modality is called generation IN-SUIT, disperse generation or distributed generation. Distributed generation is small scale generation or storage of electrical energy at the customer side, which permits the option of selling and buying energy to and from the electrical system, while taking advantage of the maximum efficiency of energy production [8]. Generally, the capacity range of distributed generation is between 100 kW and 10 MW. Figure 1 shows differences between centralized generation and distributed generation.

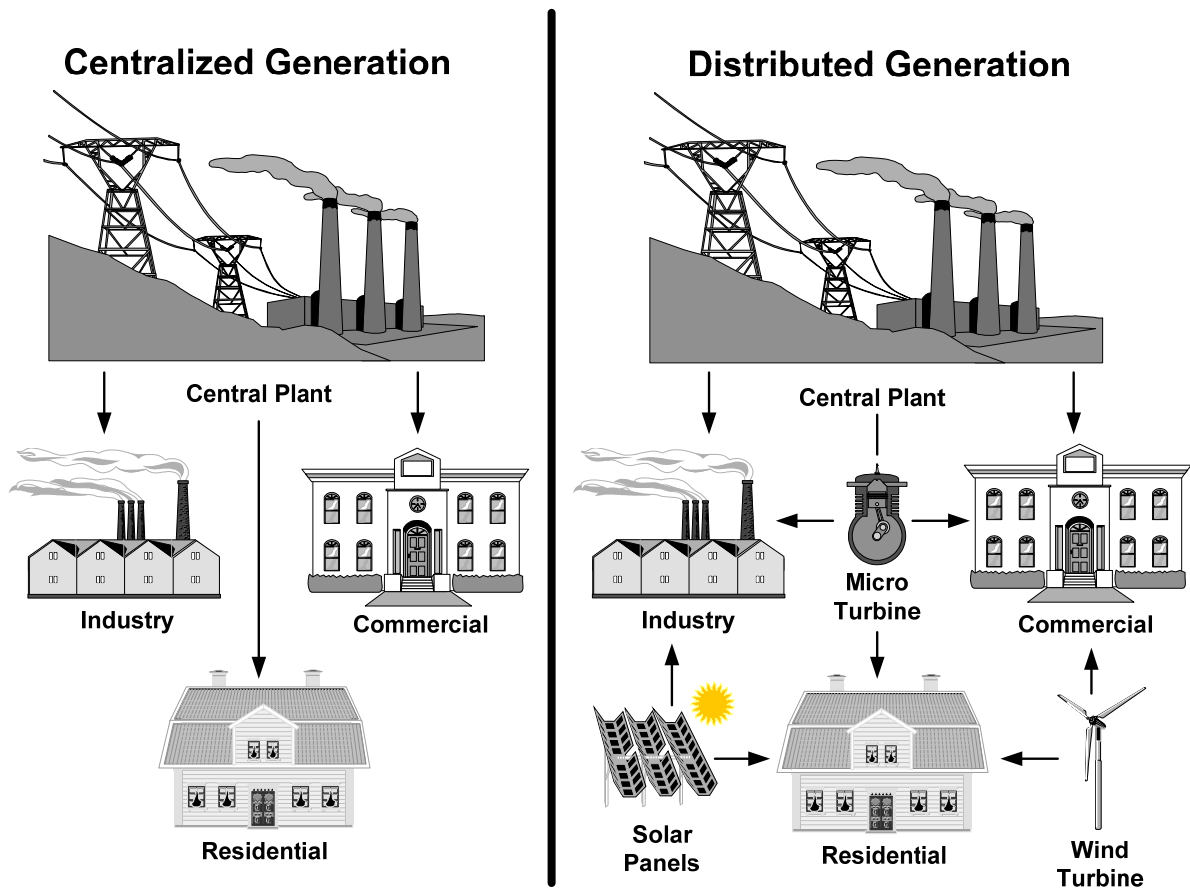


Figure 1: Centralized Generation vs. Distributed Generation

According to worldwide data from “La Cigre de 1999”, from 1995 to 1999 the percentage of installed DG capacity increased in relation with the total capacity. Some examples are [8]:

- Denmark – 37% Up 29%
- Australia, Poland, Spain and Germany – 15%
- United State – 5%

Studies from the International Agency of Energy estimate that demand for electrical energy will grow 50% in the next 20 years, mostly due to developed countries, where the 15% of demand will be supplied by DG [8]. The success of DG depends on innovative technologies that

enable small scale generation of electrical energy to operate synchronized to the power system, efficiently, reliably and maintaining the highest power quality standards.

2.1.2 Technologies

A key factor when implementing DG is the underlining technology. Technologies can be separated in generation and storage. Generation is further divided into conventional and non-conventional. Conventional includes combustion turbines, diesel engines, micro-turbines and natural gas engines. Non-conventional are mostly renewable energy technologies. Table 1 summarizes preliminary cost, size and efficiency estimates for DG technologies [9].

TABLE 1: DISTRIBUTED GENERATION TECHNOLOGIES					
Technology	Size Range (kW)	Installed Cost (\$/kW)^a	Variable O&M (\$/kWh)	Heat Rate (BTU/kWh)	Approx. Efficiency (%)
Diesel Engine	1-10,000	350-800	0.025	7,800	45
Natural Gas Engine	1-5,000	450-1,100	0.025	9,700	35
Dual Fuel Engine	1-10,000	625-1,000	0.023	9,200	37
Micro-turbine	15-60	950-1,700	0.014	12,200	28
Combustion Turbine	300-10,000	550-1,700	0.024	11,000	31
Fuel Cell	100-250	5,500+	0.01-0.05	6,850	50
Photovoltaic	Limited by Available Space	7,000-10,000	0.002	--	N/A
Wind Turbine	0.2-5,000	1,000-3,000	0.010	--	N/A

^a The high end of the range indicates costs with NO_x controls for the most severe emissions limits internal combustion technologies only.

An important factor to consider is the relation between fixed and variable costs. Depending on the technology, DG could have high installation costs, but low operation and maintenance (O&M) costs. Thus, depending on the application, investing in DG technologies could be a feasible long term alternative.

2.1.3 Applications and Advantages

DG can be applied to improve the reliability and power quality of the electrical system while supporting local utility infrastructure by reducing congestions in transmission and distribution. Some of the principal applications of DG include:

- Base Loading – DG's produce electrical energy continuously while connected to the distribution system.
- Islanding – DG generates electrical energy isolated from the grid.
- Support – DG is used to strengthen systems with high demand variation.
- Load Leveling – Supply peak demand locally to avoid transmission congestion and running more expensive units.

These applications provide advantages for the user and supplier. The available technologies supply electrical energy at low cost and good quality. They can also diminish interruptions in the electrical system, which produce great monetary losses for big industrial and commercial clients [8].

Some of the DG advantages and disadvantages include:

A. Advantages for the user:

- a) Increased reliability
- b) Increased power quality
- c) Reduction in the interruption number

- d) Efficient use of energy
- e) Lower cost of energy
- f) Use of renewable energy
- g) Reduction of pollution emissions

B. Advantages for the supplier

- a) Reduction in the transmission and distribution losses
- b) Increase the capacity system
- c) Improve the stability
- d) Extended equipment service life
- e) Reduce congestion.
- f) Voltage support
- g) Improved small signal stability, due to low constant of inertia.
- h) Loss of synchronism of a small DG unit has less impact on the local network voltage as oppose to loss of synchronism in a large power plant, which has a higher impact on the voltage, frequency and stability of the network.
- i) DG reduces post fault voltage oscillation.
- j) Increased critical clearing times.

C. Disadvantage

- a) Increased short circuit current
- b) Increased the protection cost
- c) Possibility of islanding
- d) Possibility of flicker

- e) Possibility of over voltage
- f) Retrofit costs.

2.1.4 Standards to Interconnect Distributed Resources with Power Systems

The 2005 Energy Policy Act (EPA 2005) establishes that DG interconnection should comply with the requirements of IEEE-1547 standard. The IEEE-1547 Standard for Interconnection of Distributed Resources with Electrical Power Systems was approved in the year 2003. The standard was developed to guarantee a secure and dependable interconnection between DG's and the electrical system. The standard establishes requirements that should be fulfilled when the DG is interconnected. The IEEE-1547 standard applies to DG systems with a maximum aggregated capacity of 10 MVA at the point of common coupling. The standard also establishes the operating requirements during steady state and transients conditions. It also includes a section with the specifications and requirements of tests to certify DG equipment.

The Puerto Rico Electric Power Authority (PREPA) is considering other standards for the interconnection of DG to the electrical system. The National Association of Regulatory Utility Commissioners (NARUC) developed standards to complement the IEEE-1547 standard. It provides guidelines for companies to interconnect DG. In 2003 NARUC published the Model Interconnection Procedures and Agreement or Small Distributed Generation Resources, which includes the rights and responsibilities for the supplier and client [10].

Distributed generators in compliance with NARUC's requirements, are cleared to interconnect with the electrical system. If a generator doesn't fulfill NARUC's requirements, additional studies would be required. Supplementary studies will determine the necessary changes to be applied at the DG or electrical system. NARUC establishes that the owner will be responsible to pay for any changes or studies performed.

2.2 Power System Stability

2.2.1 Introduction

In general, stability is a condition of equilibrium between opposing forces for power systems. Stability denotes the ability to maintain an acceptable equilibrium after being subjected to a physical disturbance. An acceptable equilibrium is called stable steady state condition. Otherwise, if the system doesn't reach a new equilibrium after the disturbance, the system is unstable. The main classifications of stabilities are:

- Rotor Angle Stability
- Voltage Stability

The goal of maintaining stability is to ensure the reliability of the electrical system. The main requirement for a reliable operation is to maintain synchronous generators within an adequate generation range, while fulfilling the standards to supply the demanded load.

A power system is a complex nonlinear dynamic system that operates in a constantly changing environment. When a disturbance occurs, system stability depends on the initial condition and the dynamic characteristics of the generators and control equipment. The disturbance may be small or large. Transient Stability is the ability of the power system to maintain synchronous operation following a large disturbance. The ability of the power system to maintain synchronous operation when subject to a small disturbance is called small signal stability. Small signal stability can be analyzed with linear equations [11].

2.2.2 Rotor Angle Stability

Rotor Angle Stability is the ability of synchronous generators to remain in synchronism under steady state condition and after being subjected to a disturbance [12]. It depends on the

ability of each synchronous generator in the system to maintain balance between electromagnetic torque and mechanical torque. An important factor is the variation of the synchronous generator rotor angles as they attempt to follow the variations in power demand from the system during and after a disturbance. Under steady state conditions, the input mechanical torque and output electrical torque remain in equilibrium and the rotor speed stays constant. If the system is perturbed, the synchronous generator rotor accelerates or decelerates, when power demand decreases or increases, respectively. Machine dynamics are greatly influenced by their inertia. Figure 2 illustrates the dynamics of a synchronous generator on a set of synchronous speed, and direct and quadratic axis.

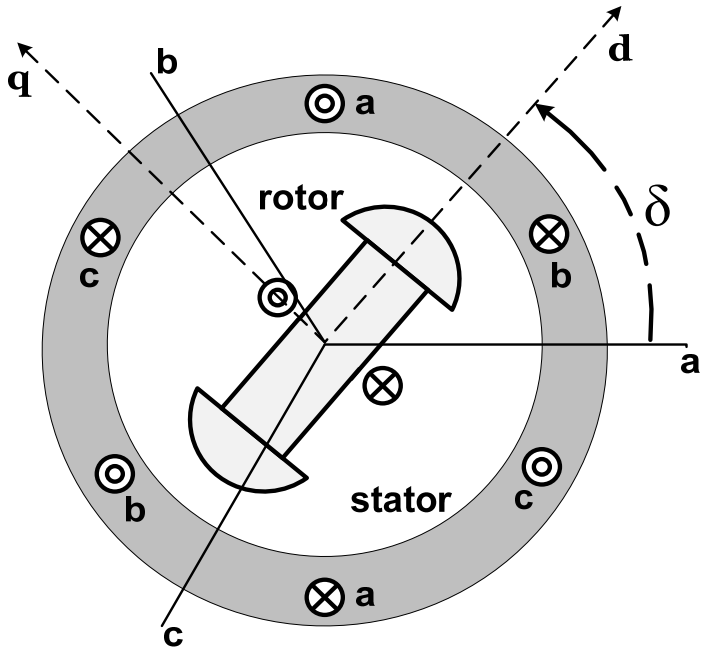


Figure 2: Synchronous Generator Representation

If a generator accelerates, the angular position of its rotor, in comparison with the other machines, will increase. Angular positions depend on the power angle relationship (see Eq. 2.2). The power angle relationship is highly nonlinear. An increase in angular separation is accompanied by a decrease in power transfer and increased instability [12].

2.2.3 Voltage Stability

Voltage stability is the ability of a power system to maintain steady state voltage at all buses in the system under normal operating condition and after to the occurrence of a disturbance [12]. The main factor contributing to voltage instability is usually the voltage drops that limit the capacity of transmission networks to transfer power between buses. Increased voltage drops could be associated with the change of rotor angles. Voltage instability occurs when load dynamics try to restore power consumption beyond the capability of the transmission system and the connected generation [12].

During power system simulations, loads are usually represented as purely static elements, where the impedance and the system could operate stably, even at low voltage. In reality, they are dynamic elements and should be represented accordingly. This is necessary to obtain good results from voltage stability simulations.

Voltage and rotor angle instability are correlated. The main difference is the control system time response. The exciter and governor are control systems that respond to maintain the voltage and rotor angle stability, respectively. The exciter response is faster, while the governor's response is slower. It is very important to recognize the difference between voltage stability and rotor angle stability to understand the cause of the problem and to develop a corrective strategy.

2.3 Transient Stability

2.3.1 Introduction

As discussed previously, transient stability is the ability of a power system to remain in synchronism when subjected to a large disturbance. These disturbances could be faults on transmission lines, loss of load, loss of generation, or loss of system components. These disturbances are critical since they entail the sudden change of electrical output, while the mechanical input doesn't have enough time to react and remains practically constant during the event. As a result, rotors may accelerate and store the extra energy.

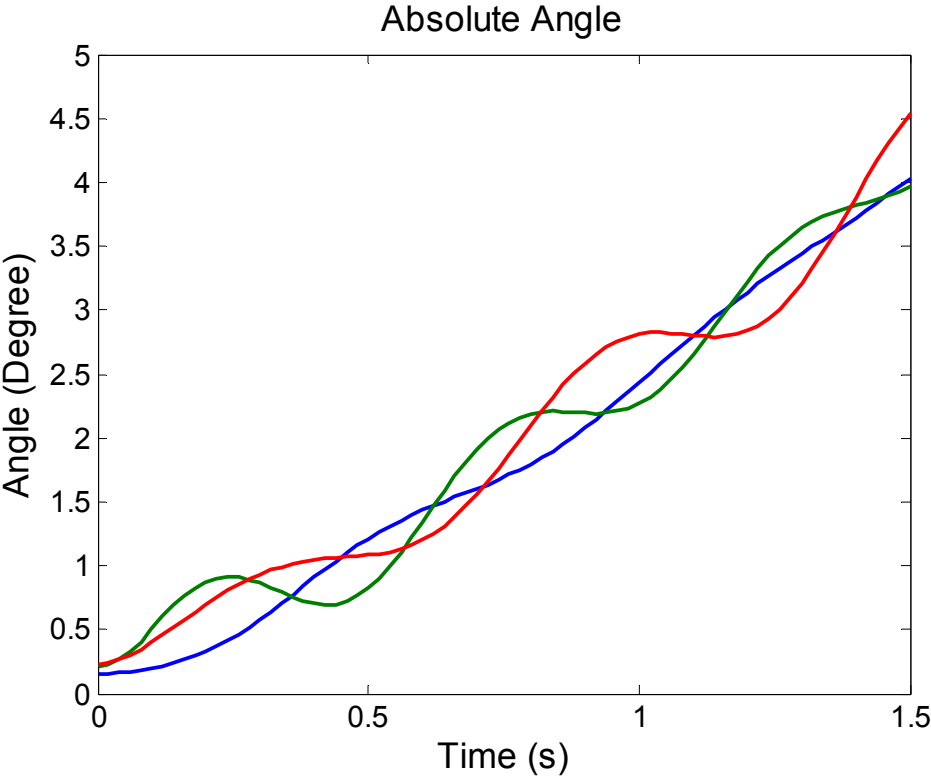


Figure 3: Absolute Angle Stable Transient

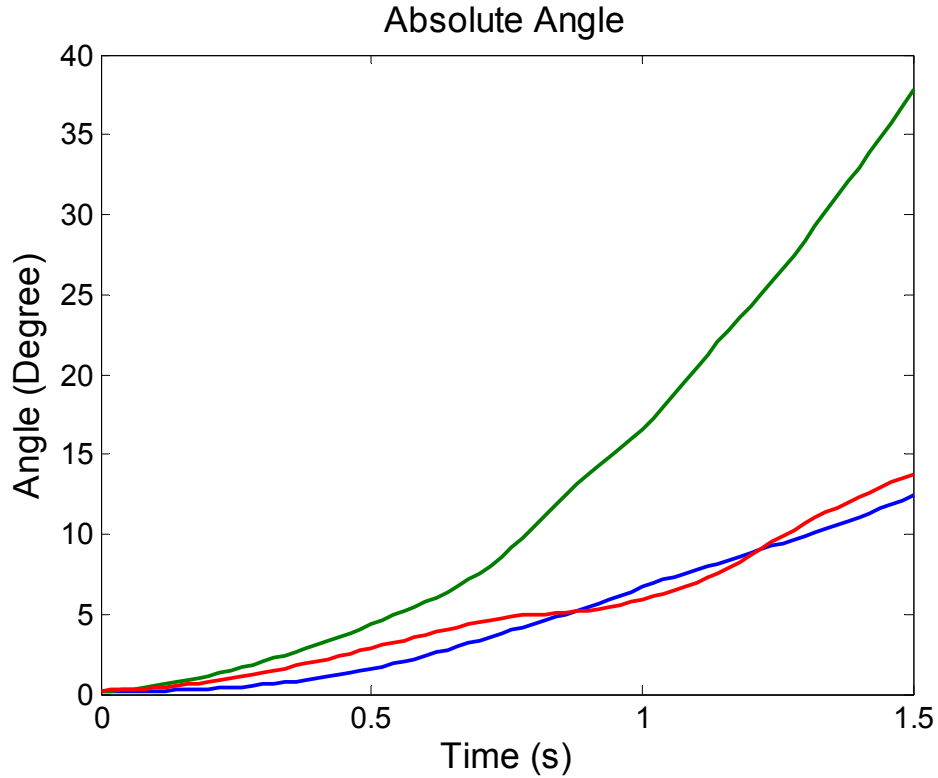


Figure 4: Absolute Angle Unstable Transient

Figure 3 and 4 show two cases of stability simulations in response to a large disturbance. Figure 3 shows a stable case where all the rotor angle differences are small. Figure 4 shows an unstable case where rotor angles continue to drift apart. Transient stability is a function of disturbance type and location to which the system is exposed. Electrical power systems can be analyzed (simulated) using computer models in order to verify how the systems behave under different disturbances. One of the main purposes of the analysis is to determine the stability limits of a system.

It is very important to consider transient stability studies when designing power systems. To obtain accurate results, it is necessary to model the dynamics of each element during and after a disturbance. Detailed mathematical models consist of differential and algebraic equations.

2.3.2 Swing Equation and Power Angle Equation

The Swing Equation describes the motion of the rotor of a synchronous machine, represented by the mismatch between the mechanical input of the turbine (P_m) and the electrical power output (P_e) of the generator.

$$\frac{2H}{\omega_r} \frac{d^2 \delta}{dt^2} = P_m - P_e = P_a \quad (2.1)$$

Equation (2.1) is characterized by the inertia constant, H (sec) and rotor speed, ω_r ($\frac{rad}{s}$).

The value of H depends on the synchronous machine size. Larger machines have larger values of H ; the opposite is true for smaller machines. Generally, the value of H is in the range of 1 to 5 seconds in per unit (Pu) [13]. This is important, because DG machines have low values of H , while centralized generators have higher values. The physical meaning of the inertia constant is the time, in seconds, the machine needs to accelerate from zero speed to rated speed when rated input power is applied [13]. Another important dynamic equation is the power angle equation.

The Power Angle Equation describes the relation between the electrical power transfer and the rotor angle of the generator. Equation (2.2) represents the power angle equation for a lossless system.

$$P_e = \frac{E' E_b}{X_T} \sin(\delta) \quad (2.2)$$

It is a function of the internal generator voltage (E'), bus voltage (E_b) and the reactance (X_T) between those two points. The power angle or rotor angle (δ) is the angle between the rotor and the reference axes in a synchronous generator. The dynamic behavior of the synchronous generator can be represented by substituting the power angle equation into the swing equation.

$$\frac{2H}{\omega_r} \frac{d^2 \delta}{dt^2} = P_m - \frac{E' E_b}{X_T} \sin \delta = P_a \quad (2.3)$$

Equation (2.3) describes the behavior of the system to change in the power angle. Figure 5 illustrates a synchronous generator connected to an infinite bus, through a pair of parallel lines. The infinite bus can absorb or deliver any amount of active or reactive power from any single generator without any change in its voltage or frequency [14].

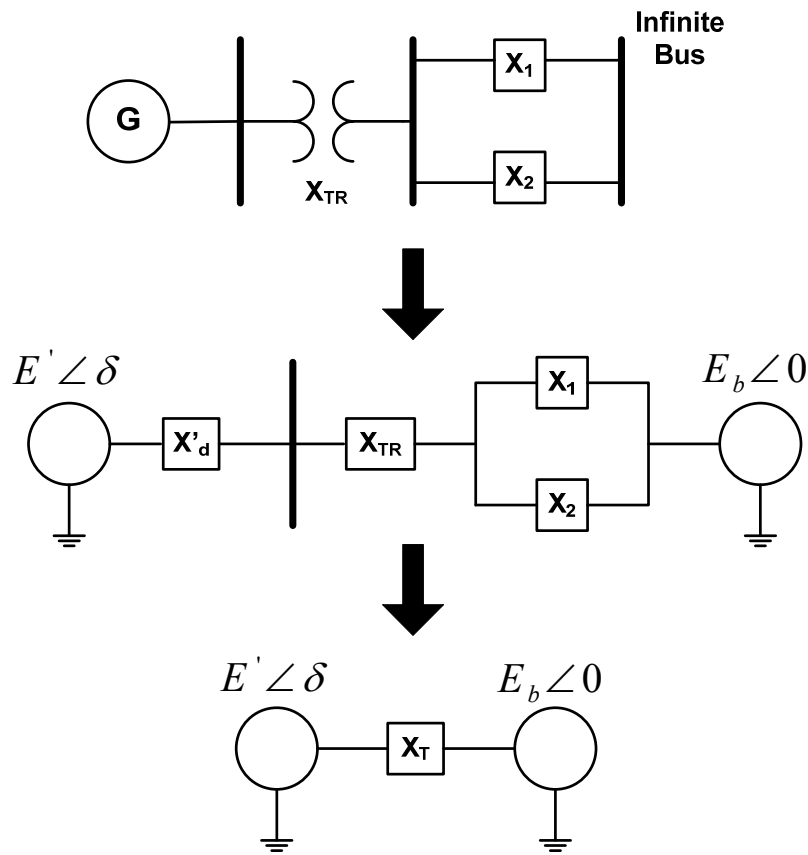


Figure 5: Synchronous Machine Infinite Bus Representation.

With the relationship between the swing and power angle equations, it is possible to analyze the fundamentals of transient stability, using the equal area criterion diagram. The equal area criterion diagram represents the transient stability through graphical means. To analyze the transient stability of the electrical system, it is necessary to understand the dynamic behavior of

the synchronous generator. Figure 6 and 7 illustrate the equal area criterion diagram to a stable and unstable case respectively. These figures summarize Equation (2.2) pre-fault, during and post-fault conditions.

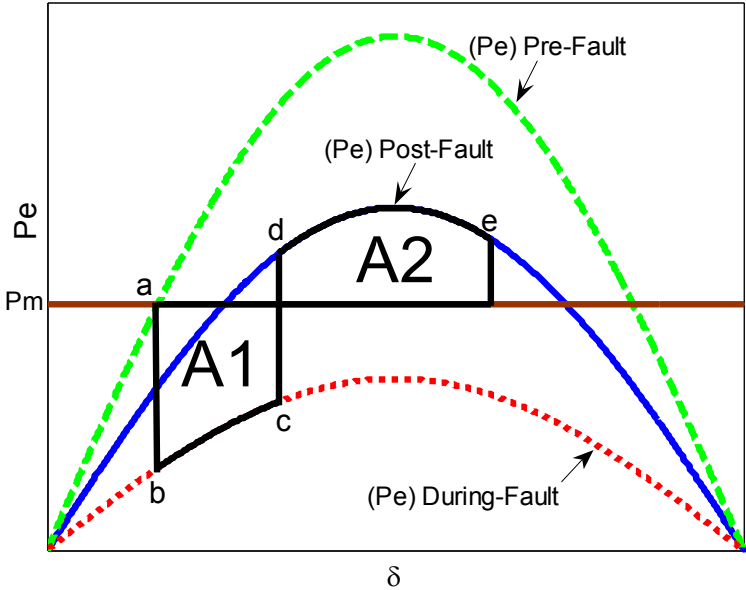


Figure 6: Power Angle Curve - Stable Case

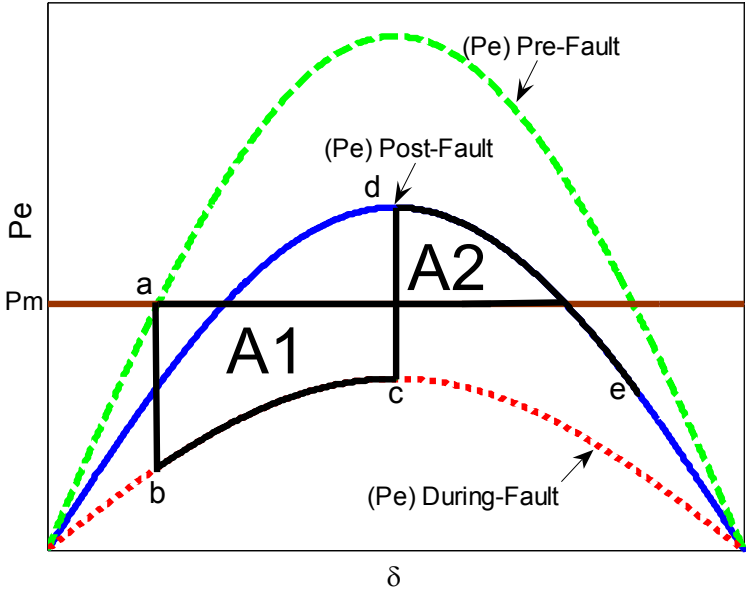


Figure 7: Power Angle Curve - Unstable Case

Initially, at operating point *a* (Figure 6), the system is operating in steady state condition, where the generator is operating at synchronous speed ($P_m = P_e$). Momentarily, a fault occurs in a transmission line, see Figure 5. The disturbance causes a reduction in P_e and a difference between the input and output powers ($P_m > P_e$). The operating point moves from *a* to *b*. To reach equilibrium, the synchronous machine accelerates and the power angle increases. The operating point moves to the “during fault” curve from *b* to *c*. The protection system removes the fault quickly, opening the breaker in transmission line X_2 . Instantly, the removals of X_2 cause an increase in X_T and a decrease of P_e , when compared to the pre-fault conditions. The operating point moves from *c* to *d*. After the fault is eliminated, a difference between the input and output power ($P_m < P_e$) exists and the synchronous machine decelerates to reach the equilibrium point, hence the power angle decrease. The operating point moves over the “post-fault” curve from *d* to *e*.

Figure 6 illustrates a scenario where the fault was cleared before the critical clearing time and the electrical system returns to a stable operation point. The critical clearing time is the maximum permissible fault duration before the generators lose the ability to regain stability in the electrical system. The energy gained during a disturbance caused by the acceleration is equal to the energy dissipated after the disturbance caused by the deceleration ($A_1=A_2$). Figure 7 illustrates an unstable case, where the fault is removed after the critical clearing time and the generator cannot return to stability. The energy gained during the disturbance is greater than the energy dissipated after the disturbance ($A_1>A_2$). In this case, the rotor speed begins to increase and does not recover.

3 Power System Models

3.1 Introduction

The electrical power system has numerous equipments that interact simultaneously to maintain stability and a safe operating condition. The principal components affecting the dynamic analysis are generators, turbines, governors, exciters and loads. The dynamics of these devices are affected when a disturbance occurs. The principal control systems are the exciter and governor, which act on the generator and turbine respectively.

Stability analysis programs include a variety of generator, exciter, turbine, governor and load models. The electrical system is described by algebraic and differential equations. Differential equations describe the dynamics of the system and the algebraic equations are known as static equations.

3.2 Synchronous Generator Model

The synchronous generator model is very complicated when analyzed in a three phase frame of reference. Generally, the three phases are transformed into two equivalents, direct and quadratic axes, using Park's transformation [11]. The direct axis is in phase with the rotor field winding and the quadratic axis is leading the direct axis by 90 degrees, see Figure 2. The equivalent circuit has some assumptions to simplify the analysis. Figure 8 and 9 illustrates the generator's direct and quadratic axis equivalent circuit, respectively [15].

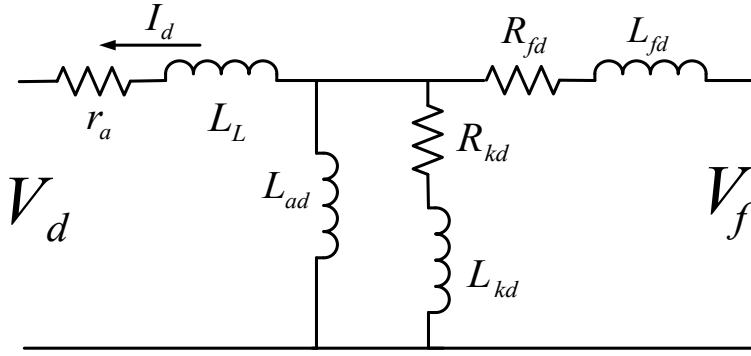


Figure 8: Generator Equivalent Circuit direct axis

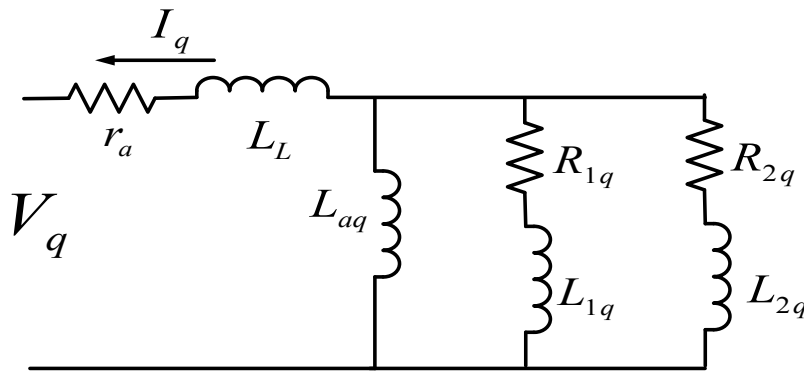


Figure 9: Generator Equivalent Circuit quadratic axis

The direct and quadratic axes include r_a , L_L , L_{ad} , L_{aq} , V_d and V_q which are the stator resistance, stator leakage inductance and the mutual inductance between stator and rotor, direct axis voltage and quadratic axis voltage, respectively. The other elements represent the rotor equivalent winding.

The synchronous generator model has six (6) algebraic variables and equations. The algebraic variables are represented by the active power (P), reactive power (Q), voltage magnitude (V), voltage angle (θ), mechanical power (p_m) and field voltage (v_f). The algebraic equations are represented by the power injection (P , Q), and the following equations [15]:

$$0 = v_d i_d + v_q i_q - P \quad (3.1a)$$

$$0 = v_q i_d - v_d i_q - Q \quad (3.1b)$$

$$0 = p_{m0} - p_m \quad (3.1c)$$

$$0 = v_{f0} - v_f \quad (3.1d)$$

To describe the dynamic behavior, differential equations were derived from the models shown in the Figure 8 and 9. This model considers a field circuit and an additional rotor circuit along the direct axis, two additional circuits along the quadratic axis and electromagnetic flux dynamics. The state variables are δ , ω , e'_q and e'_d , which represent the rotor angle, rotor speed, quadratic axis transient voltage and direct axis transient voltage, respectively. Equation (3.2) represents the synchronous generator differential equations.

$$\dot{\delta} = \Omega_b (\omega - 1) \quad (3.2a)$$

$$\dot{\omega} = \frac{(p_m - p_e - D(\omega - 1))}{M} \quad (3.2b)$$

$$\dot{e}'_q = \frac{(-f_s(e'_q) - (x_d - x'_d)i_d + v_f^*)}{T'_{d0}} \quad (3.2c)$$

$$\dot{e}'_d = \frac{(-e'_d + (x_q - x'_q)i_q)}{T'_{q0}} \quad (3.2d)$$

3.3 Exciter System Model

The excitation system is an automatic feedback controller, whose primary function is to regulate the generator field current to maintain a reference voltage at the synchronous machine terminals. Its components are the main exciter, automatic voltage regulator (AVR) and the amplifier. The exciter provides the field current for the synchronous generator. AVR couples the terminal voltage to the input of the main exciter. The amplifier increases the power of the regulation signal to that required by the exciter. Figure 10 shows the exciter control system diagram.

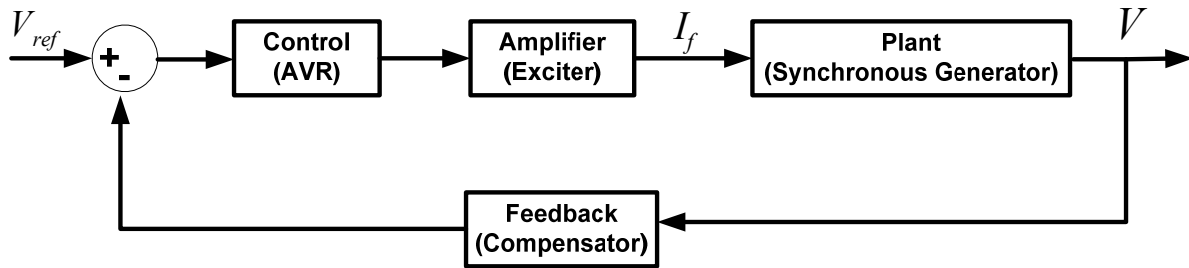


Figure 10: Exciter Control System

To reach an adequate generator voltage the exciter should respond instantly when a disturbance occurs. Figure 11 shows the AVR control system.

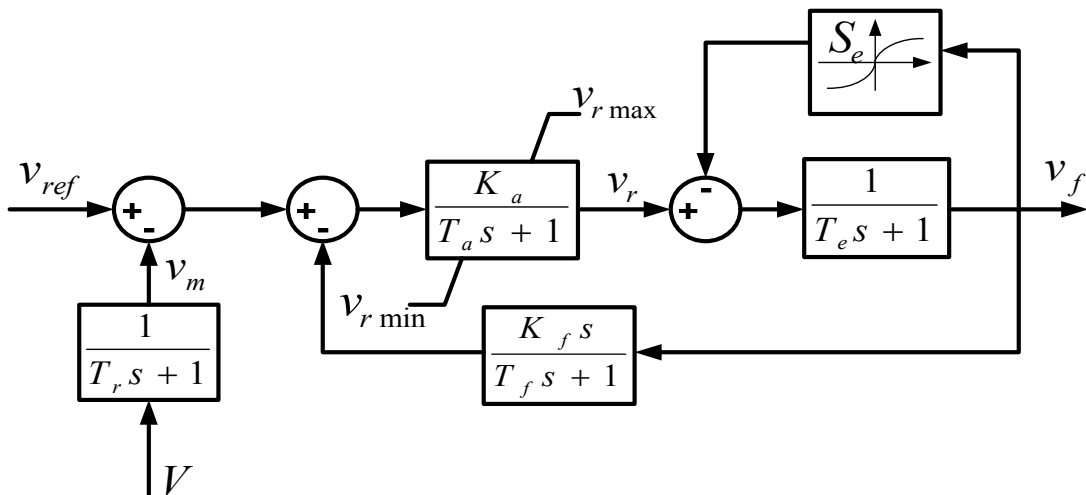


Figure 11: AVR System

Equation (3.3), represents the link between AVR, the generator and the reference voltage, where v_f^{syn} , v_f , v_0 , v_{ref} are the synchronous field voltage, field voltage, initial reference voltage and reference voltage, respectively.

$$0 = v_f - v_f^{syn} \quad (3.3a)$$

$$0 = v_0 - v_{ref} \quad (3.3b)$$

If a disturbance occurs in the electrical system, the terminal voltage of the synchronous generator is perturbed and the exciter responds to maintain the voltage within an operational range. The maximum exciter limit is fixed to prevent excessive rotor heating, while a minimum excitation limit is fixed to prevent potential loss [3]. Equation (3.4), describes the dynamic behavior of the exciter during a disturbance.

$$\dot{v}_m = \frac{(V - v_m)}{T_r} \quad (3.4a)$$

$$\dot{v}_{r1} = \frac{\left(K_a \left(v_{ref} - v_m - v_{r2} - \frac{K_f}{T_f} v_f \right) - v_{r1} \right)}{T_a} \quad (3.4b)$$

$$\dot{v}_{r2} = - \frac{\left(\frac{K_f}{T_f} v_f + v_{r2} \right)}{T_f} \quad (3.4c)$$

$$\dot{v}_f = - \frac{\left(v_f \left(1 + S_e(v_f) \right) - v_r \right)}{T_r} \quad (3.4d)$$

3.4 Governor Model

The main function of a governor is to control the rotor speed. Continuous variations in real power cause a change in system frequency. It is necessary to maintain the frequency close to 60 Hz to obtain a stable operation. When a disturbance occurs, caused by a mismatch between the mechanical torque (T_m) and the electrical torque (T_e), the governor modifies the mechanical power. Figure 12 represents the governor control system.

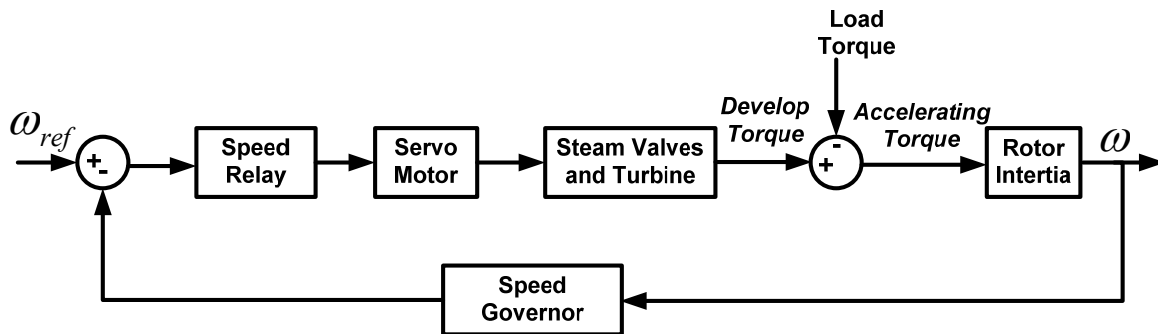


Figure 12: Governor Control System

If a fault or a load change occurs, the electrical torque of the synchronous generator changes, almost instantaneously. This difference causes rotors speed variation. In order to obtain a new equilibrium point, the governor tries to accelerate or decelerate the rotor, increasing or decreasing the mechanical torque. Figure 13 represents the governor transfer function, which relates speed and torque.

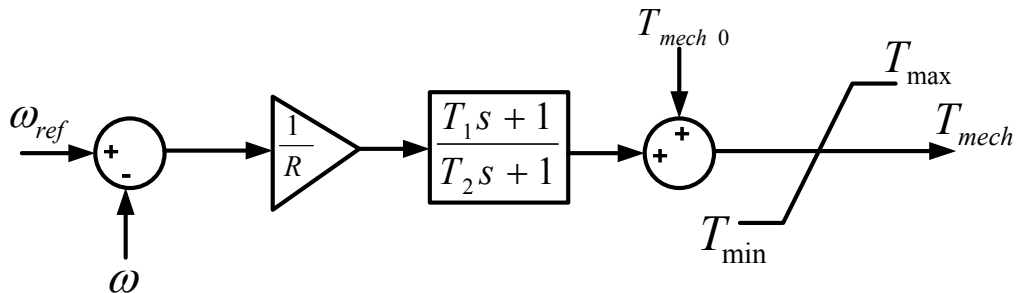


Figure 13: Governor Transfer Function

To maintain stability in the power system the governor operation is necessary. It has two (2) algebraic equations, Equation (3.5), where p_m^{syn} , p_m , ω_0 and ω_{ref} are the synchronous mechanical power, mechanical power, initial reference speed and reference speed, respectively. Equation (3.6) represents the link between the governor and the synchronous generator, and the governor reference rotor speed [15].

$$0 = p_m - p_m^{syn} \quad (3.5a)$$

$$0 = \omega_0 - \omega_{ref} \quad (3.5b)$$

The differential equations that describe the dynamic behavior are:

$$\dot{t}_g = \left(\frac{\frac{1}{R} \left(1 - \frac{T_1}{T_2} \right) (\omega_{ref} - \omega) - t_g}{T_2} \right) \quad (3.6a)$$

$$T_{mech} = \left(t_g + \left(\frac{1}{R} \right) \left(\frac{T_1}{T_2} \right) (\omega_{ref} - \omega) + T_{mech 0} \right) \quad (3.6b)$$

3.5 Load Model

Load modeling is very challenging when implemented in stability analysis, because the electrical system has a large number of devices whose characteristics vary continuously. Therefore, it is not useful to exactly represent each individual component. To increase the performance of the dynamic analysis, load models have been implemented.

$$P = \frac{k_p}{100} \left(\frac{V}{V_0} \right)^{\alpha_p} (1 + \Delta\omega)^{\beta_p} \quad (3.7a)$$

$$Q = \frac{k_Q}{100} \left(\frac{V}{V_0} \right)^{\alpha_Q} (1 + \Delta\omega)^{\beta_Q} \quad (3.7b)$$

Power system analysis refers loads as real and reactive power demand. Generally, the load is represented by a static model. The model simulates the characteristics of the load at any given time as algebraic function of voltage and frequency [16] [11]. Active and reactive power are considered separately. Equation (3.7) represents the voltage and frequency dependency of loads. Typical load coefficient values have been shown in previous publications [15].

4 Electrical System of Puerto Rico

4.1 History

Initially, the generation and distribution of electrical energy in Puerto Rico (PR) depended on hydroelectric generators. The first system of irrigation in the south coast was created through the approval of “Ley de Riego” in the year 1908. The law motivated an interest to create different artificial lakes around the island, with the objective to expand the irrigation system. In 1915, the PR government built hydroelectric plants to distribute and sell energy that was generated by the irrigation systems, of which 85% was used for the irrigation system, and the remaining 15 % was sold for industrial use.

The increase in demand for electrical energy and the success of the hydroelectric plants, caused Legislative interest, and thus more hydroelectric generators were building. In 1935, the total capacity was 5.8 MW. That same year, construction began for three (3) additional power plants, which were finished by 1937. The total capacity of the island increased to 19 MW. The development of hydroelectric plants continued to expand due to the increasing demand for electrical energy.

After the Second World War, the island began a heavy industrialization process. The electrical energy demand increased, but the water resources were limited. PREPA began to incorporate fossil fuel based thermoelectric plants into the electrical system. The hydroelectric plants were moved to the second level; those considered less efficient were shut down.

Today, the hydroelectric system incorporates 21 generation units, which are operated by PREPA. It has an aggregated capacity of 100 MW which represents about 2% of the total generation capacity in PR.

4.2 Generation

Puerto Rico has a generation capacity of 5,365 MW, while the peak demand is nearly 3,685 MW, still allowing for a reserve margin [17] [18]. The transmission system is designed such that the principal generation units are located in the south and the main concentration of load is located in the north of the island. Figure 14 illustrates the geographic locations of the principal generation units [17].



Figure 14: Geographic Location of Generations Units

PREPA has five (5) principals units of generation, which are: Cambalache, Palo Seco, Costa Sur, San Juan and Aguirre. These generators use petroleum fuel derivates. Table 2 shows the capacity of each generating plant [17].

TABLE 2: PRINCIPAL GENERATION UNITS		
Localization	Generation	Construction Year
Cambalache	247.5 MW	1997
Palo Seco	602 MW	1960
Costa Sur	1090 MW	1958
San Juan	400 MW	1956
Aguirre	900 MW	1973
	Total = 3,239.5 MW	

The San Juan, Palo Seco, Costa Sur and Aguirre thermoelectric plants use bunker #6 fuel. These can be considered as the base units of the system, because most of the time they are dispatched at their maximum capacity. The rest of PREPA’s thermal units use bunkers #2 fuels. These are “peak” units, because bunker #2 is more expensive. Table 3 presents the different types of fuel used and the capacity installed [19].

TABLE 3: GENERATION IN THE ELECTRICAL SYSTEM OF PUERTO RICO				
<i>PREPA System</i>				
Steam System: Generator Using fuel Bunker #6		Localization	Number of Units	Capacity of each unit (MW)
		Aguirre	2	450
		Costa Sur	2	410
			2	85
			2	50
		Palo Seco	2	216
			2	85
San Juan	4	100		
Generator using fuel bunker #2	Gas Turbine	Cambalache	3	83
		Others	22	21
	Combined Cycle Each Unit Consists of 4 combustion turbine of 50 MW and one steam turbine of 96 MW	Aguirre	2	296
Diesel Motor				2
				7
Hydro				100
Total Capacity of PREPA				4,404
<i>Cogeneration</i>				
Gas Turbine - Eco Electric Combined Cycle: Two combustion turbine of 165 MW and one steam turbine of 177 MW.				507
AES – Coal Two units of 227 MW.				454
Total Capacity Currently Installed in Puerto Rico				5,365

About 80% of the electrical energy produced in PR is derived from petroleum [17]. This fact is very concerning, because petroleum cost is increasing daily and the pollution caused by these generators is higher [20]. In order to improve the electrical system, PREPA is developing different plans to generate electrical energy at a lower cost.

4.3 Transmission and Distribution Systems

The transmission system carries large amounts of electrical power from generating stations to consumption areas. Transmission voltages in PR are 230 kV, 115 kV and 38 kV. The system is composed of 45 substations of 115 and 230 kV, and has an approximate extension of 2,182 miles of transmission lines. Figure 15 illustrates the 230 kV and 115 kV transmission systems [19].

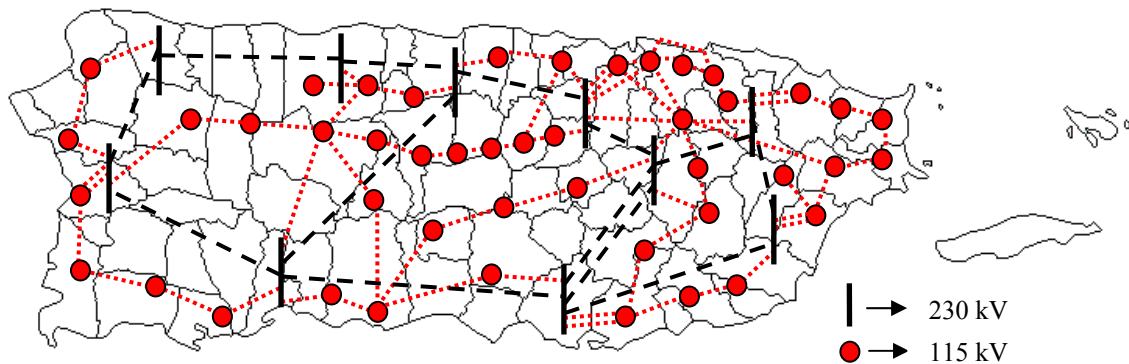


Figure 15: Transmission System

The 230 kV transmission network is composed of three main loops. The central loop has an extension of approximately 170 miles and links the electrical system from north to south of the island. The other two loops have a total extension of approximately 123 miles, and connect the electrical systems to the east and west parts of the island. The configuration of the 38 kV network in the electrical system is very complex. At present, there are 278 substations at this voltage level, which are connected with the distributions substations mentioned.

Distribution substations receive power from one or more transmission or sub-transmission lines. It provides power to one or more distribution feeders that originate in substations and comprise the primary distribution network. Most distribution substations carry between 5 and 60 MVA. The primary distribution system consists of feeders “emanating” from the substation and supplying power to one or more secondary distribution systems. Such feeders are usually 3-phase circuits. A total of 326 distribution substations are installed through the island. Standard primary distribution voltage level and number of distribution substation corresponding to each level of voltage used in PR are: 4.16kV (178), 7.2kV (NA), 8.32 kV (53) and 13.2kV (86).

4.4 Puerto Rico Case Study Scope and Description

4.4.1 Scope

The following items summarize the conditions and limitations of the study.

1. All 115 kV load busses were chosen as suitable locations for DG. These busses supply the 38 kV and subsequently the 13.2/4.16 kV systems (neglected on the system model.). Including the 38kV system on the actual model, would have increased the computational complexity by a factor of 4 (3760 x Time Step variables as oppose to 850xTime Strep variables neglecting the 38 kV and lower voltages.)
2. Each DG was connected to a step-up transformer with a voltage ratio of 11.4 kV to 115 kV.
3. Loads were modeled with standard polynomials corresponding to industrial customers.

4. Low inertia (see Appendix C) generators, typical for DG systems, were incorporated to the system.

The scope of the study was greatly influenced by items 1-4 above. The only modeling element not considered, see item 1, was the impedance between the 38kV system and the 115kV load busses. Such impedance, it is speculated, will not have a significant effect on results because grid tie operation was implemented in all case studies. Therefore, given the DG models used and the 115kV load busses DG locations (supplying all lower voltage busses) results from the study closest resemble the conditions for Distributed Generation as oppose to the conditions for Dispersed Generation [21].

4.4.2 Description

The electrical system of Puerto Rico was simulated considering all the buses at 115 kV and 230 kV. The network is composed of ninety-five (95) buses, eighty-nine (89) transmission lines, thirty-nine (39) transformer, twenty-nine (29) generators and fifty-four (54) loads. The complexity of the model is produced by the high order of state variables. Each generator and excitation system models consist of four (4) state variables while the governor has one (1) state variable. To improve the accuracy of results, each synchronous generator model includes a transformer, excitation system and governor. Overall, the electrical system of Puerto Rico is composed of two hundred sixty four (264) state variables for the base case. The simulations considered solely the transmission system.

In order to have a better appreciation of the buses location, Figure 16 shows the single line diagram of the electrical system of Puerto Rico. Buses at 115 kV are represented with a circle while the buses at 230 kV are represented by a line.

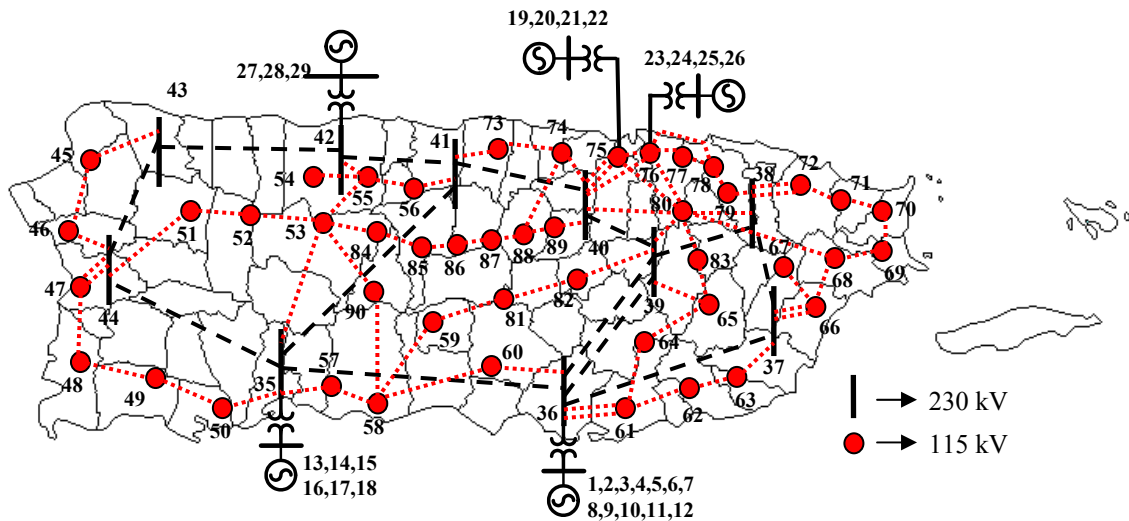


Figure 16: Electrical System of Puerto Rico

Due to homeland security regulations, implemented after September 11 2001, PREPA doesn't provide information about the electrical system. However, the PV data, PQ data and branches data were obtained from preview PREPA's publications [19] [22]. The parameters of the generators, excitation system and governor were estimated from similar generation units available elsewhere [16] [11]. Numeric values for all system parameters are shown in Appendix B.

In order to improve the accuracy of the results, the real power and the reactive power of the loads were obtained by an approximation of the power flow solution of the electrical system of Puerto Rico. The power flow data was obtained at a high peak period. Otherwise, branch data was obtained from PREPA's reports [22]. Each transmission line is represented by the same name that PREPA uses to identify its transmission lines. The transmission lines were represented by their series impedance. Based in the length of the transmission lines of the electrical system of Puerto Rico, the lines are considered as short lines, because the lengths are less than fifty (50) miles. Hence, the shunt capacitances are considered negligible [11]. The resistance (R) and reactance (X) are in ohm per miles (ohm/km). The R and X values were determined in accordance the real distance and cable used in each transmission lines.

5 Optimal Capacity of Distributed Generation

5.1 Introduction

The study is focused on developing computer algorithm to estimate the optimal capacity and location of distributed generation. Optimization is the technique which seeks a maximum or minimum value of a function of several variables subject to a set of constraints, as linear or nonlinear programming [23]. To make use of optimization techniques, it is important to firstly identify the objective function and control variables. The goal is to find the values of the control variables that optimize the objective function. The process to determine the objective function, control variables, and constraints is known as modeling. The power system is modeled by algebraic and differential equations represented in the following form.

$$0 = g(x, y, u) \quad (5.1)$$

$$\dot{x} = f(x, y, u) \quad (5.2)$$

Equation (5.2) was represented by \mathcal{H} , in order to consider it as an equality constraint:

$$\mathcal{H} = \dot{x} - f(x, y, u) = 0 \quad (5.3)$$

The study presents a methodology, based on nonlinear programming to estimate DG size and location to improve transient response during and after a disturbance. Similar methods have been presented elsewhere [24] [25] [26]. The idea of the Optimal Capacity of Distributed Generation algorithm (OCDG) is to minimize the objective function, subject to inequality and equality constraints. In order to satisfy a practical requirement, the inequality constraints define

the trajectory of the system. Equality constraints are represented by the algebraic equations and the discretization at each time step of the system's differential equations.

The integration method used is the trapezoidal method, which uses a complete Jacobian matrix to evaluate the algebraic and state variable direction at each time step, to estimate the dynamics of the system. The following equations represent the discretization of Equation (5.3):

$$H_k = x^{k+1} - x^k - 0.5\Delta t \left(f(x^{k+1}, y^{k+1}, u^{k+1}) + f(x^k, y^k, u^k) \right) \quad (5.4)$$

Equation (5.4) is nonlinear and its solution, together with Equation (5.1), represents a discretized dynamic trajectory of a power system.

5.2 OCDG Model

The objective function is given by:

$$C(x, y, u) = C_1(x) + C_2(y) + C_3(u) \quad (5.5)$$

Where

$$C_1(x) = (x - x^*)^T Q_x \Delta t (x - x^*) \quad (5.5a)$$

$$C_2(y) = (y - y^*)^T Q_y \Delta t (y - y^*) \quad (5.5b)$$

$$C_3(u) = (u)^T Q_u (u) \quad (5.5c)$$

The objective function consists of quadratic functions $C_1(x)$, $C_2(y)$ and $C_3(u)$ which represent costs related to the state, algebraic and control variables deviations from known stable values. The weight matrix (Q) determines the importance given to the variables in the objective function. The weights increase the cost of the objective function when the system trajectory deviates from the stable operating point. Since the overall objective is to minimize the cost

function, a new control variable will be generated to drive the system towards the known stable operating point. Therefore, each weight effectively guides the system trajectory according to its physical meaning. For example, higher values of Q_x will result in smaller deviations for state variables. Meanwhile, higher values of Q_u will result in less DG penetration. The time step (Δt) determines the accuracy of the time domain simulation required on each optimization iteration.

The optimization problem is:

$$\text{minimize } C(x, y, u)$$

subject to

$$H_k(x, y, u) = 0$$

$$g(x, y, u) = 0$$

In order to establish the necessary conditions for a possible solution, constrain functions are added to the objective function and multiplied by the Lagrange multiplier. The augmented goal function is given by:

$$L = C_1(x) + C_2(y) + C_3(u) + [H_k(x, y, u)]^T \lambda + [g(x, y, u)]^T \beta \quad (5.6)$$

The First Order Necessary Conditions (FONC) is the necessary condition for the objective function. These conditions take the first derivate of the augmented goal function with respect to each of the independent variable and set the derivates equal to zero.

$$\frac{\partial L}{\partial x} = \frac{\partial C_1}{\partial x} + \frac{\partial H_k^T}{\partial x} \lambda + \frac{\partial g^T}{\partial x} \beta = 0 \quad (5.7)$$

$$\frac{\partial L}{\partial y} = \frac{\partial C_2}{\partial y} + \frac{\partial H_k^T}{\partial y} \lambda + \frac{\partial g^T}{\partial y} \beta = 0 \quad (5.8)$$

$$\frac{\partial L}{\partial u} = \frac{\partial C_3}{\partial u} + \frac{\partial H_k^T}{\partial u} \lambda + \frac{\partial g^T}{\partial u} \beta = 0 \quad (5.9)$$

$$\frac{\partial L}{\partial \lambda} = H_k(x, y, u) = 0 \quad (5.10)$$

$$\frac{\partial L}{\partial \beta} = g(x, y, u) = 0 \quad (5.11)$$

Equations (5.7) and (5.8) were used to determine the values of the Lagrange multipliers (λ) and (β). Solving for λ and β is obtained:

$$\lambda = - \left[\left(\frac{\partial H^T}{\partial x} \right)^{-1} \left(\frac{\partial g^T}{\partial x} \right) \beta + \left(\frac{\partial H^T}{\partial x} \right)^{-1} \left(\frac{\partial C_1}{\partial x} \right) \right] \quad (5.12)$$

$$\beta = - \left[\left(\frac{\partial g^T}{\partial y} \right)^{-1} \left(\frac{\partial H^T}{\partial y} \right) \lambda + \left(\frac{\partial g^T}{\partial y} \right)^{-1} \left(\frac{\partial C_2}{\partial y} \right) \right] \quad (5.13)$$

Substituting the Equation (5.12) into Equation (5.13), the value of β is obtained by:

$$\beta = \left[\left(\frac{\partial H^T}{\partial y} \right) \left(\frac{\partial H^T}{\partial x} \right)^{-1} \left(\frac{\partial C_1}{\partial x} \right) - \frac{\partial C_2}{\partial y} \right] \cdot \left[\frac{\partial g}{\partial y} - \left(\frac{\partial H^T}{\partial y} \right) \left(\frac{\partial H^T}{\partial x} \right)^{-1} \left(\frac{\partial g^T}{\partial x} \right) \right]^{-1} \quad (5.14)$$

Then, the value of β was substituted in the Equation (5.12) in order to determine the values of λ . Once the values of λ and β are determined, Equation (5.9) can be solved. However,

the values of λ and β can be obtained by an alternate solution. Solving the Equation (5.7) and (5.8) the following results are obtained:

$$\frac{\partial H_k^T}{\partial x} \lambda + \frac{\partial g^T}{\partial x} \beta = -\frac{\partial C_1}{\partial x} \quad (5.15)$$

$$\frac{\partial H_k^T}{\partial y} \lambda + \frac{\partial g^T}{\partial y} \beta = -\frac{\partial C_2}{\partial y} \quad (5.16)$$

Solving Equations (5.15) and (5.16) through matrices yields the values of λ and β .

$$\begin{bmatrix} \lambda \\ \beta \end{bmatrix} = - \begin{bmatrix} \frac{\partial H_k^T}{\partial x} & \frac{\partial g^T}{\partial x} \\ \frac{\partial H_k^T}{\partial y} & \frac{\partial g^T}{\partial y} \end{bmatrix}^{-1} \begin{bmatrix} \frac{\partial C_1}{\partial x} \\ \frac{\partial C_2}{\partial y} \end{bmatrix} \quad (5.17)$$

The values of λ and β are substituted into Equation (5.9) in order to determine the change in the control variable (u). If the change is less than a tolerance value (ϵ) the algorithm reached the optimal condition.

$$u^{k+1} = u^k + \alpha \frac{\partial L}{\partial u} \quad (5.18)$$

Otherwise, the control variable is modified and a new iteration would once again begin by initializing the system. In order to obtain a faster convergence the control multiplier (α) is applied. The best value of α must be determined empirically [23].

Figure 17 shows a flowchart of the OCDG optimization process. The goal of the algorithm is to determine the value of (u) that minimizes the objective function (Equation (5.5)).

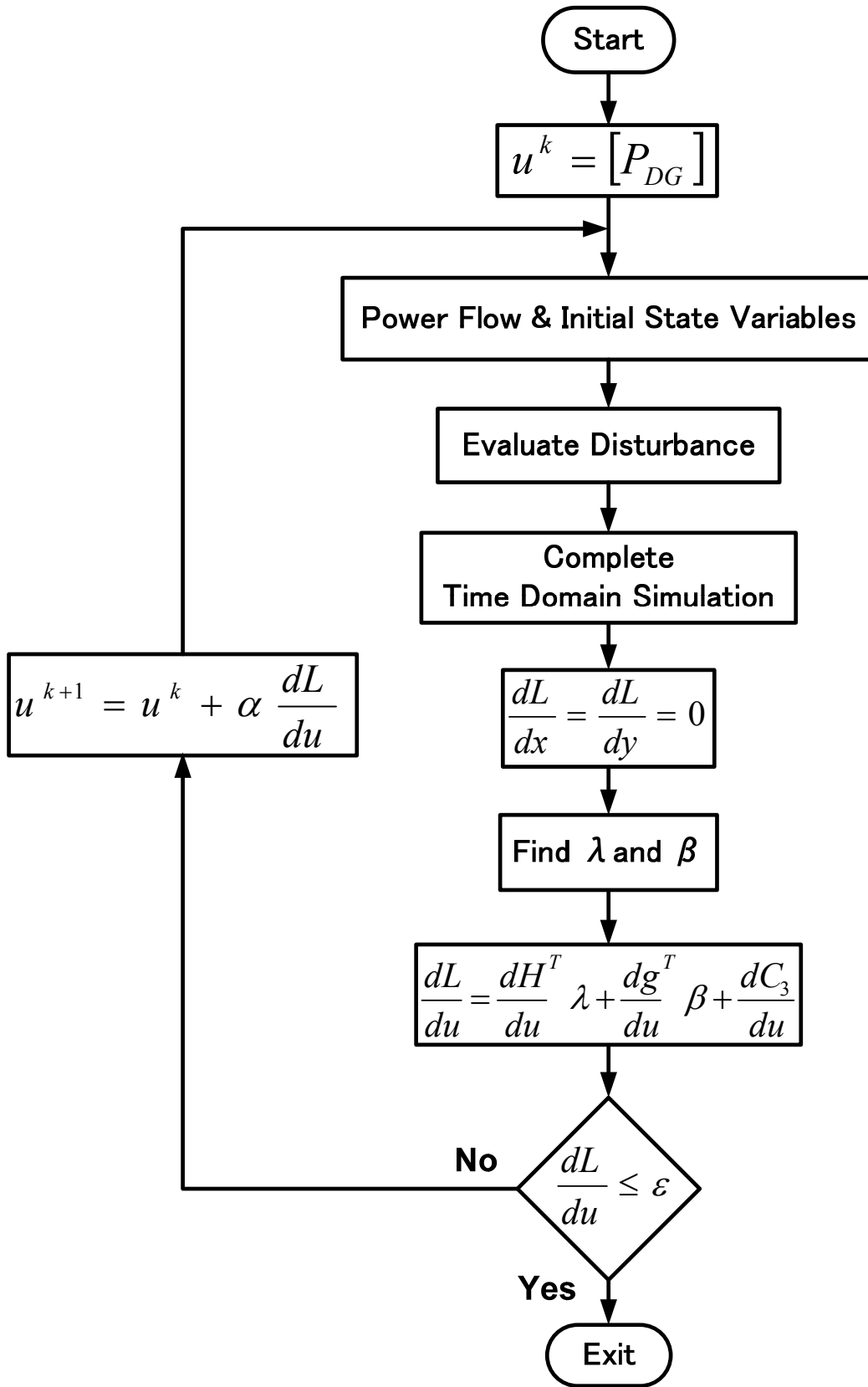


Figure 17: OCDG Flowchart

The control variable is part of the governor's algebraic and differential equations. To initiate the algorithm it is necessary to input the values of the control variable u^k which represents the real power output of the DG (P_{DG}), in per unit. The algorithm computes the power flow solution and initializes the algebraic and state variables $[x_0 \ y_0]$. Then, the algorithm evaluates the disturbance in order to determine the dynamic response of the power system, completing the time domain simulation. The Reduce Gradient Method, used to solve the nonlinear programming problem, calls for the sequential calculation of the increment Δu in order to update the actual value of the control variable (u).

This method reaches the minimum of the objective function by a series of steps taking a (steepest) downward direction. From any initial point, Equation (5.18) finds the direction of steepest decent to the local optimal value. The method only considers the first derivate without computing Hessian matrices of second derivatives, which would increase significantly the algorithmic complexity and computational burden.

Different techniques to solve the linear system represented by equation (5.12), (5.13) or (5.17) were discussed previously in the chapter. The length of λ depends on the number of state variables times the number of time steps ($N_x * N_T$). The length of β is given by the number of algebraic variables times the number of time steps ($N_y * N_T$). The trapezoidal rule technique is applied to Equation (5.4) producing an off-diagonal matrix, per time step, corresponding to the derivate with respect to the $(k + 1)$ term. The derivate with respect to the (k^{th}) term, produces a diagonal matrix per time step. Equations (5.19) and (5.20) show the derivatives with respect to present and future terms.

$$\frac{\partial H_k}{\partial x^k} = -I - 0.5\Delta t \frac{\partial f(x^k, y^k, u^k)}{\partial x^k} \quad (5.19)$$

$$\frac{\partial H_k}{\partial x^{k+1}} = I - 0.5\Delta t \frac{\partial f(x^{k+1}, y^{k+1}, u^{k+1})}{\partial x^{k+1}} \quad (5.20)$$

Each equation represents a matrix. The resultant matrix of Equation (5.4) is square. The matrix size depends of the number of state variables and the number of time steps ($N_x * N_T$). Equation (5.21) shows the general structure of Equations (5.19) and (5.20).

$$\frac{\partial H_k}{\partial x} = \begin{bmatrix} \frac{\partial H_1}{\partial x_1} & \frac{\partial H_1}{\partial x_2} & 0 & \dots & 0 \\ 0 & \frac{\partial H_2}{\partial x_2} & \frac{\partial H_2}{\partial x_3} & 0 & 0 \\ 0 & 0 & \ddots & \ddots & 0 \\ \vdots & \vdots & 0 & \frac{\partial H_{n-1}}{\partial x_{n-1}} & \frac{\partial H_{n-1}}{\partial x_n} \\ 0 & 0 & 0 & 0 & \frac{\partial H_n}{\partial x_n} \end{bmatrix} \quad (5.21)$$

Partial derivative of the Equation (5.4) with respect to y is similar to the previous case. However, the resultant matrix is not square. The number of rows depends on the number of state variables and the number of time step ($N_x * N_T$). The number of columns depends on the number of algebraic variables and the number of time step ($N_y * N_T$).

$$\frac{\partial H_k}{\partial y^k} = -0.5\Delta t \frac{\partial f(x^k, y^k, u^k)}{\partial y^k} \quad (5.22)$$

$$\frac{\partial H_k}{\partial y^{k+1}} = -0.5\Delta t \frac{\partial f(x^{k+1}, y^{k+1}, u^{k+1})}{\partial y^{k+1}} \quad (5.23)$$

Equation (5.24) shows the general structure of Equations (5.22) and (5.23).

$$\frac{\partial H}{\partial y} = \begin{bmatrix} \frac{\partial H_1}{\partial y_1} & \frac{\partial H_1}{\partial y_2} & 0 & \dots & 0 \\ 0 & \frac{\partial H_2}{\partial y_2} & \frac{\partial H_2}{\partial y_3} & 0 & 0 \\ 0 & 0 & \ddots & \ddots & 0 \\ \vdots & \vdots & 0 & \frac{\partial H_{n-1}}{\partial y_{n-1}} & \frac{\partial H_{n-1}}{\partial y_n} \\ 0 & 0 & 0 & 0 & \frac{\partial H_n}{\partial y_n} \end{bmatrix} \quad (5.24)$$

The partial derivative with respect the Equation (5.1) required less computation than the previous cases, because for algebraic equations it is not necessary to difference between a present and future term [24]. Equation (5.25) shows the matrix array from the partial derivative of the Equation (5.1) respect to x (state variables).

$$\frac{\partial g}{\partial x} = \begin{bmatrix} \frac{\partial g_1}{\partial x_1} & 0 & \dots & 0 \\ 0 & \frac{\partial g_2}{\partial x_2} & 0 & \vdots \\ \vdots & 0 & \ddots & 0 \\ 0 & \dots & 0 & \frac{\partial g_n}{\partial x_n} \end{bmatrix} \quad (5.25)$$

Each element in the diagonal represents a matrix. The resultant matrix is not square. The number of rows depends on the number of algebraic variables times the number of time steps ($N_y * N_T$). The number of columns depends on the number of state variables and time steps ($N_x * N_T$).

Partial derivative of Equation (5.1) with respect to y is similar to the previous case, but the resultant matrix is square. Equation (5.26) shows the matrix array for the partial derivative of Equation (5.1) respect to y . The size of the matrix depends on the number of algebraic equations and the number of time steps ($N_y * N_T$).

$$\frac{\partial g}{\partial y} = \begin{bmatrix} \frac{\partial g_1}{\partial y_1} & 0 & \dots & 0 \\ 0 & \frac{\partial g_2}{\partial y_2} & 0 & \vdots \\ \vdots & 0 & \ddots & 0 \\ 0 & \dots & 0 & \frac{\partial g_n}{\partial y_n} \end{bmatrix} \quad (5.26)$$

The time domain simulations and power flow solutions required by the OCDG algorithm were implemented on Power System Analysis Toolbox (PSAT) a Matlab[®] Toolbox. PSAT permits access to its equations and subroutines. This toolbox is used around the world to perform stability studies [15]

6 Results and Analysis

The IEEE 14 Bus Test System and the Electrical System of Puerto Rico were used as case studies. Electrical systems were modeled for different disturbances through dynamic simulation, in order to obtain the optimal size and location to implement distributed generation and to improve the stability response of the electrical system. During a disturbance, system voltage drops and synchronous machines begin to accelerate, as result of an imbalance between the electrical power and mechanical power. The OCDG algorithm determines the optimal active power of each DG in order to reduce the oscillation of the synchronous machines. The physical interpretation is that the DG machines have low values of inertia, while the central generation has higher values of inertia. When a disturbance occurs, the response of DG is faster than central generation. Thus, DG helps to reduce the imbalance of the synchronous generator with large capacity. The overall goal of the OCDG algorithm is to minimize voltage oscillations and acceleration (or deceleration) of synchronous machines following a severe disturbance, thus improving the stability of the electrical system.

Several cases have been studied. The base case was simulated without DG. Then, DGs were connected to the network with a real power value equal to zero MW ($P_{DG} = 0$ MW). The OCDG algorithm determines the real power of each DG in order to obtain the optimal condition during and after the disturbance. In order to appreciate the dynamic response of the electrical system the results of the simulations are represented by several plots. The time domain simulation has time duration of 10 seconds. Additionally, contour plots in two dimensions are used to illustrate the convergence of the OCDG algorithm, in order to show the decent trajectory to reach an optimal value.

6.1 IEEE 14-Bus Test System

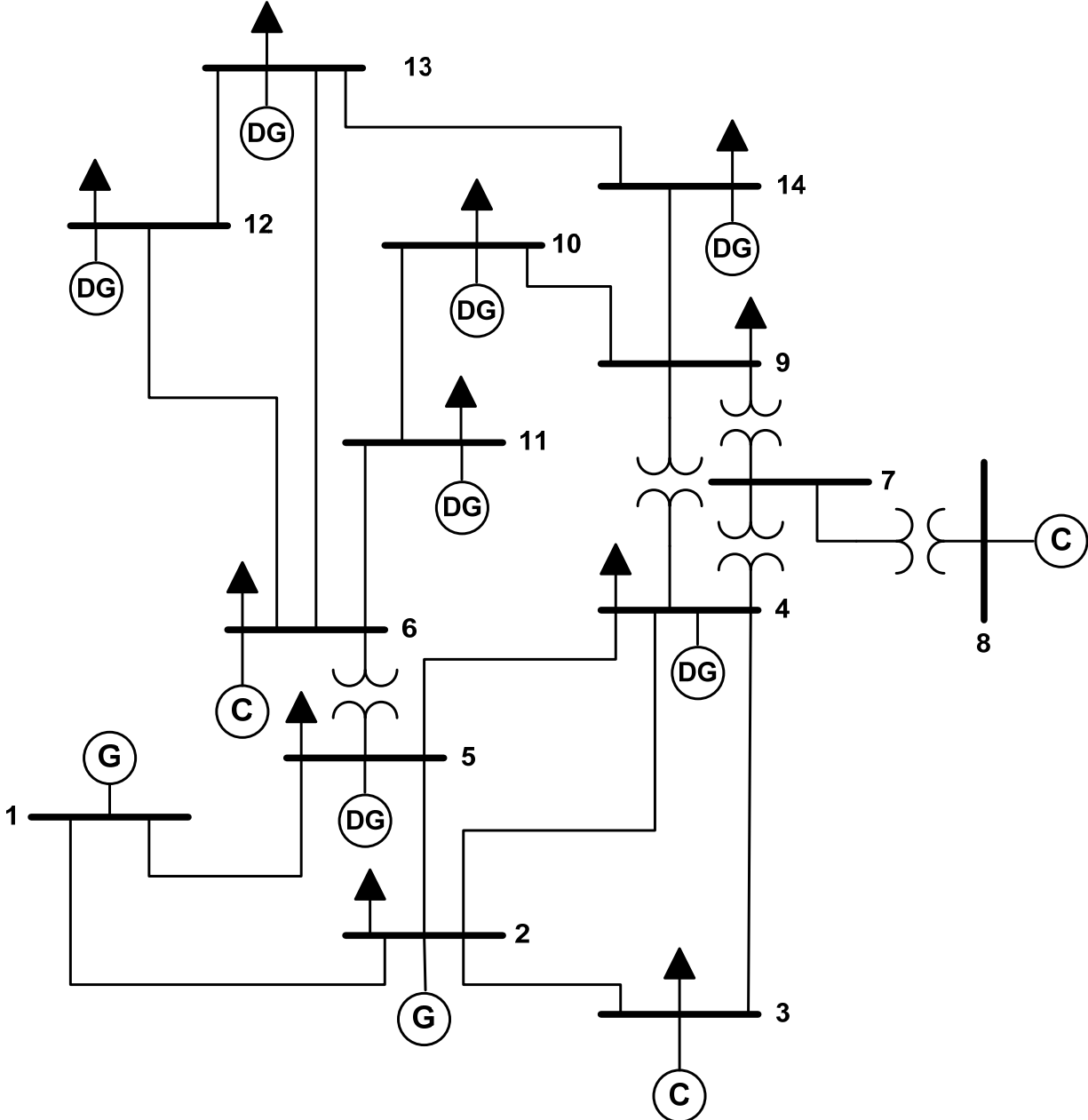


Figure 18: IEEE 14-Bus Test System with Distributed Generation

The IEEE 14-Bus test system is used to validate the convergence characteristics of the OCDG algorithm. This system is simple enough to easily interpret all results while at the same time it is complex enough show the robustness and ability of the algorithm to handle larger

systems. System parameters are shown in appendix A [15]. Seven (7) synchronous DGs were incorporated to the test system as seen in the single line diagram shown in Figure 18. The power rating and terminal voltage of each DG is 7 MVA and 4.16 kV, respectively. Each DG is connected to a transformer. Appendix C shows the DG parameters. All the DGs, synchronous generator and synchronous condenser, were modeled with 4th order dynamic models. Additionally, each synchronous generators and DGs has an excitation and governor system.

6.1.1 Case 1: Synchronous DG Connected at Bus 4 (One Dimension)

A three phase fault was applied to the electrical system at bus 5 (see Figure 18). The disturbance produced rotor speed and bus voltages oscillations. In order to appreciate the convergence characteristics of the OCDG algorithm, only one (1) DG was connected at bus 4. Thus, the system is simplified into a single dimensional problem. The objective function considered frequency and voltage deviations.

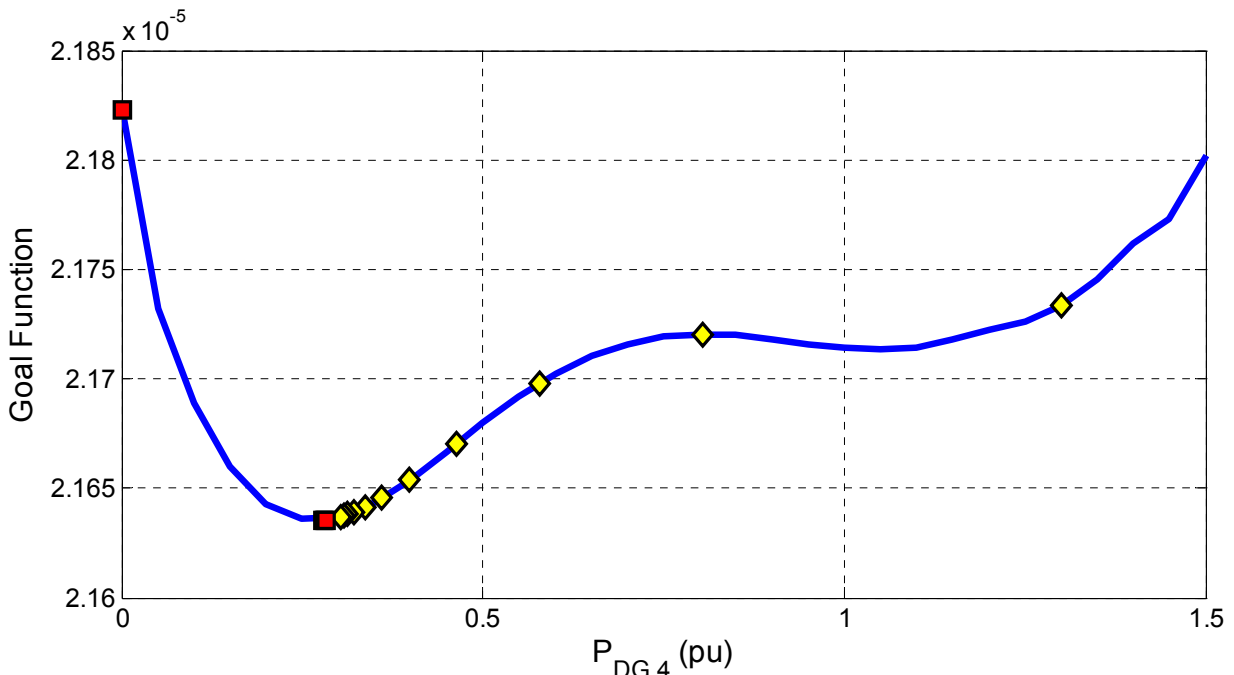


Figure 19: Optimal Penetration of P_{DG4} Goal Function Curve

Figure 19 shows the convergence of the OCDG algorithm for two different initial points, $P_{DG} = 0$ and $P_{DG} = 1.3$ pu. In both cases, the OCDG algorithm iterated its way to the same optimal power output. The optimal value of P_{DG} is 0.25 in per unit (Pu), which represents a power output of 1.75 MW. It is important to emphasize that the step size (alpha) was large enough to avoid the shallow local minima near $PDG = 1.1$ pu.

6.1.2 Case 2: Synchronous DG Connected at Buses 4 and 5 (Two Dimensions)

The second case is similar to the previous one, this time two (2) DGs are connected at buses 4 and 5. Two dimension contours plots are used to appreciate the convergence. The goal function varies with frequency and voltage deviations.

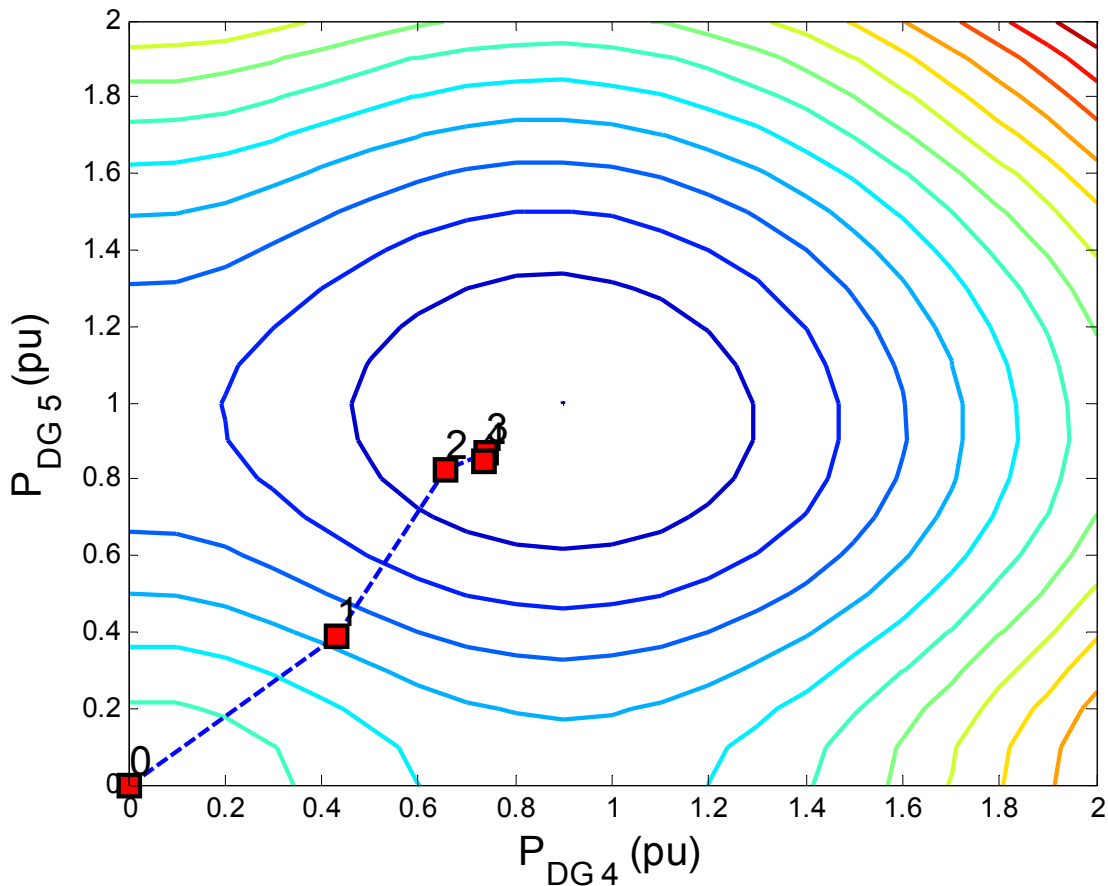


Figure 20: Optimal Penetration of P_{DG4} and P_{DG5} , Two Dimension Contour Plot

Contour lines are a set of points where the objective function has a constant value for different values of P_{DG4} and P_{DG5} . The contour plot shows the feasible region, which is a set of points that satisfy all the constraints. In a three dimensional appreciation, the contour plots have the shape of a bowl formed by the contour lines. The convergence moves from the high to the deep point of the bowl, which represents the minimum value. The numbers along the curve show the iterations needed to reach the optimal solution.

Initially, real power of P_{DG4} and P_{DG5} were equal to zero (0) MW. At that point, the gradient is computed making a straight line descent to reach the optimal solution. The length and direction of each step is in accordance with the value of the control multiplier and the iteration value. It is necessary to determine the correct value of the multiplier to reach the optimal solution. The first iteration was distant from the optimal value producing a big step, followed by shorter steps because the iterations are closer to the optimal solution. In order to reduce the voltage and frequency oscillations, the power output needed of P_{DG4} and P_{DG5} should be 0.77 Pu (5.4 MW) and 0.83 Pu (5.81 MW), respectively.

6.1.3 Rotor Speed and Voltage Response

Initially, the electrical system is stable, and then a three phase fault is applied at bus 5, producing rotor speed and bus voltages oscillations. The stability improvement produced by the two previous cases was insignificant. Hence, if a small amount of DG is connected to the electrical system, the impact in the stability could be negligible. However, increased DG penetration influences the stability response.

This case studied the effects produced in the electrical system by DG penetration. The DG penetration was calculated by the following equation, where P_{DG} and P_{CG} are the total power produced by DG and CG, respectively.

$$\%DG_{\text{penetration}} = \frac{P_{\text{DG}}}{P_{\text{DG}} + P_{\text{CG}}} * 100 \quad (6.1)$$

The P_{CG} of the system is 146 MVA and the capacity of each DG is 7 MVA. In order to determine the stability response one (1), two (2) and seven (7) DGs were connected to the network where the DG penetration is 4.58%, 8.75% and 25.13%, respectively. Figure 21 shows the rotor speed response of the synchronous generators ($\omega_{\text{syn } 1}$ and $\omega_{\text{syn } 2}$) and synchronous condenser ($\omega_{\text{syn } 3}$, $\omega_{\text{syn } 4}$ and $\omega_{\text{syn } 5}$) for the three cases mentioned. Figure 18 shows the location of the synchronous generator and synchronous condenser.

Initially, the rotor speed is constant which indicated the stability of the system. After one (1) second a three fault was applied at bus 5, producing an imbalance between the mechanical power and electrical power. The disturbance caused great oscillations in synchronous condenser. The oscillations of the other synchronous generators were moderated. Finally, the electrical system continued oscillating, but the oscillation decayed rapidly.

The OCDG algorithm determined the optimal DG penetration for each case, in order to reduce the rotor speed and voltage oscillation. Figure 21 shows the rotor speed response to determine the effect produced by the DG penetration in the stability of the system.

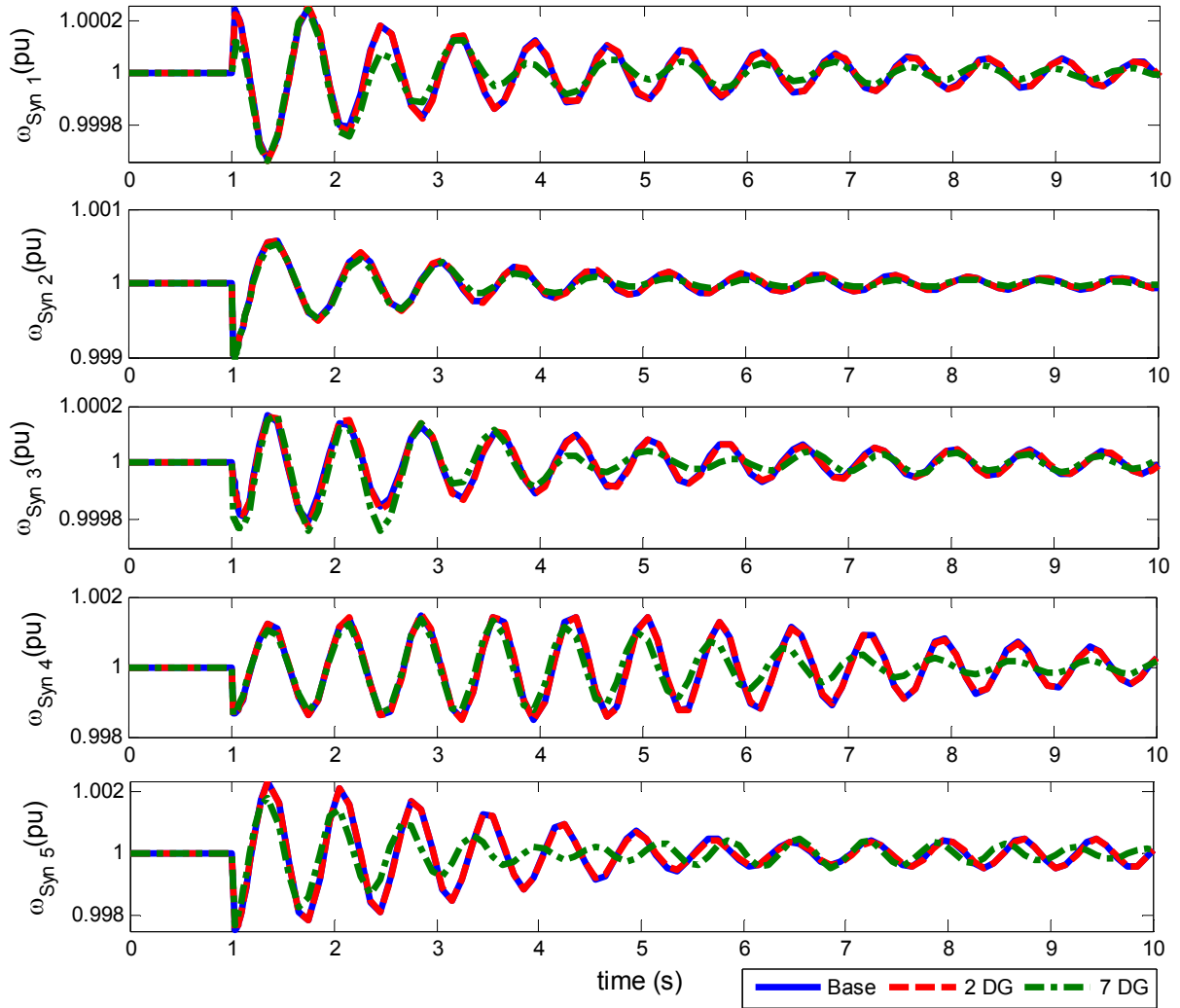


Figure 21: Rotor Speed Response – IEEE 14-Bus Test System

Figure 21 shows negligible effects in response of 4.58% and 8.75% DG increase. However, with 25.13% DG penetration showed an improvement in the rotor speed stability response. As expected, increased DG penetration led to increased system stability. Oscillations were lower, especially in the rotor speed of the synchronous condenser number five ($\omega_{syn 5}$). Increased DG penetration reduced the acceleration of the synchronous generators and synchronous condenser during and after the disturbance. A similar behavior occurred in bus voltages.

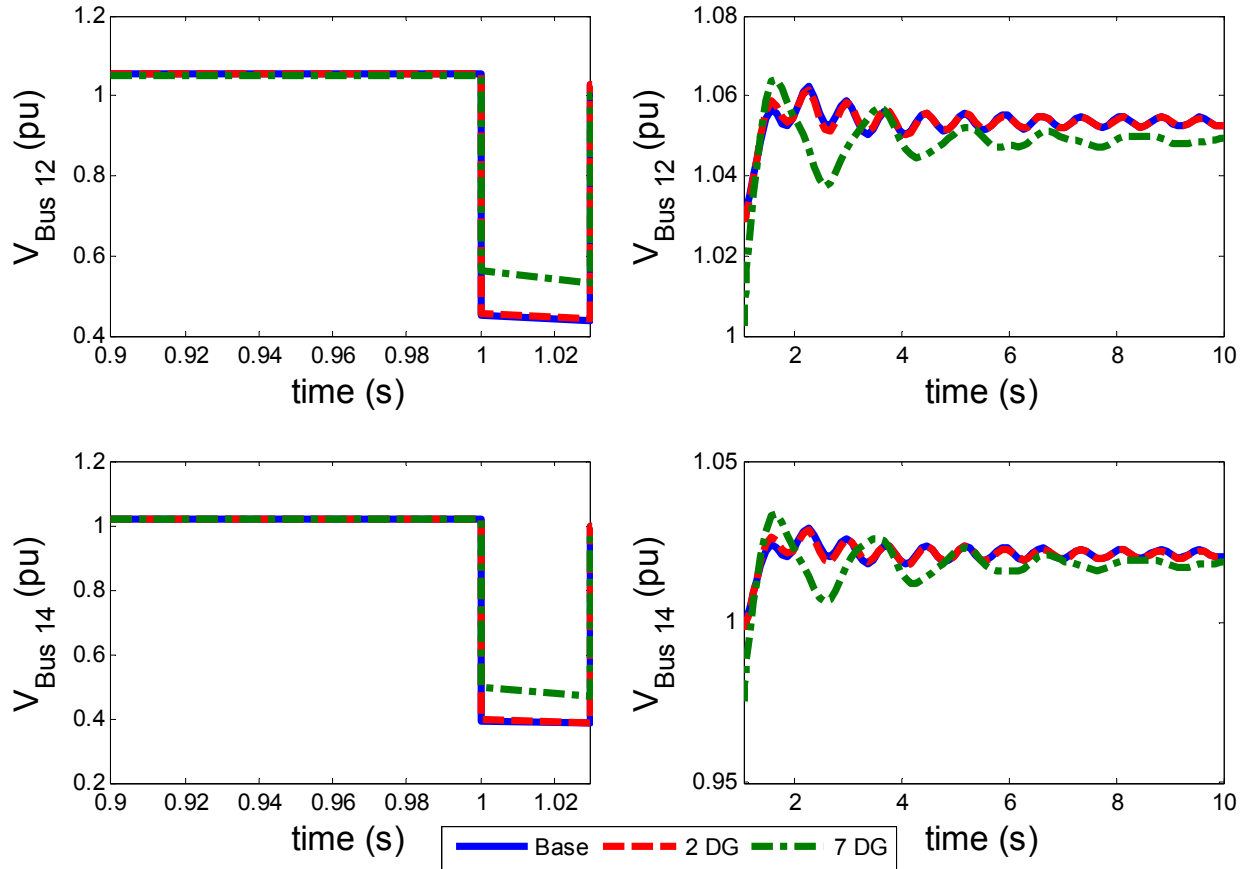


Figure 22: Voltage Response – IEEE 14-Bus Test System

Figure 22 shows the voltage response of bus 12 and 14. Initially, from 0.9s to 1s bus voltages are stable. Then a disturbance (1.0s to 1.03s) produced voltages drop, which limit the capacity of the network to transfer power between buses. The voltage drop and the oscillations were smaller under on increased DG penetration conditions (1.03s to 10s). The case with 25.3% of DG penetration produced an increased damping of voltage oscillation and a new equilibrium was obtained faster than the other cases. The post fault voltage responses were closer to the initial condition with 25.3% of DG penetration in comparison with the others cases. Additionally, voltage drops during the fault were lowers when 25.3% were connected. The base case showed a voltage drop of 0.6 Pu at bus voltage 14, while the case with seven (7) DGs

produced a voltage drop of 0.54 Pu. The DG penetration improved and maintained an acceptable equilibrium, after being subjected to a physical disturbance.

6.1.4 Critical Disturbance

In this section, transient stability was measured as a function of the Critical Clear Time (the allowable fault duration to avoid system collapse). The critical disturbance was implemented with a three phase fault at bus 2 and subsequently cleared opening breakers. The fault persisted long enough until rotor speed increased continuously and synchronism was lost. Seven (7) DGs were connected at the network to improve the stability of the system.

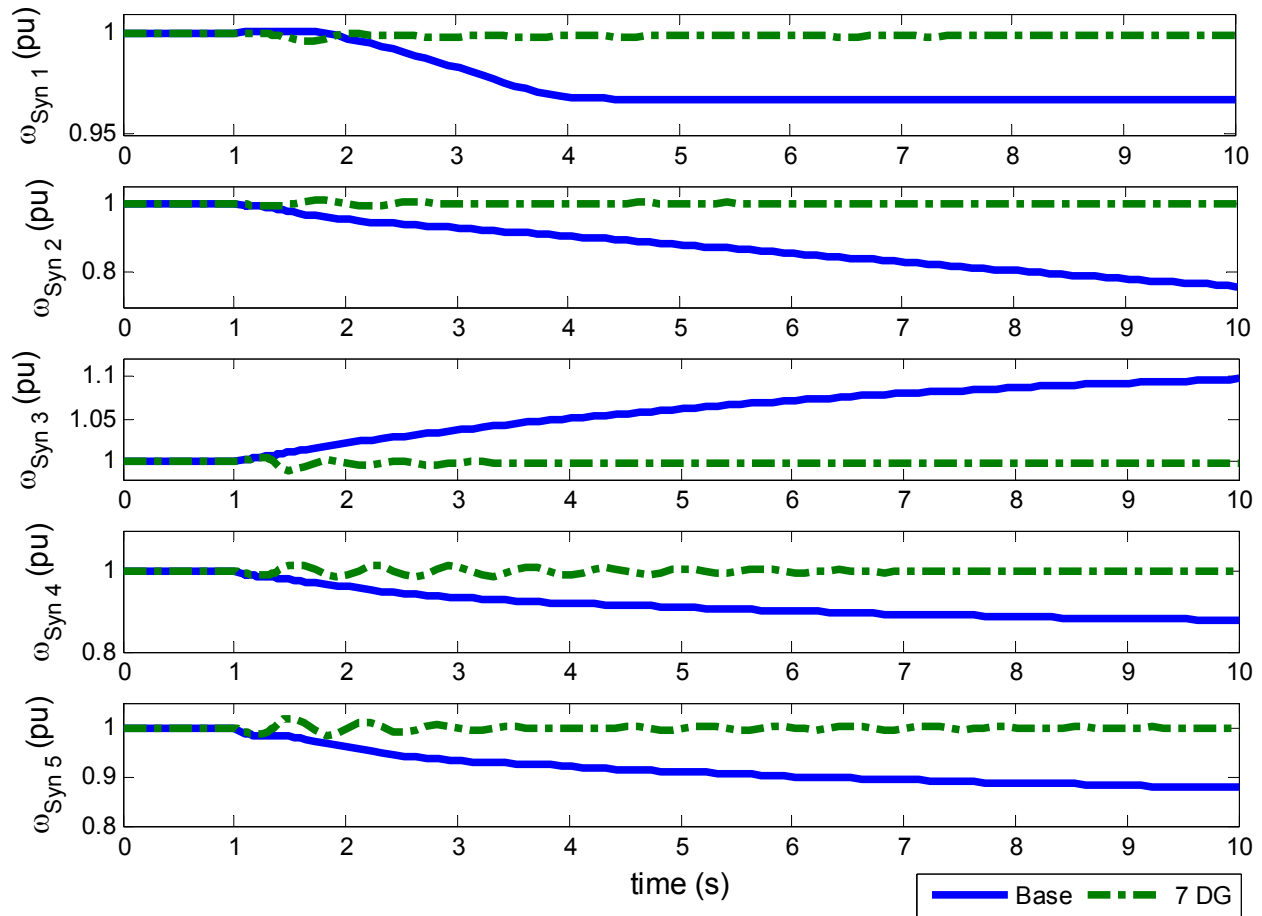


Figure 23: Rotor Speed Response - Unstable and Stable Cases

Figure 23 show the rotor speed response for the base case and the case with seven (7) DGs connected. The base case shows the unstable case where the system did not return to synchronism. However, DG penetration improved the transient stability and returned the electrical system to a stable steady state condition. Machine dynamics were greatly influenced by their inertia. DG rotors were accelerated or decelerated faster than the centralized generators, reducing the absorption of energy during the disturbance by the CG. Thus, DGs reduced the separation between the angular positions of the synchronous machines when a disturbance occurred. An increase in angular separation was matched by a decrease in power transfer and increased instability. Additionally, DGs improved voltage stability during and after a disturbance

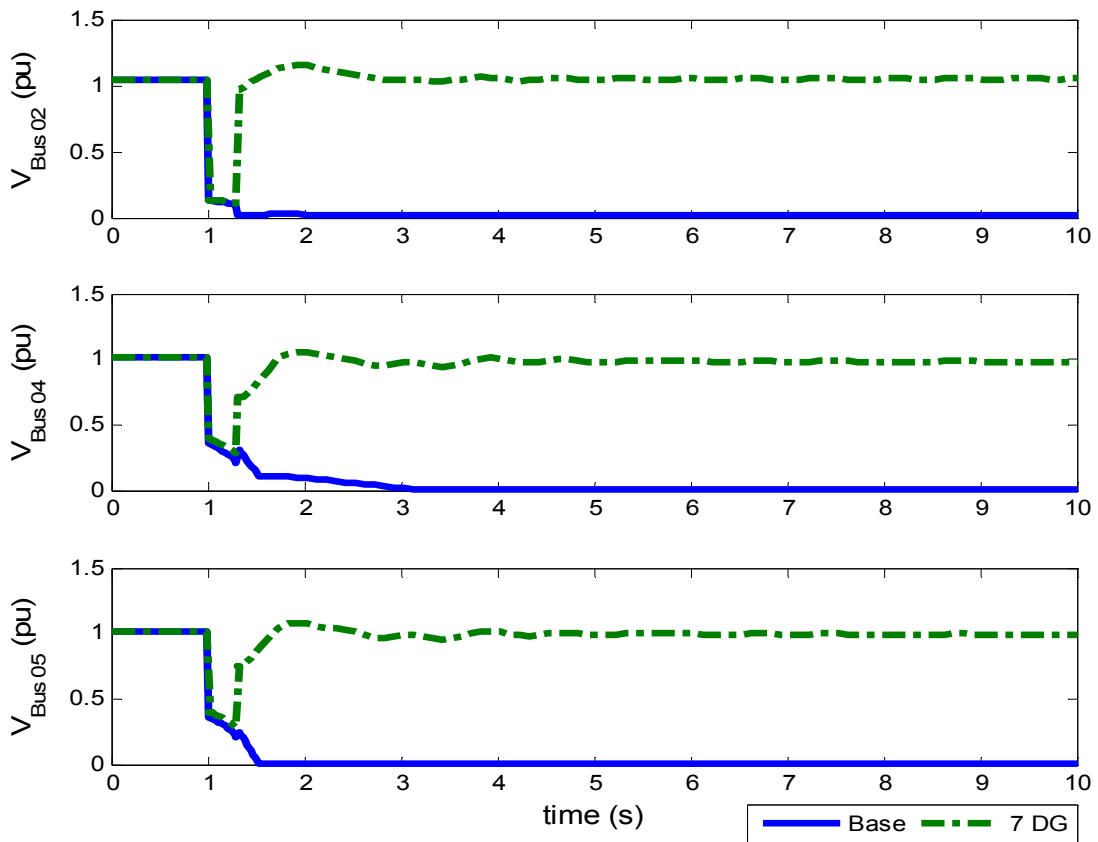


Figure 24: Bus Voltage – Unstable and Stable Cases

Figure 24 shows voltage stability response for the base case and 25.3% DG penetration. The base case shows the unstable case, which the load tried to restore power consumption beyond the capability of the transmission system and the connected generation. The voltage drops limits the capacity of the networks to transfer power between buses. In contrast, the case with 25.3% DG penetration shows the stable case. The DGs reduced the voltage drop during the disturbance and returned the electrical system to a stable steady state condition, avoiding a collapse of the electrical system. Therefore, increased DG penetration significantly improved transient stability of the system.

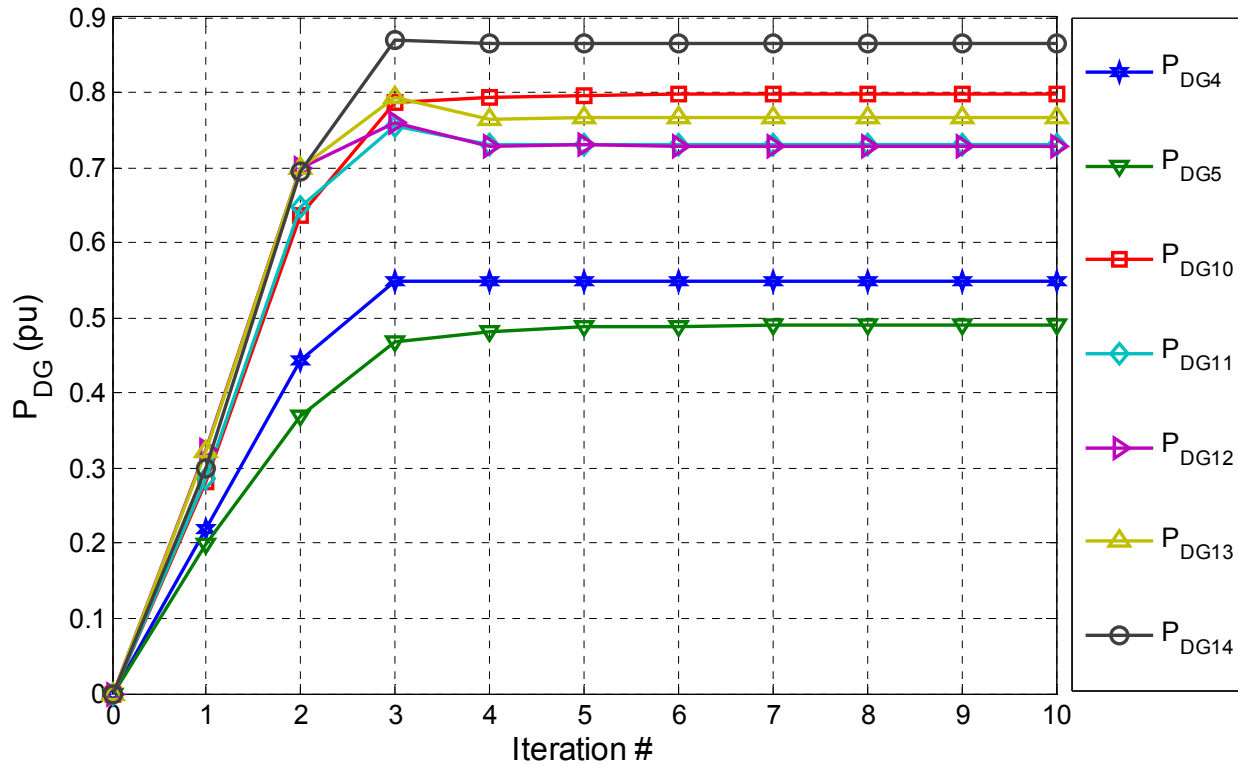


Figure 25: Optimal Penetration of Distributed Generation

Figure 25 shows the optimal real power and location of each DG in order to maximize system stability. The OCDG algorithm determined the optimal DG penetration in three (3) iterations. After the 3rd iteration, the real power remained constant indicating the OCDG

algorithm reached on optimal solution. The result showed that the main DG penetrations occurred at 13.8 kV buses. P_{DG} values are shown in per unit on a 7MVA base. The capacities of the DGs were 3.85 MW, 3.7 MW, 5.6 MW, 5.04 MW, 5.04 MW, 5.25 MW and 6.16 MW which were connected at buses 4, 5, 10, 11, 12, 13 and 14, respectively. The OCDG algorithm determined the optimal DG location and capacity.

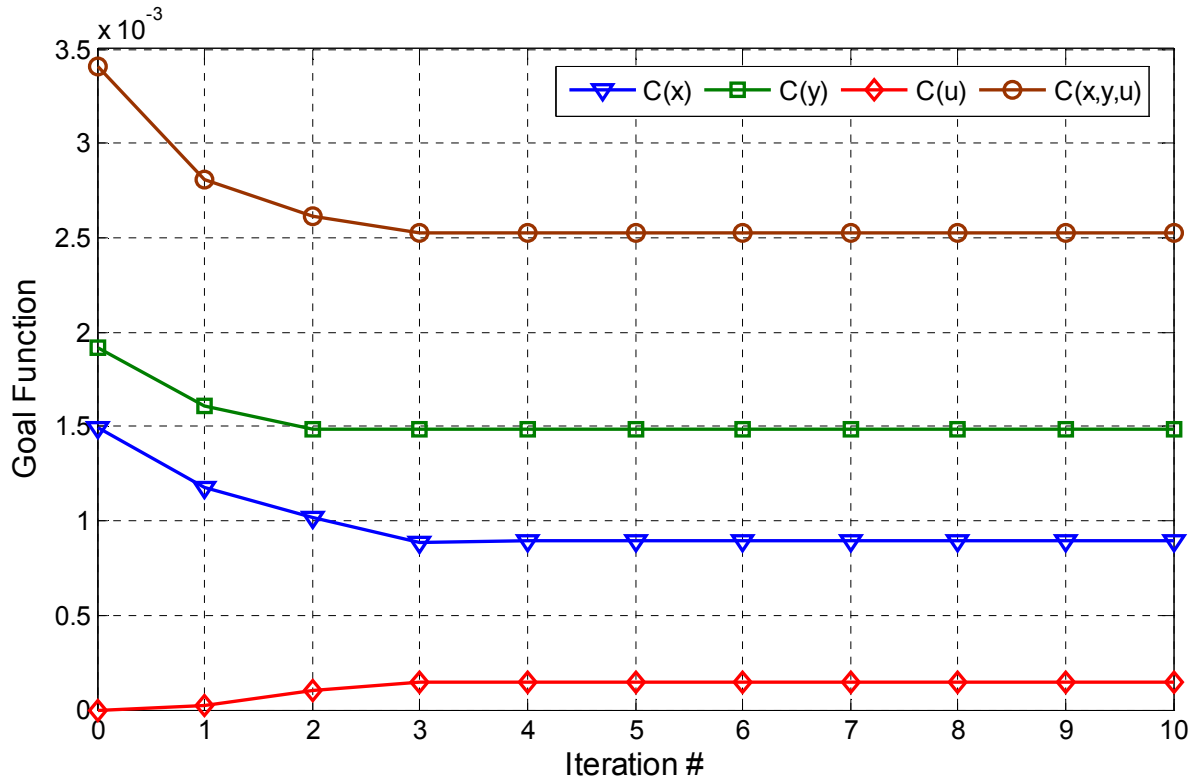


Figure 26: Goal Function

Figure 26 shows the performance of the OCDG algorithm as a function of the iteration number. The goal function $C(x,y,u)$ consist of quadratic functions $C(x)$, $C(y)$ and $C(u)$ represent the costs related to rotor speed, bus voltage and P_{DG} of after ten (10) iterations. Only, three (3) iterations were necessary to reach the optimal value. Lower value of the goal function means less rotor speed and voltage oscillation. The OCDG algorithm reduced the goal function value in order to improve stability of the electrical system.

6.1.5 Critical Clearing Time (CCT)

The critical clearing time is the maximum permissible fault duration before the generators lose the ability to regain stability in the electrical system. The DG penetration increased the critical clearing time helping the electrical system to maintain a stable operation. Figure 27 shows the critical clearing time for a DG penetration of 0%, 4.58%, 8.75% and 25.13%.

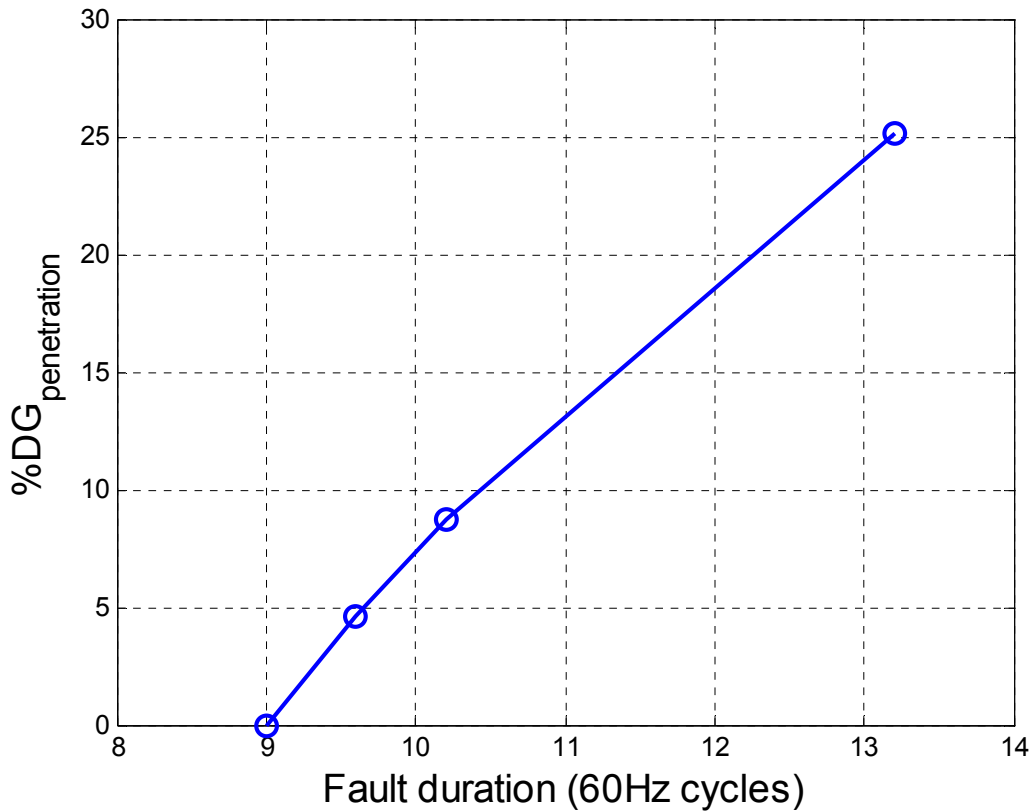


Figure 27: Critical Clearing Time

The case with 0% of DG penetration has a CCT of 9 cycles (0.15 sec). The cases with a DG penetration of 4.58% and 8.75% did not produce a significant improvement over the CCT. However, the case with a DG penetration of 25.13% increased the CCT to 13 cycles (0.22 sec). DG penetration increased the fault duration, thus improved the stability and reliability of the electrical system.

6.1.6 Goal Function Weights

The weight matrix determines the importance weight given to the variables in the objective function according to the desired physical means. The objective function consists of quadratic functions C_1 , C_2 and C_3 which represent the cost related to rotor speed, bus voltage and the DG penetration, respectively.

An experiment was conducted to study the effect of the weight matrix in the objective function. Starting from an initial optimal solution (a_0 , b_0 and c_0), one (1) weight value was shifted to determine the displacement on the objective function. The following equations show the assumptions were made, where the factor a , b and c were shifted individually.

- $Q_x = Q_y = Q_u = I$
- $cost = aC_1 + bC_2 + cC_3$
- $a_0 = 10 \quad 10 \leq a \leq 50$
- $b_0 = 0 \quad 0 \leq b \leq 0.05$
- $c_0 = 0 \quad 0 \leq c \leq 0.005$

Figure 28 shows the effects of shifting weights on the solution of the OCDG algorithm. The shift in trajectory for $a > a_0$, represents a higher importance to the frequency performance (less deviation). Increase DG penetration reduced the imbalance between the mechanical and electric powers. The DG response is faster than centralized generation, when a disturbance occurs. Hence, DG absorbs energy during the disturbance, thus reduces the acceleration on the synchronous generator.

For the voltage deviations, $b > b_0$, represents a higher importance of the voltage performance over the others. This is equivalent to increase the DG penetration, in order to increase the capacity of the networks to transfer power between buses when a disturbance

occurs. DG penetration helps to reduce the voltage drop during a disturbance and reduce the oscillation post-disturbance.

The last optimal trajectory, determines the amount of DG penetration. When $c > c_0$, DG penetration is reduced. It continues in this way until the optimal amount of P_{DG} is zero.

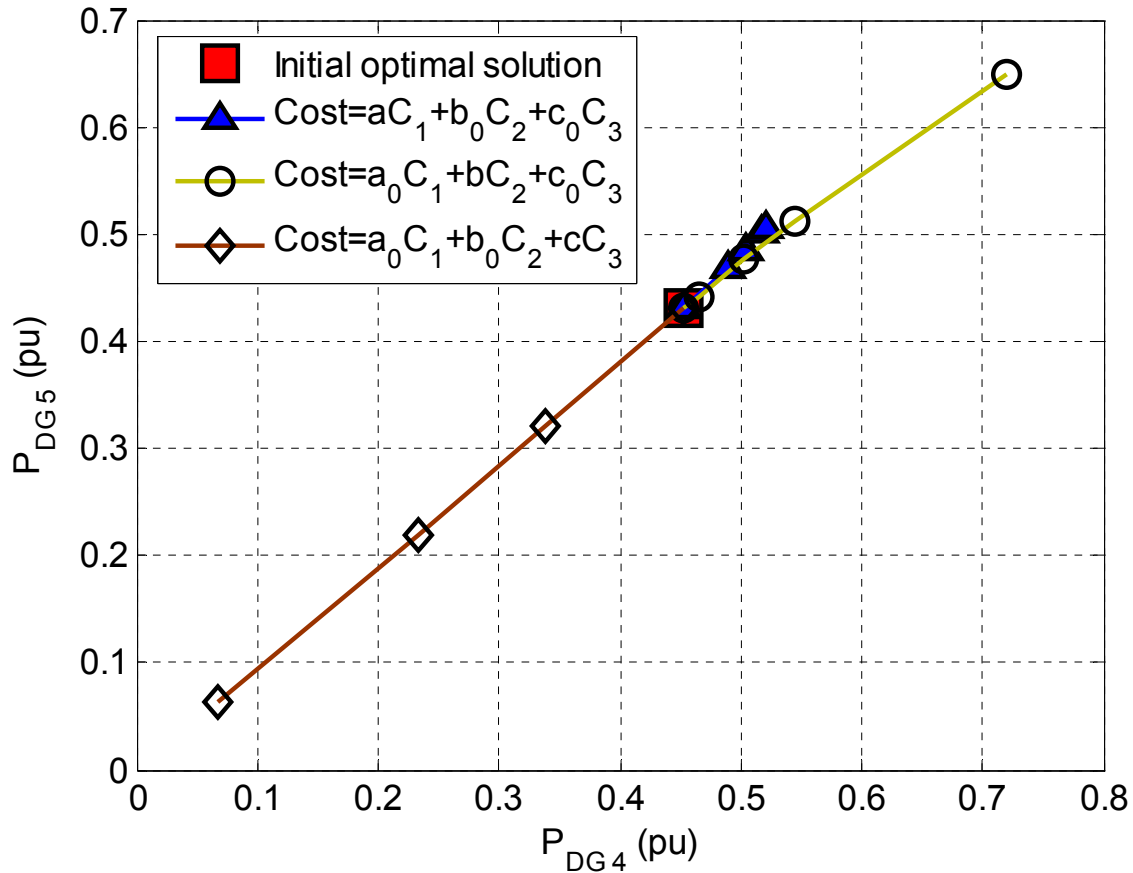


Figure 28: Goal Function Weights

6.1.7 Step Size

The control multiplier (α) is applied to obtain a faster convergence. The OCDG algorithm is based on a gradient search method, and the control multiplier is used to accelerate the convergence. Usually, the control multiplier value is determined by experiment. Figure 29 shows the effect of step size on the convergence of the algorithm.

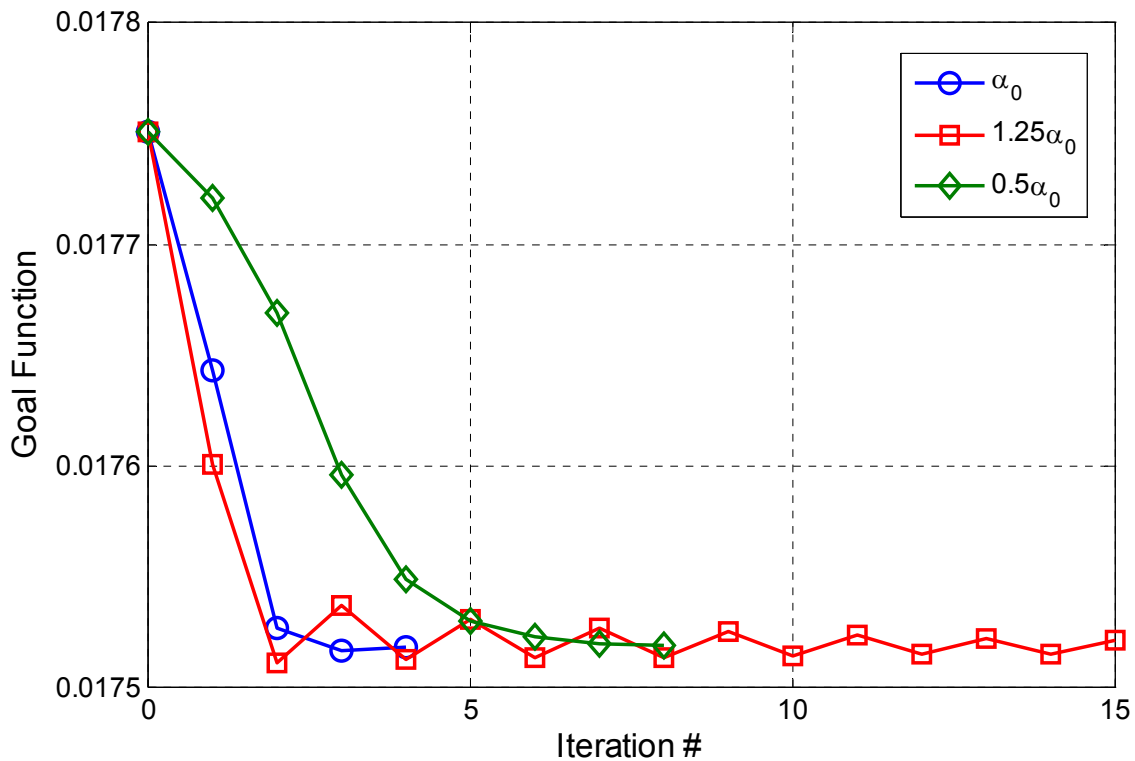


Figure 29: Step Size

For a large step size ($1.25\alpha_0$) the algorithm oscillated near the optimal solution, overshooting it on every iteration. For a small step size ($0.5\alpha_0$) the algorithm reach the optimal solution in eight (8) iterations, slowing down the performance of the algorithm. A right choice produces faster convergence. In this particular case (α_0), convergence was achieved at a minimum of 4 iterations. This test was performed on the IEEE 14-bus test system with DG penetration of 8.75%.

6.2 Simulations of the Electrical System of Puerto Rico

The following section summarizes results and analysis obtained from the application of the OCDG algorithm to the electrical system of PR. The investigation focused on three (3) strategic cases. The overall goal was to obtain the optimal conditions necessary to improve stability, with DG, during and after a disturbance. The electrical system of PR was simulated under different faults, to determine the optimal amount and location of distributed generation.

The OCDG algorithm determined the optimal capacity of each DG based on stability criterion. The disturbances occurred at the 230kV transmission system. In order to determine the DG locations, all 115kV buses have DG connected. Each DG was connected to a transformer. Table 4 shows the location of the DG connected with the 115kV buses.

From Bus	To Bus						
96	45	107	56	118	67	129	80
97	46	108	57	119	68	130	81
98	47	109	58	120	69	131	82
99	48	110	59	121	70	132	83
100	49	111	60	122	71	133	84
101	50	112	61	123	72	134	85
102	51	113	62	124	73	135	86
103	52	114	63	125	74	136	87
104	53	115	64	126	77	137	88
105	54	116	65	127	78	138	89
106	55	117	66	128	79	139	90

The power rating and the terminal voltage of each DG are 12.5 MVA and 11.4 kV, respectively. All the DGs and centralized generators were modeled with a 4th dynamic order system. Additionally, each synchronous machine has an excitation system and governor. The number of DG connected was 44 and each case has a total penetration of approximately 14.65%.

In order to determine the optimal capacity of each DG, the real and reactive powers were not constrained.

TABLE 5: COMPONENTS IN THE ELECTRICAL SYSTEM OF PUERTO RICO	
Base Case	
Bus Number	95
Transformer	39
Centralized Generators	29
Load	56
Transmission Lines	89
State Variables	261
Algebraic Variables	364
DG Connected	
Bus Number	139
Transformer	83
Centralized Generators	29
DG	44
Load	56
Transmission Lines	89
State Variables	710
Algebraic Variables	713

The number of components connected in the electrical system of Puerto Rico is summarized above (Table 5). Simulation complexity increased significantly with the added number of DGs and other components. Due to the complexity of the electrical system, only 230 kV buses were considered for the voltage stability analysis. To analyze rotor speed stability, only the impact of DG on centralized generation was considered. To improve accuracy, loads were modeled as function of frequency and voltage. Typical load coefficients for industrial loads are available elsewhere [15].

Under typical loading conditions, a base case was simulated without DG. Figure 30, 31, 32 and 33 show power flow simulation results (voltage magnitude, voltage angle, real power and

reactive power) for the base case. These were used to determine critical areas of the electrical system. The weakest areas were found near the northeast and eastern sections of the island. Disturbances were applied over those zones, because they may inflict the most severe contingences to the network.

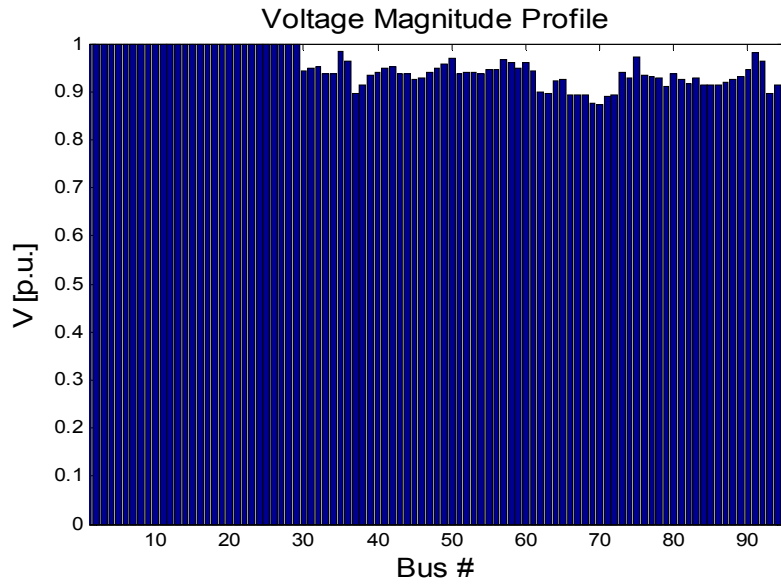


Figure 30: Puerto Rico Power Flow Solution - Voltage Magnitude

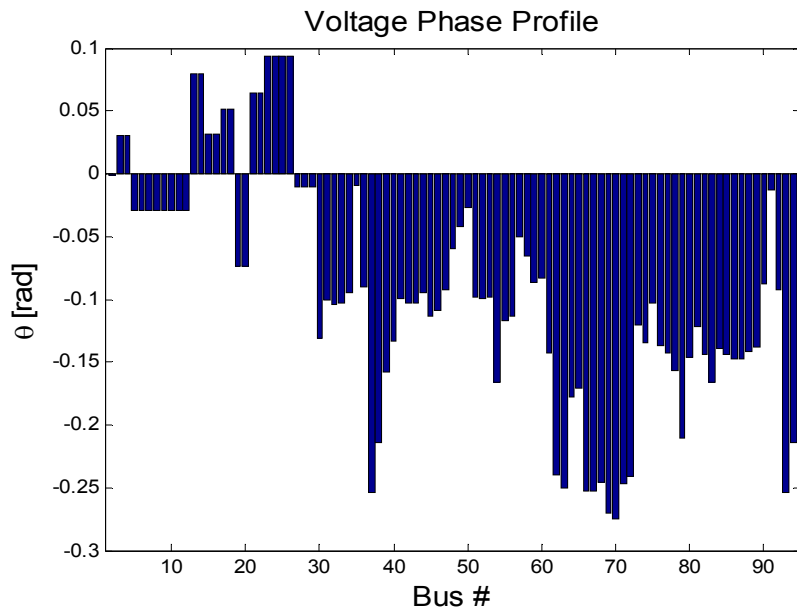


Figure 31: Puerto Rico Power Flow Solution - Voltage Angle

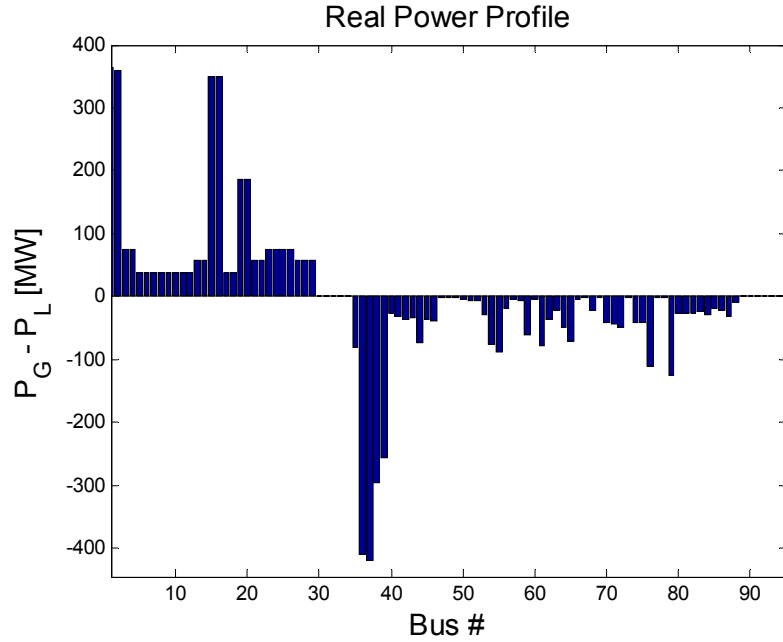


Figure 32: Puerto Rico Power Flow Solution - Real Power

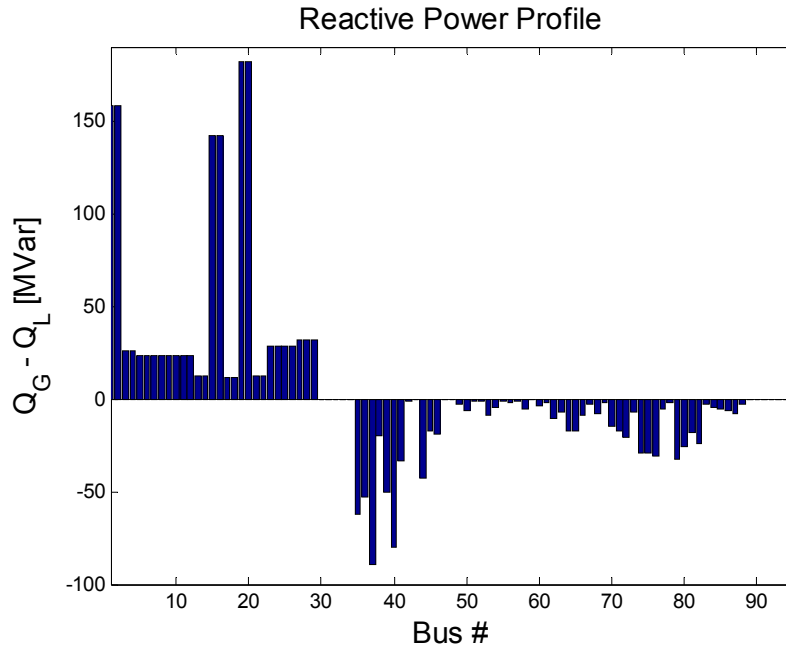


Figure 33: Puerto Rico Power Flow Solution - Reactive Power

6.2.1 Case #1: Fault at Bus 41, then open breaker between buses 35 and 41

The first case analyzed the stability response to a disturbance over a main transmission line. A three phase fault was applied at bus 41 (See Figure 16) with duration of 0.0167 seconds,

and later cleared opening breakers between buses 35 and 41. The disconnection of the transmission line produced a serious contingency in the electrical system because it transported a vital amount of electrical energy from south to the north of the island. Figure 34 shows rotor speed response for the base case and the case with DG connected.

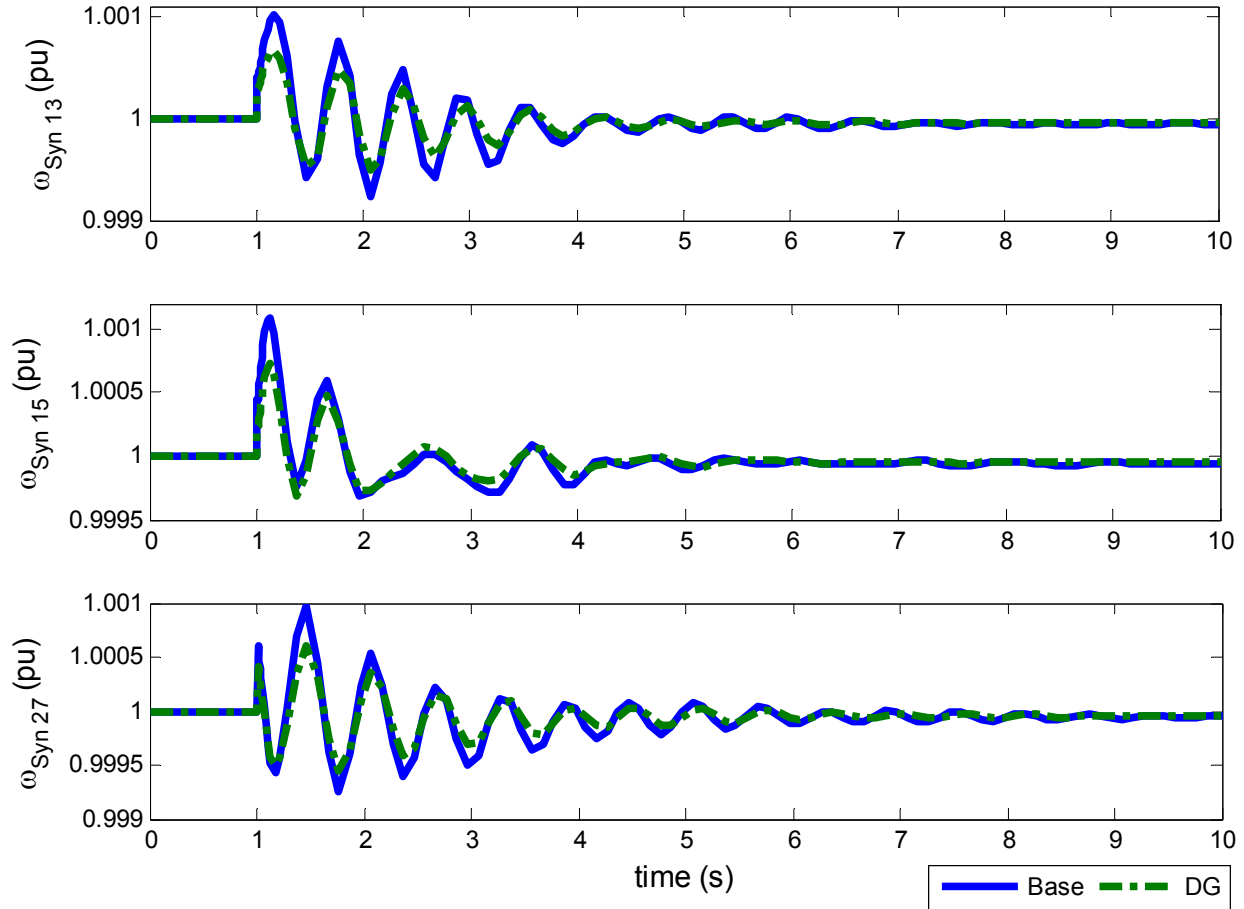


Figure 34: Case 1 - Rotor Speed Response

The disturbance produced an imbalance between the mechanical and electrical power on the centralized synchronous generators. Maximum oscillations occurred at the generators connected to buses 13, 15 and 27. The base case shows that rotor speed continued oscillating 7 seconds after the disturbance and then reached a new stable condition. The maximum frequency change produced by the disturbance was 0.0011 Pu which represents 0.066 Hz. DG reduced the

magnitude of the oscillation during the fault. The maximum frequency change with DG was 0.0007 Pu which represents approximately 0.042 Hz. Additionally, DG reduced the oscillations and a new equilibrium point was obtained faster than the base case. DG improved rotor speed stability during and after the fault.

A similar behavior occurred to bus voltages. Figure 35 shows voltage stability response before and after DG was added.

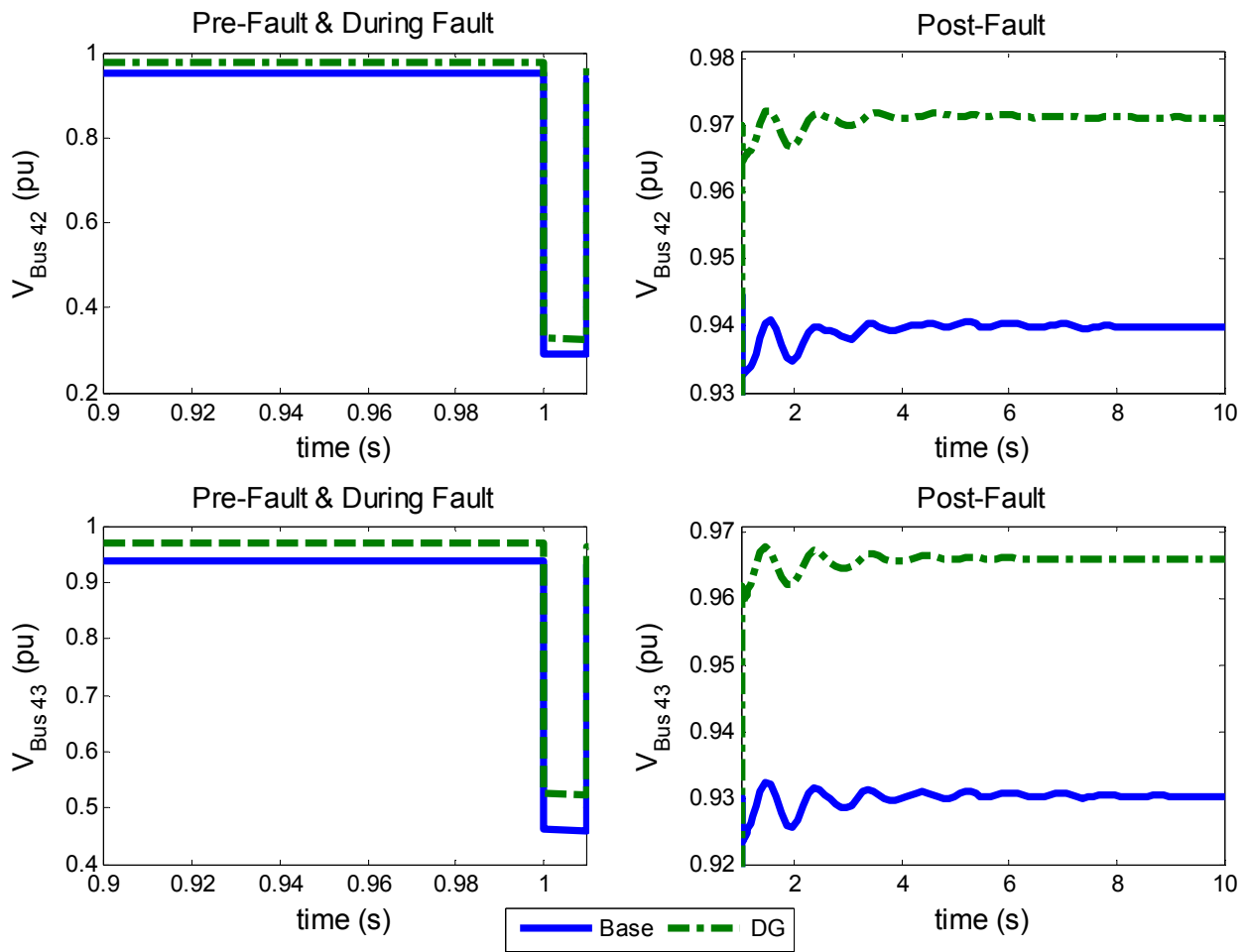


Figure 35: Case 1 – Bus Voltage Response

Initially the system was stable (0 to 1s). During the disturbance (1.0s to 1.03s) the maximum voltage drop occurred at buses 42 and 43, which were located in the north of the island (closest to the fault). After the fault (1.03s to 10.0s) the disturbance produced voltage oscillations lasting

4 seconds followed by a new stable condition. The base case also shows that transmission buses have voltage problems, pre-fault bus voltages were near 0.9 Pu. However, DG increased the steady state voltage in the transmission system, improving voltage regulation. Additionally, DGs were able to reduce the voltage drop during the fault and reduce the post-fault voltage oscillation. Figure 36 and 37 show the real and reactive power produced by DG and centralized generation.

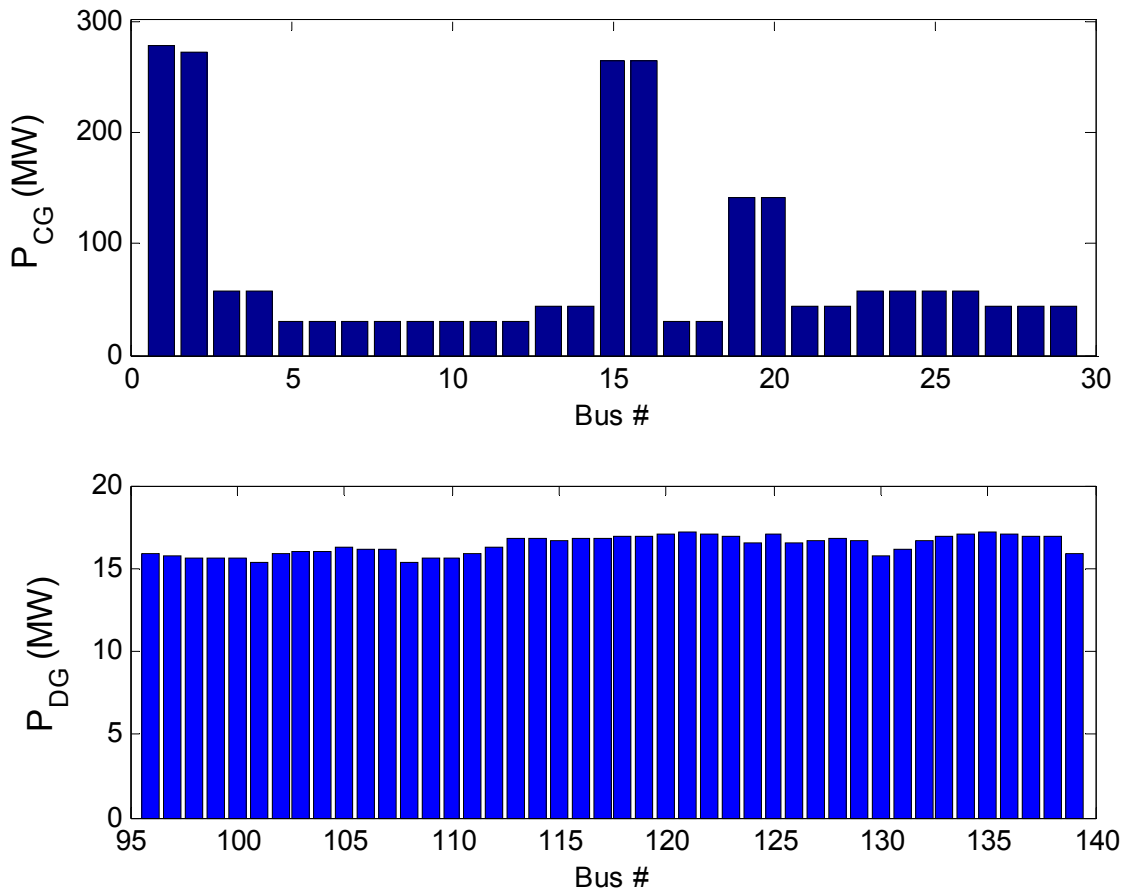


Figure 36: Case 1 – Real Power

The maximum DG penetration occurred at buses 120, 121 and 125 which were connected to the 115 kV system through buses 69, 70 and 74, respectively. Those buses were located in the east and north of the island. DG penetration was approximately uniform with an average DG real power of 16 MW. DGs produced a power reduction on the centralized synchronous

generators. The main reduction occurred on the synchronous generators connected to buses 1, 2, 15 and 16, which were located in the south of the island. Figure 37 shows the reactive power produced by the centralized and distributed synchronous generators.

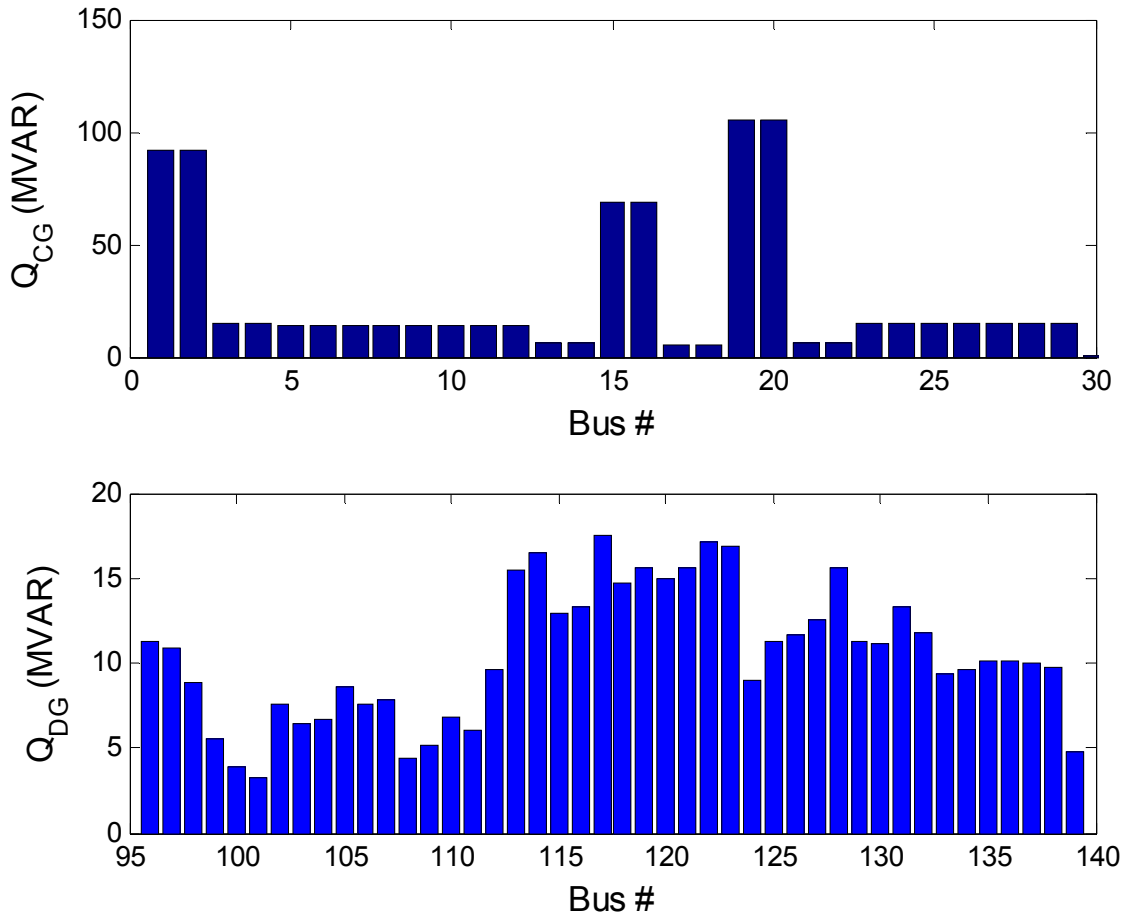


Figure 37: Case 1 – Reactive Power

The main production of DG reactive power occurred at buses 114, 117, 122 and 123 which were connected to transmission buses 63, 66, 71 and 72, respectively. Those buses were located in the south-east and east of the island. The penetration of DG reactive power increased the post-fault bus voltage, in order to improve the performance of the electrical system. Thus, DG penetrations supported the electrical system to maintain viable operation condition before, during and after a disturbance. DG also reduced the reactive power produced by the centralized

synchronous generator. The main reduction of reactive power was approximately 72 MVAR at buses 1, 2, 19 and 20. Those buses are located on the south and north of the island.

6.2.2 Case #2: Fault at bus 39, then open breakers between buses 36 and 39

The second case studies the transient response to a disturbance over parallel transmission lines. The disturbance was produced when a three phase fault was applied at bus 39 with duration of 0.016 second, later cleared opening breakers between buses 36 and 39. Figure 38 shows rotor speed response before and after DG was added.

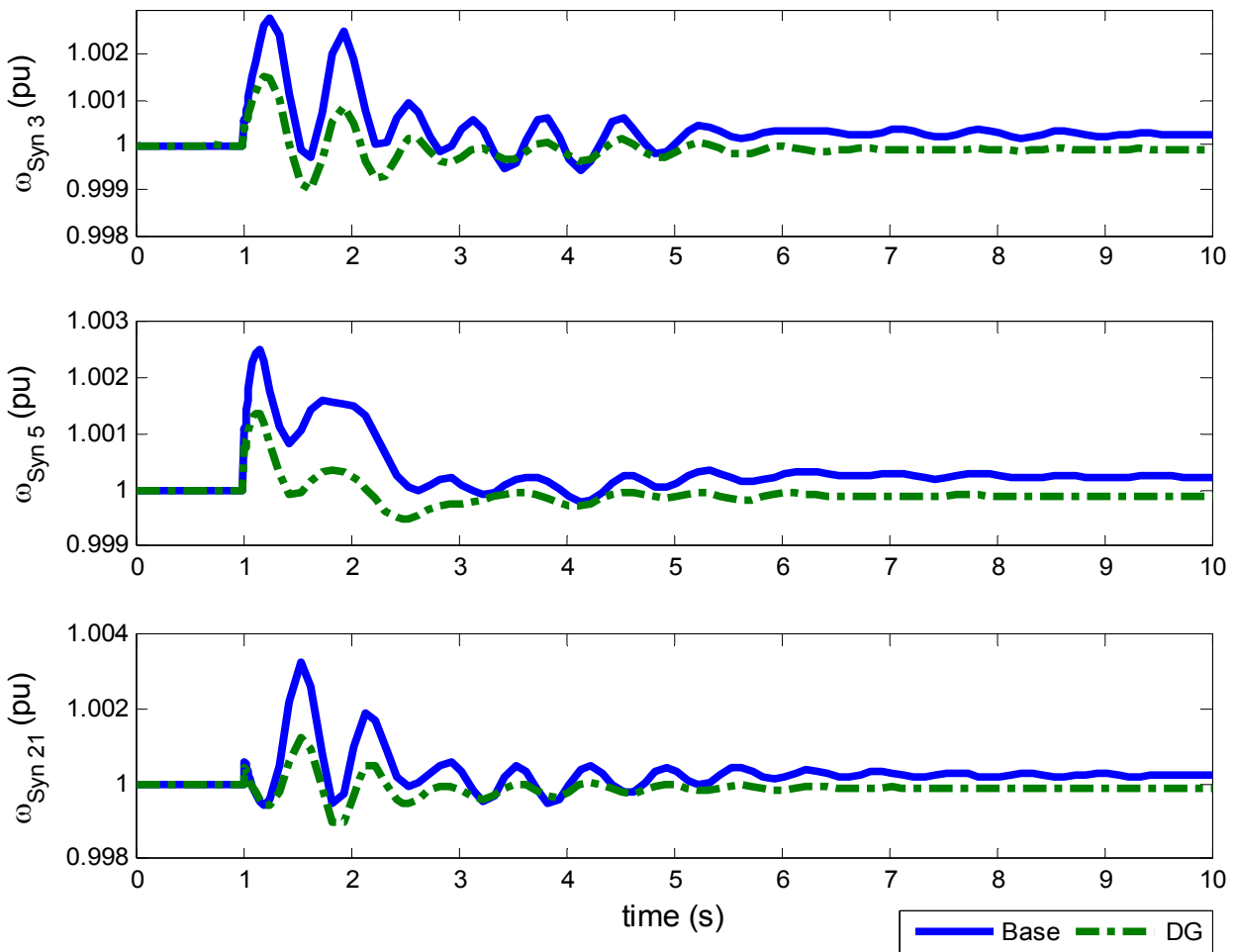


Figure 38: Case 2 – Rotor Speed Response

The maximum oscillations occurred in the synchronous generators connected at buses 3, 5 and 21. Base case shows that the disturbance produced a maximum frequency change of 0.0031 Pu, which represent approximately 0.186 Hz. The rotor speeds of the synchronous generator continued oscillating 8 seconds after the disturbance. The optimal DG penetration estimated with the OCDG algorithm damped the oscillations and led the system to a stable condition faster than the base case. DG improved the system stability reducing the maximum frequency change to 0.0015 Pu, which represent 0.09 Hz. The main improvements from the optimal DG penetration occurred in the synchronous generator connected at bus 21, because the magnitude of oscillation was reduced significantly when the DGs were connected. Figure 39 shows voltage stability response before and after DG was added

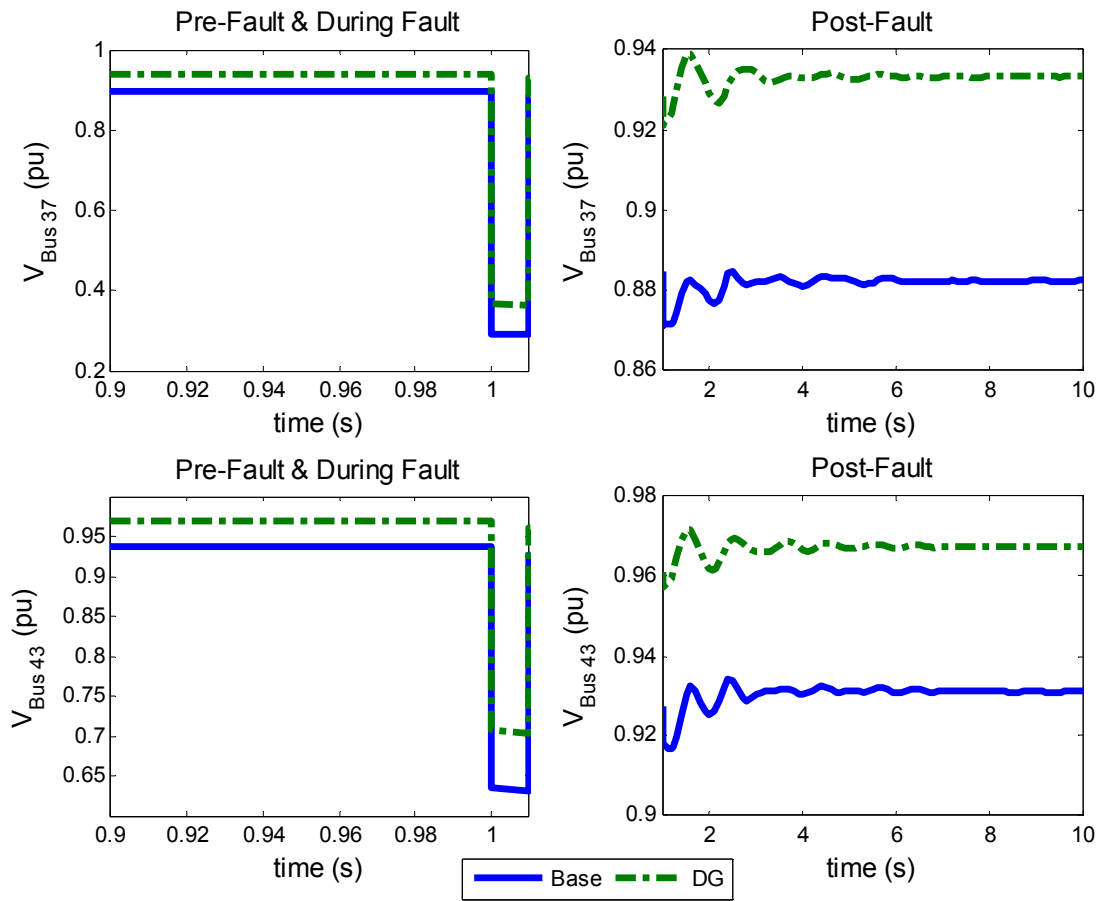


Figure 39: Case 2 – Bus Voltage Response

During the disturbance, DG improved significantly the voltage (about .1 Pu increase) at buses 37 and 43. The base case shows that the disturbance produced voltage oscillations lasting 5 seconds after the fault and then reached a new stable condition. DG improved the bus voltages before, during and after the disturbance. The reactive power supplied by the DG helped to increase bus voltages on the transmission system. Hence, the case with DG produced a better voltage regulation than the base case. Figure 40 and 41 show the real and reactive power supplied by the synchronous machines.

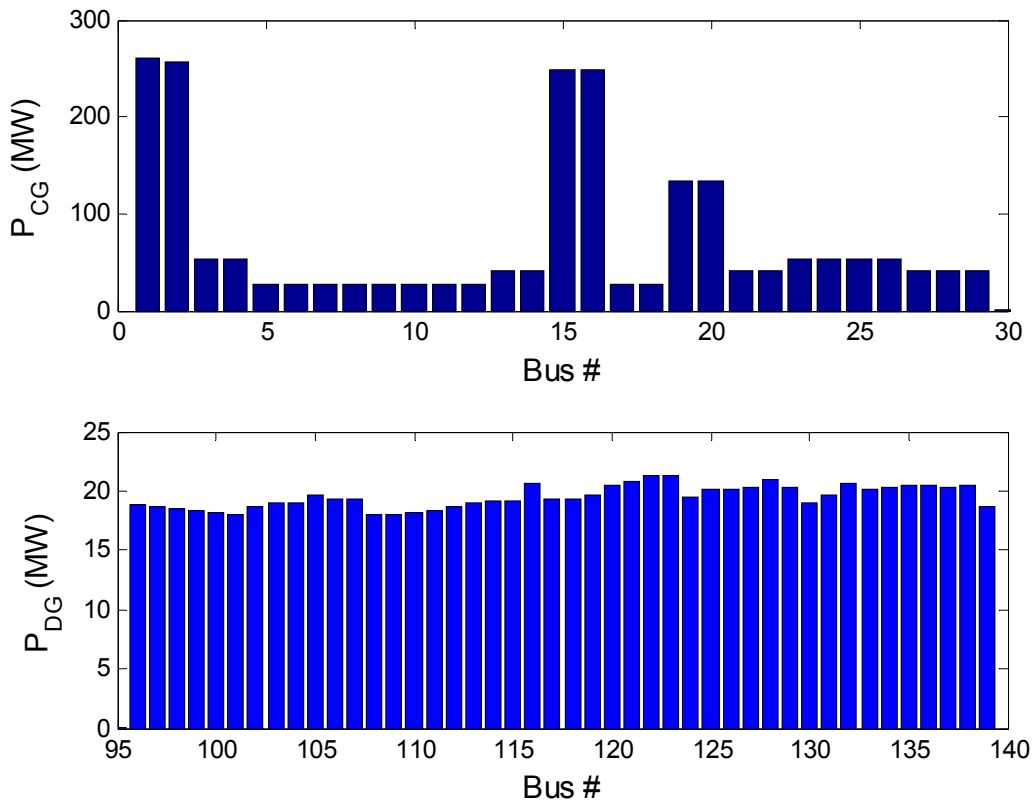


Figure 40: Case 2 - Real Power

The main DG penetration was at buses 122, 123 and 128, which were connected to the transmission buses 71, 72 and 73, respectively. Those buses were located in the north and north-east of the island. The maximum real power produced by a DG was 21 MW, while the minimum was 18 MW. In comparison with case #1, this case shows a higher DG penetration and produced

a higher reduction on the power output of the centralized generations. DG penetration reduced approximately 108 MW from the synchronous generators connected at buses 1 and 2. The removal of the parallel transmission lines between buses 36 and 39, produced a power output reduction of the centralized generation connected in the south of the island. DG connected at the north of the island supported the electrical system supplying the necessary energy to the load. Hence, DG helped the electrical system to maintain a stable condition during and after the disturbance. Figure 41 shows the effects on DG reactive power.

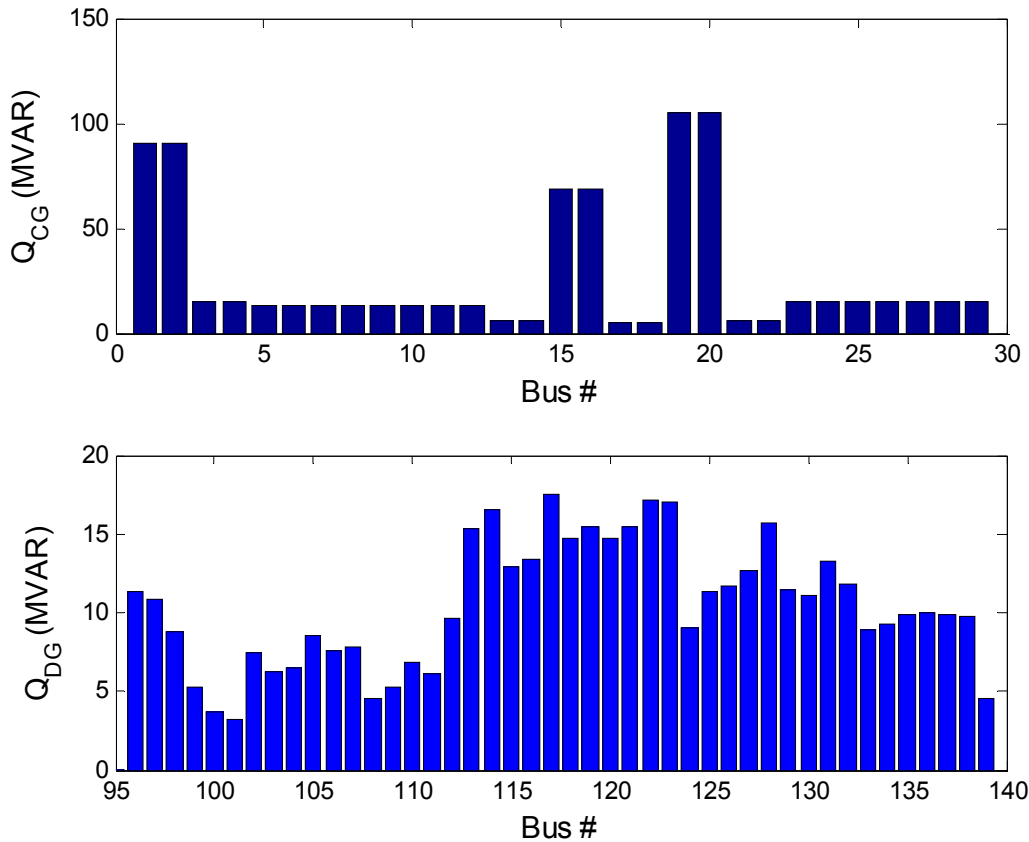


Figure 41: Case 2 – Reactive Power

The maximum production of reactive power occurred between buses 113 and 123, which were located in the east of the island. The base case shows that those buses had voltage regulation problems (see Figure 30). DG supported the electrical system, principally in the east of the island, supplying reactive power to maintain an acceptable condition before, during and

after the disturbance. DG penetration produced a reduction of approximately 73 MVAR of the centralized synchronous generators connected at buses 1, 2, 19 and 20. DG penetration reduced the reactive power supplied by the centralized synchronous generators to prevent excessive rotor heating.

6.2.3 Case #3: Fault at bus 44, then open breaker between buses 35 and 44

The third case studied the transient response to a disturbance applied in the west of the electrical system of PR. A three phase fault with duration of 0.1 second was applied at bus 44, and then the transmission line was removed opening breakers between buses 35 and 44. Figure 42 shows rotor speed response before and after the optimal amount of DG was added.

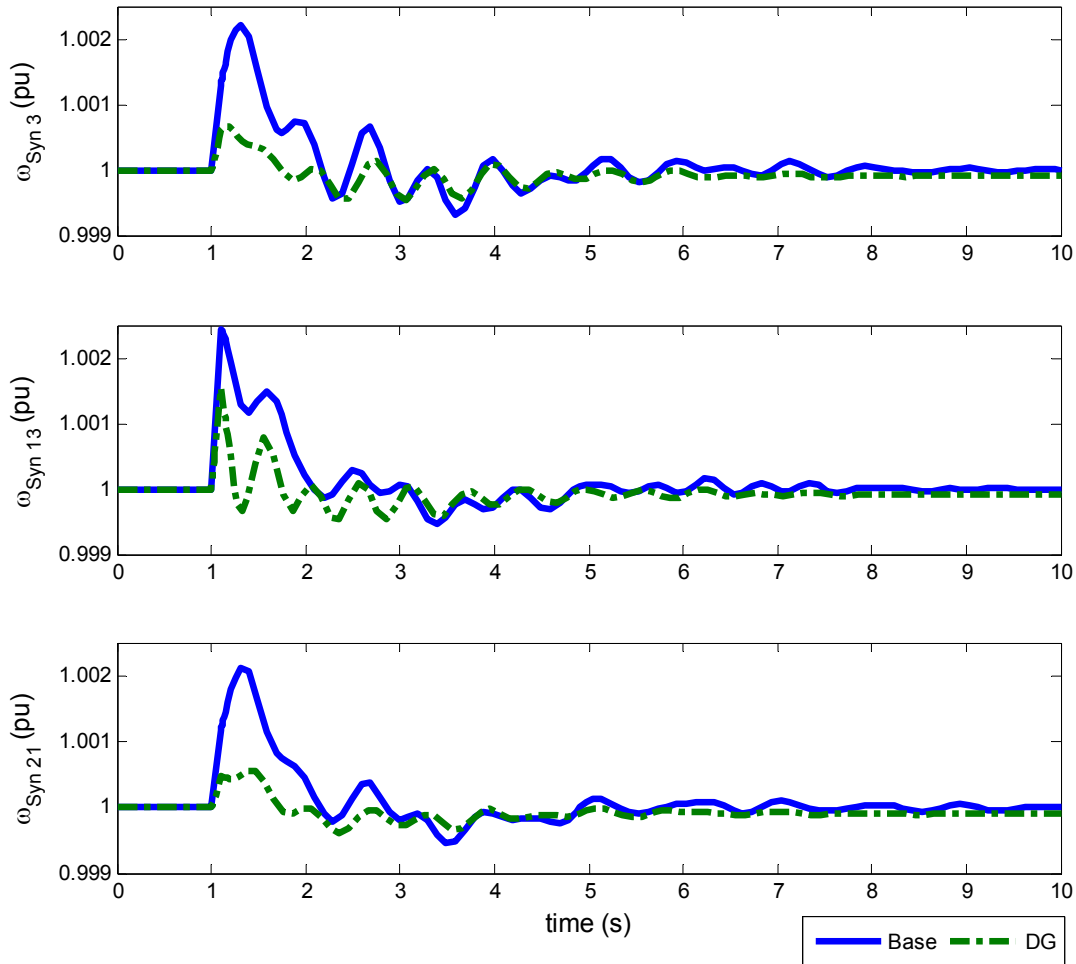


Figure 42: Case 3 – Rotor Speed Response

The disturbance produced maximum oscillations over the synchronous generators connected at buses 3, 13 and 21. The base case showed continued rotor speed oscillation lasting 8 seconds after the disturbance followed by a stable condition. Additionally, the base case shows a maximum frequency change of 0.0029 Pu (0.174 Hz), while the case with DG connected shows a maximum frequency change of 0.0016 Pu (0.096 Hz). Optimal DG reduced oscillations and reached a stable condition faster than the base case, thus improving rotor stability response. Figure 43 shows the voltage stability response for the base case and the case with DG connected.

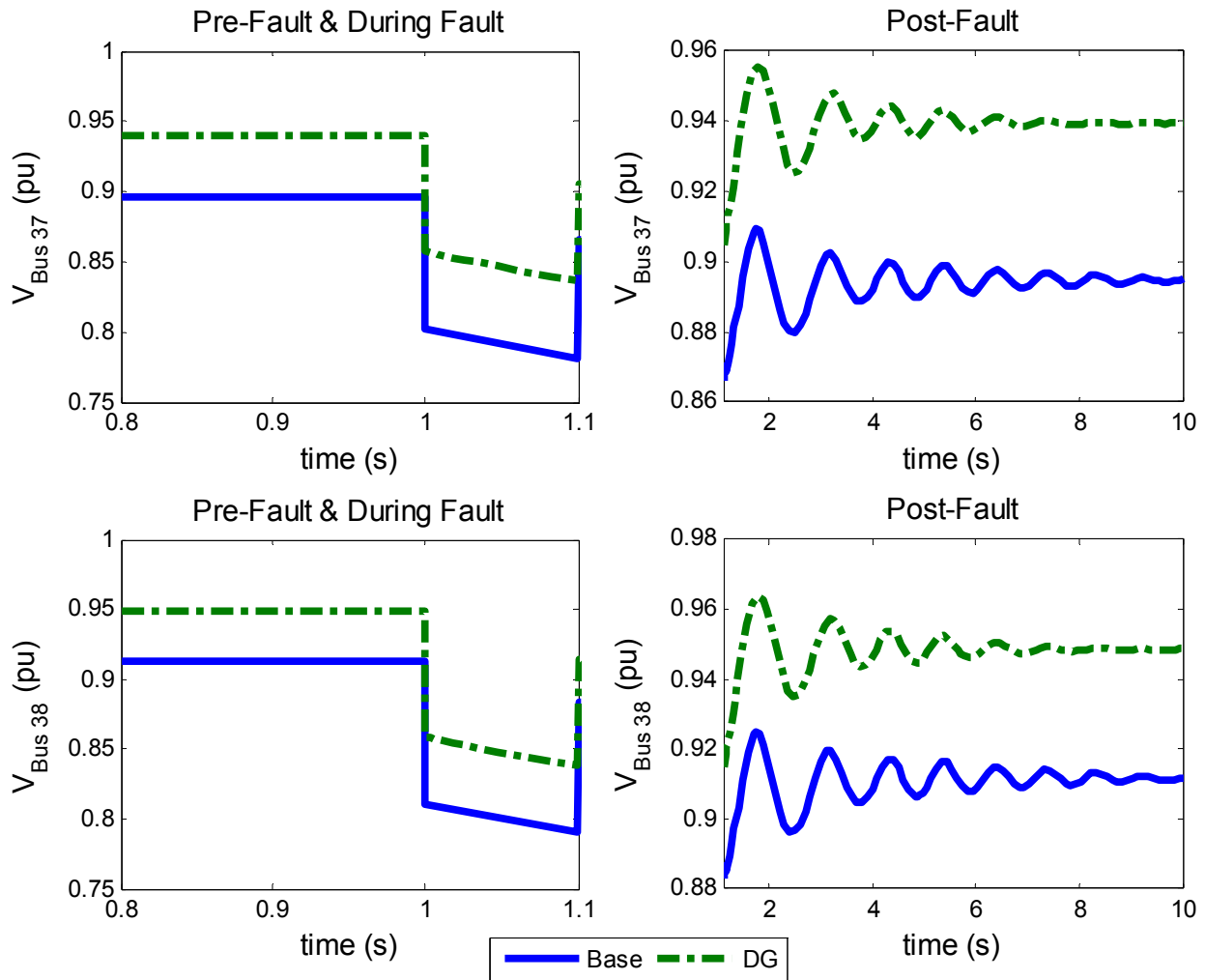


Figure 43: Case 3 – Bus Voltage Response

The base case shows a bus voltage of 0.92 Pu (211 kV) at the bus 38, while the case with DG connected shows a bus voltage of 0.95 Pu (218 kV). The reactive power supplied by the DG improved the bus voltage to maintain a better regulation. The base case shows a high voltage drop during the disturbance than the case with DG connected. Additionally, DGs reduced the post-fault voltage oscillation, obtaining a stable condition faster than the base case. Figure 44 shows the real power produced by the synchronous generators.

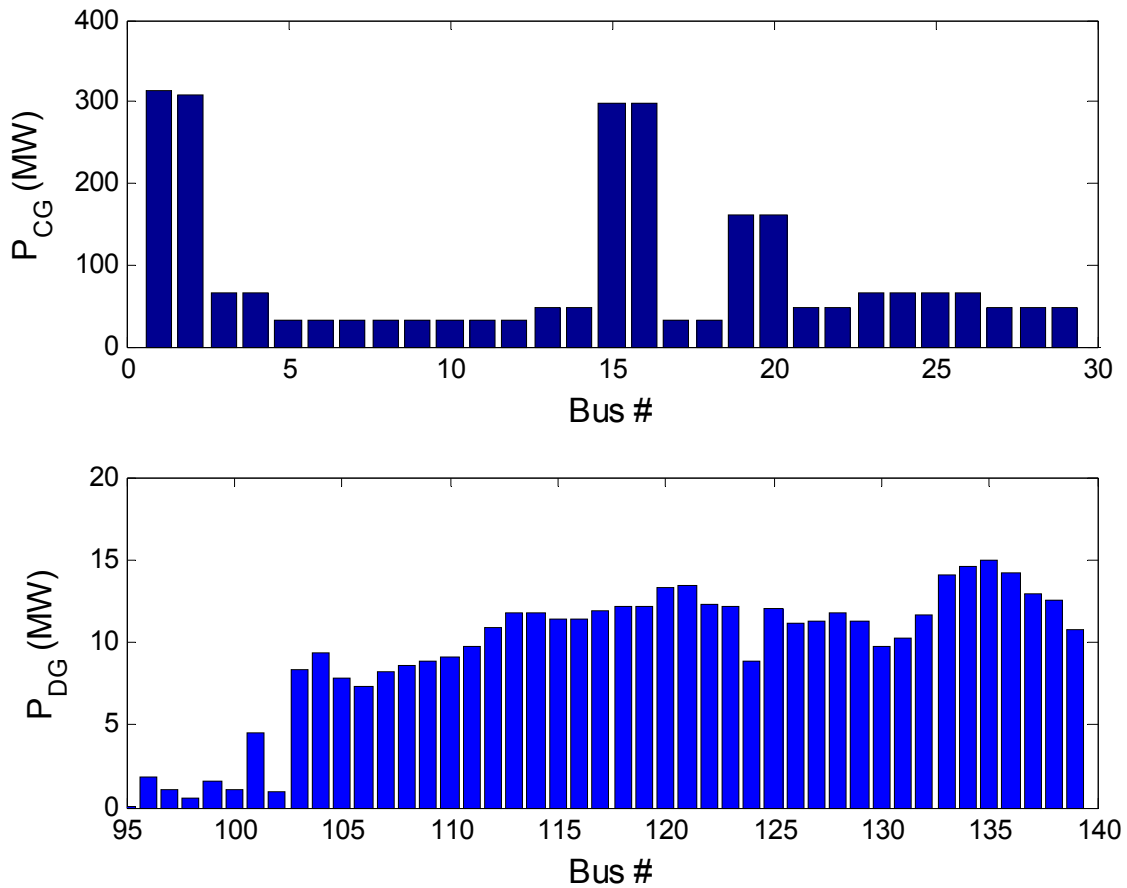


Figure 44: Case 3 – Real Power

The main production of real power occurred at buses 133, 134, 135 and 136, which were connect to transmission buses 84, 85, 86 and 87, respectively. Those buses are located in the center of the island. The maximum real power produced by a DG was 15 MW, while the minimum was 0.63 MW. The main DG penetration was in the center and north of the island

close to the main concentration of load. This case shows a lower DG penetration than case #1 and #2. Hence, the real power reduction of the centralized generation was lower for this case. DG penetration reduce approximately 56 MW on the synchronous generators connected at buses 1 and 2. That reduction was half than the case #2. The removal of the transmission lines between buses 35 and 44 produced lower effect on the stability of the electrical system. Figure 44 also shows the location capabilities of the algorithm. Initially, the programmer chooses all busses where DG is to be evaluated. After the initial results, when a DG is located at a bus where its output is negligible, see busses 96-102 on Figure 44, the programmer could label those locations as not suitable for a DG installation. A second output could be generated, neglecting the locations previously identified, to fine-tune the remaining locations. Figure 45 shows the reactive powers supplied by the synchronous generators.

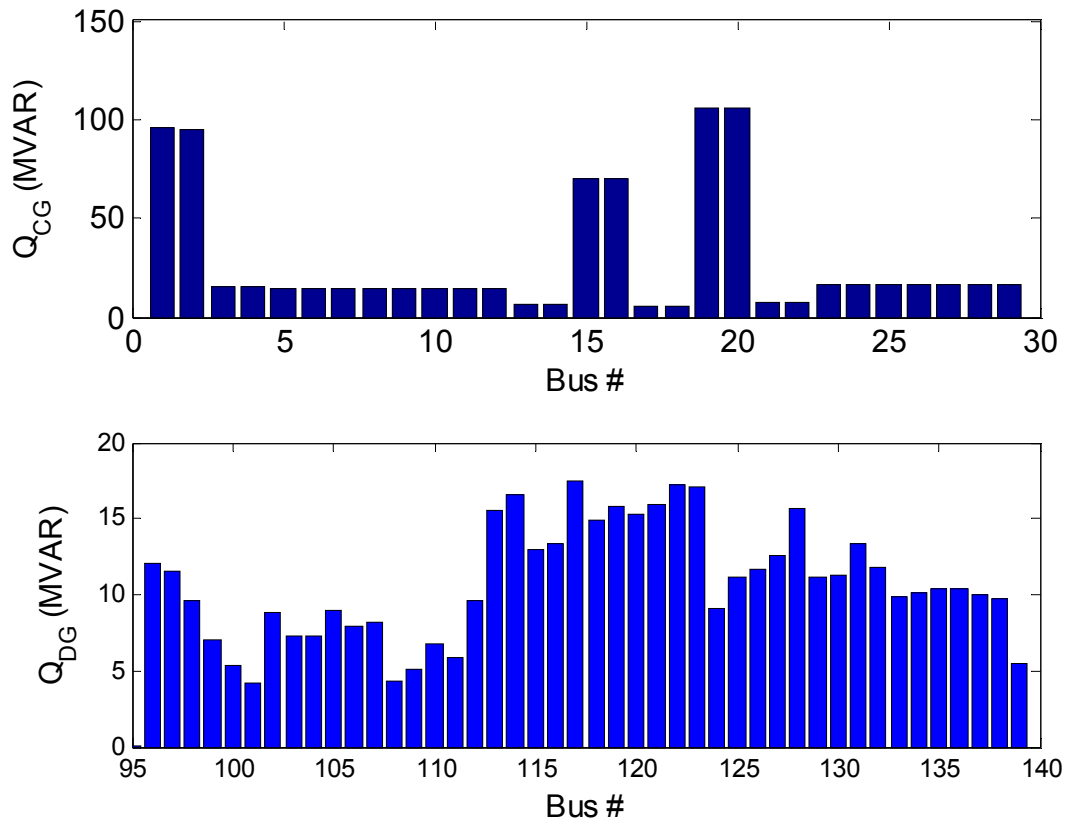


Figure 45: Case 3 – Reactive Power

This case is similar to the case #1 and #2. The main production of reactive power was located in the east of the island. DG penetration improved the voltage regulation over that zone. The case with DG connected reduced approximately 70 MVAR on the centralized synchronous generators connected at buses 1, 2, 19 and 20. Similarly than previous cases, the reactive power produced by DG helps to regulate the bus voltage on the transmission system, thus improved the voltage stability in the electrical system.

6.2.4 Summary of the Electrical System of PR

The investigation studied several cases in order to obtain the optimal conditions to implement distributed generation and improve the stability of the electrical system of Puerto Rico. DGs were connected to generate electrical power, closer to consumption areas, taking advantage of the maximum efficiency of energy production. Figure 46 and 47 show a summary of real and reactive power produced for each case.

Figure 46 shows DG penetration reduced the power output of the centralized synchronous generator and the losses in the transmission lines. Case #2 produced the maximum DG penetration, reducing 30% the power output of the centralized generation. Case #3 showed the minimum DG penetration with a reduction of 14% on the centralized generation. Stability is a function of disturbance type and location to which the system is exposed. The disturbance for case #2, had greater effect on the stability of the electrical system than the disturbance for cases #1 and #3. The disturbance for case #2 was the worst case, removing a parallel circuit, equivalent to two transmission lines limiting the transfer capability to the centralized synchronous generators connected in the south. Hence, DG penetration increased in the north of the island to supply the necessary power.

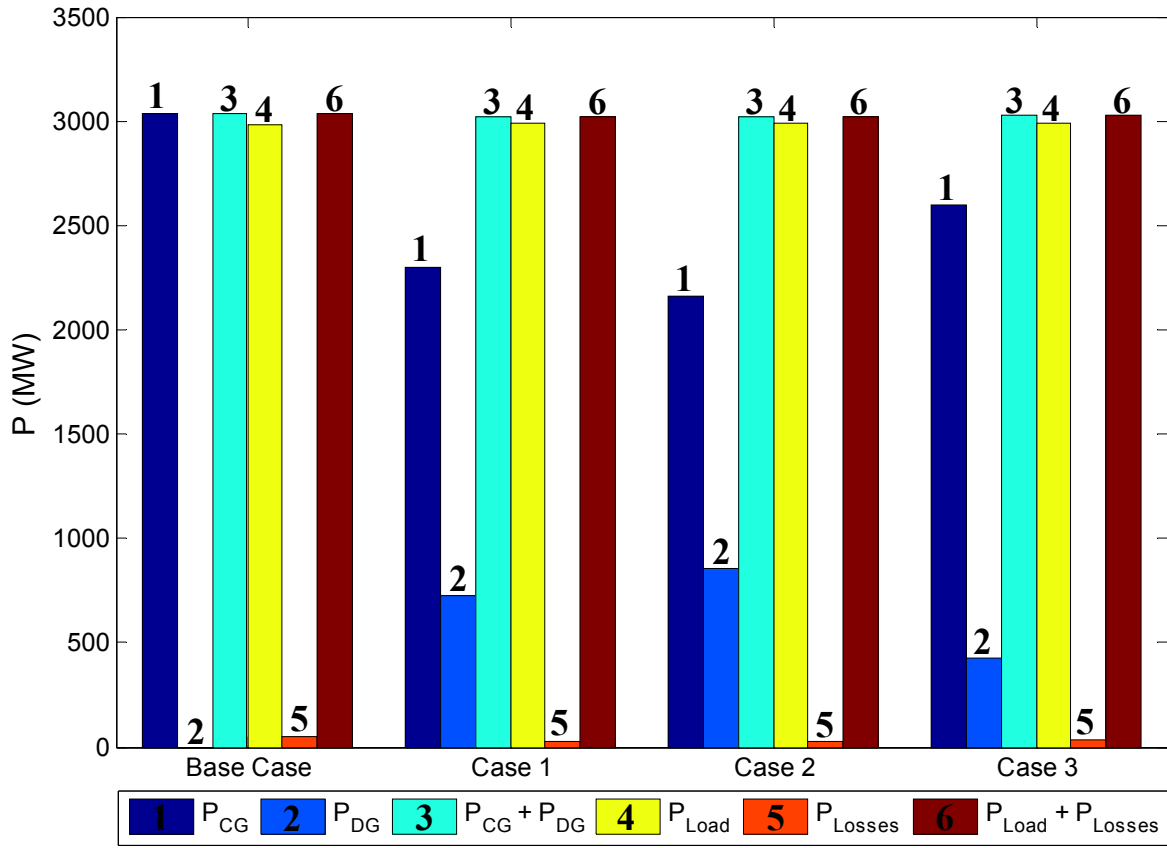


Figure 46: Real Power Summary

The OCDG algorithm could be used to control the location of DG assets (see Section 6.1.6). Increased weights on P_{DG} (Q_u) reduce DG penetration on the specified zone or busses. Figure 44 proves the algorithm is location sensitive when busses with lower DG values are interpreted as non suitable for DG installation.

Figure 47 shows that cases with DG connected significantly reduced the reactive demand from centralized generators. The three (3) cases with DG connected reduced, approximately, 45% of the reactive power supplied by the centralized generators. Hence, DG reduced the reactive power supplied by the centralized synchronous generators preventing excessive rotor heating and maintaining a better regulation on bus voltages. Additionally, DG improved the performance reducing losses in the electrical system. Figure 48 shows the real and reactive power losses for each case.

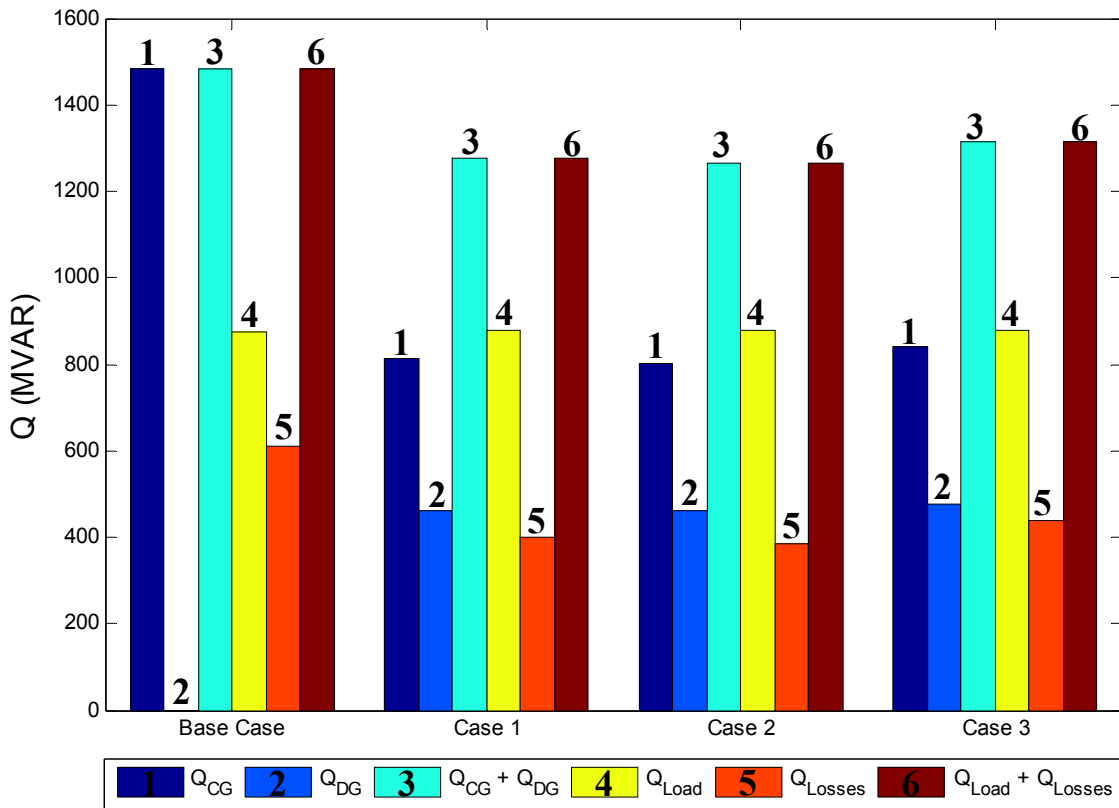


Figure 47: Reactive Power Summary

The cases with DG show a significant loss reduction of the electrical system. DG reduced real power losses by 45%. It also improved the reliability and power quality of the electrical system reducing congestions in transmission lines. Additionally, DG reduced by 35% the reactive power losses. The MVAR reduction on the reactive power losses was higher than the real power losses because of the inductive characteristic of transmission lines. Hence, the reduction of real and reactive power losses caused a reduction in the production from the centralized synchronous machines.

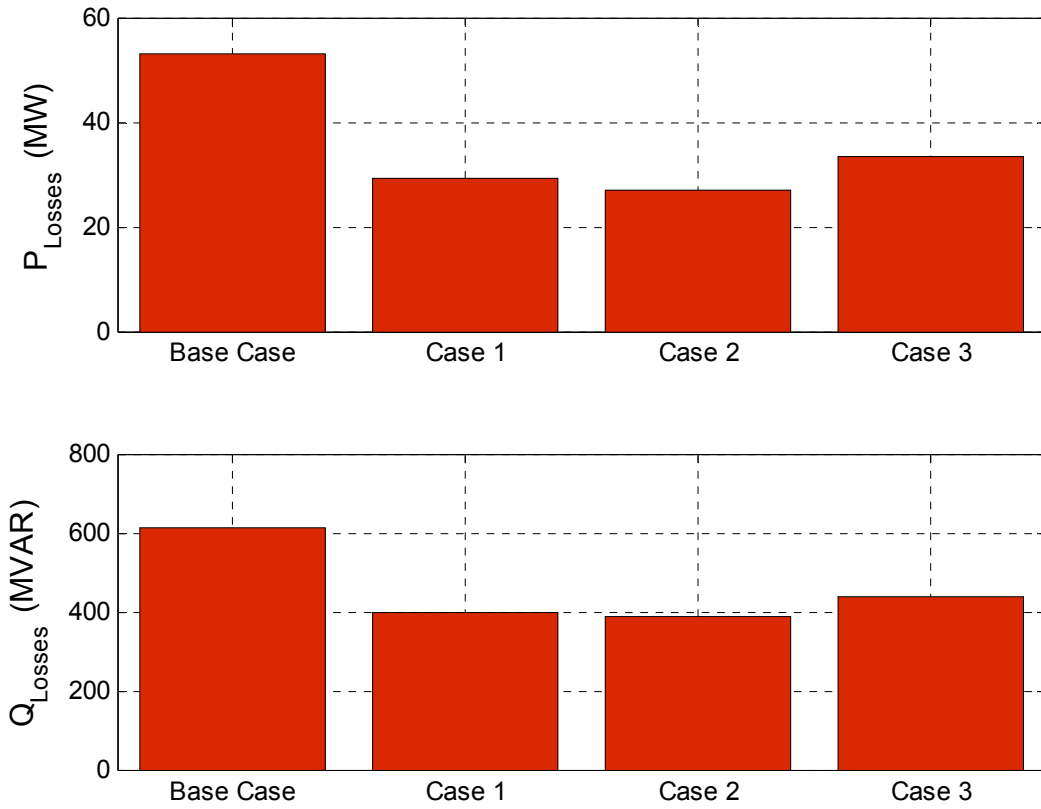


Figure 48: Real and Reactive Power Losses

7 Conclusion and Future Work

7.1 Conclusion

This document presented an optimization technique to determine the optimal location and capacity of distributed generation in order to improve the stability response during and after a disturbance. The OCDG algorithm has been developed as a nonlinear programming tool. In this approach, dynamic trajectories of a power system were discretized and used as equality constraints, together with algebraic equations representing the network interface. The methodology presented in this work was shown to be robust enough to handle a small 14 bus system and a complex system, the Puerto Rico power system.

The IEEE 14-Bus test system was used to validate the convergence of the OCDG algorithm. Simulation results were presented in several plots to show the convergence and dynamic response of the electrical system. The OCDG algorithm was able to reach the optimal solution for each case. Minimal values of the goal function meant fewer oscillations of rotor speed and voltage. The OCDG algorithm determined the optimal localization and capacity to connect DG based on stability criteria.

As expected, results have shown that negligible effects from DG are seen at low penetration values. However, increased DG penetration improved the stability response of the electrical system. When a disturbance, known to be critical without DG, was applied to the electrical system, DG supported the network and avoided the collapse of the system. DG penetration improved the stability of the electrical system during and after a disturbance, reducing rotor and voltage oscillations. Simulation complexity increased significantly with added

number of DGs. Higher order of state variable and algebraic variables limited the computation performance during simulations.

Several test cases, focusing on system stability, demonstrated the advantages of distributed generation in the electrical system of Puerto Rico. The OCDG algorithm was used to determine the optimal location and capacity of DGs in the electrical system of Puerto Rico. The investigation focused on three (3) strategic cases. Power flow solution showed that weak bus voltage areas were located in the northeast and east of the island. Results showed that the main penetration of DG was in the northeast and east of the electrical system of Puerto Rico. Simulations results showed that the reactive power supplied by DG supported the electrical system in order to maintain an acceptable operation condition before, during and after the disturbance. Higher DG penetration increased the steady state bus voltages and reduced the voltage drop during the disturbance. It also reduced voltage oscillations after a disturbance reaching a new steady state condition faster than the base case.

Additionally, optimal DG penetration improved the rotor angle stability in the electrical system. Lower inertias allowed DGs to respond faster than centralized generation. All cases showed greater oscillations occurring on centralized synchronous generators connected in the south of the island. Optimal DG penetration reduced the magnitude of the oscillations during and after a disturbance. Hence, optimal DG penetration supported the electrical system in order to maintain the frequency closer to its nominal value.

The results by the OCDG algorithm showed that the main DG penetration was in the north and east of the island. Power flow studies from the optimal DG penetration showed reduced flows between transmission buses producing a significant loss reduction of electrical

system. In general the study demonstrated the advantages of distributed generation in the electrical system of Puerto Rico, with a principal focus on system stability.

7.2 Future Work

The following are recommendations for future work:

- The model of the electrical system of Puerto Rico was created using actual cable data, while loads were determined through a power flow solution. Future models should include actual parameters for synchronous machines, excitation system and governor in order to improve accuracy (collaboration with PREPA).
- Consider the effects of DG on short circuit currents and system protection.
- Include renewable energy models.
- DG Cost Analysis.
- Environmental Considerations (noise and emissions).

Bibliography

- [1] M. Reza, P. H. Schavemaker, J. G. Slootweg, W. L. Kling, and L. Van der Sluis, "Impacts of Distributed Generation Penetration Levels on Power Systems Transient Stability," IEEE, 2004.

- [2] D. Chatterjee, A. Ghosh, and M. A. Pai, "Systems, Trajectory Sensitivity Analysis in Distributed Generation," IEEE, 2006.

- [3] T. Tran-Quoc, et al., "Stability Analysis for the Distribution Networks with Distributed Generation," IEEE, 2006.

- [4] H. Chen, J. Chen, D. Shi, and X. Duan, "Power flow study and voltage stability analysis for distribution systems with distributed generation," IEEE, 2006.

- [5] K. Bosworth, "A Distributed and Community-Based Electrical Grid: Building the Energy, Economy, and Democracy for Tomorrow," Macalester College, 2008.

- [6] P. Ng, "Draft Unit Cost Guide for Transmission Lines," Pacific Gas and Electric Company, 2009.

- [7] U. S. C. C. T. Program, "Transmission and Distribution Technologies," p. 35, Nov. 2003.

- [8] C. Galarza. (2008, Dec.) Comisión Nacional Para el Uso de la Energía Eficiente. [Online]. HYPERLINK "http://www.conae.gob.mx/wb/CONAE/CONA_1917_generacion_distribui"
http://www.conae.gob.mx/wb/CONAE/CONA_1917_generacion_distribui

- [9] (2007, Feb.) U.S. Department of Energy. [Online]. HYPERLINK "http://www1.eere.energy.gov/femp/der/derchp_derbasics.html"
http://www1.eere.energy.gov/femp/der/derchp_derbasics.html

- [10] "Model Interconnection Procedures and Agreement for Small Distributed Resources," NARUC, 2003.

- [11] P. Kundur, *Power System Stability and Control*. McGraw - Hill Professional, 1994.
- [12] L. L. Grigsby, *The Electric Power Engineering Handbook*, 2nd ed. CRC, 2007.
- [13] A. L. Shenkman, *Transient Analysis of Electric Power Circuits Handbook*, 1st ed. Springer, 2005.
- [14] M. A. El-Sharkawi, *Electric Energy: An Introduction Power Electronics and Applications Series*, 2nd ed. Florida, United States of America: CRC Press, 2005.
- [15] F. Milano. (2008, Feb.) Power System Analysis Toolbox. Manual.
- [16] P. M. Anderson and A. A. Fouad, *Power System Control and Stability*, 2nd ed. Wiley-IEEE Press, 2002.
- [17] A. A. Irizarry, "Energía eléctrica en Puerto Rico: generación, transmisión y conservación," University of Puerto Rico.
- [18] J. A. Rodríguez, "Iniciativa para Reducir el Costo de la Electricidad," AEE, 2007.
- [19] S. Miranda, M. Franco, A. Román, and A. Anazagasty, "La generación, transmisión y distribución de la energía eléctrica," CIAPR, 2001.
- [20] A. Williams, "Role of fossil fuels in electricity generation and their environmental impact," IEEE, 1993.
- [21] J. Haskard. (2008, Jun.) Clean Energy Resources Team. [Online]. HYPERLINK "http://www.cleanenergyresourceteams.org/get-answers/26/06/2008/what-is-DG" <http://www.cleanenergyresourceteams.org/get-answers/26/06/2008/what-is-DG>
- [22] Puerto Rico Electric Power Authority, "Lianas de Transmisión y Subtransmisión Datos de Construcción," December 2007.

- [23] J. Nocedal and S. J. Wright, *Numerical Optimization*, 2nd ed. Springer, 2006.
- [24] E. E. Aponte, "Time Optimal Load Shedding for Power System with Distributed Resources," Rensselaer Polytechnic Institute D.Eng Tesis, 2005.
- [25] E. De Tugile, M. La Scala, and P. Scarpellini, "Real Time Preventive Action for the Enhancement of Voltage Degraded Trajectories," *IEEE*, May 1999.
- [26] M. La Scala, M. Trovato, and C. Antonelli, "On-Line Dynamic Preventive Control: An Algorithm for Transient Security Despatch," *IEEE*, May 1998.
- [27] Chen, C S; Hsu, C T; Lee, Y D; Huang, J F; Chen, H S; Hsu, R T; Huang, C B;, "Design of Protective Scheme for Tie Line Tripping of an Industrial Power System," 199.
- [28] "Connection Assessment & Approval Process," Independent Electricity Market Operator, Report, 2004.
- [29] "Standard for Interconnecting Distributed Resources with Electric Power Systems," IEEE Standard 1547, 2003.
- [30] "Consideración de los Estándares del E pact 2005: Time-Based Metering and Communications Interconnection Standards for Distributed Resources ," AEE, 2007.
- [31] J. G. Slootweg and W. L. Kling, "Impacts of distributed generation on power system transient stability," *IEEE*, 2002.
- [32] L. Zhengyi, Z. Xiangjun, T. Shuntao, and G. Zigang, "A novel scheme of stability control for distributed generation systems," *IEEE*, 2004.
- [33] K. E. Brenan, S. L. Campbell, and L. Petzold, *Numerical Solution of Initial-Value Problems in Differential-Algebraic Equations*. Philadelphia: SIAM, 1995.
- [34] "IEEE Recommended Practice for Excitation System Models for Power System Stability Studies," IEEE Power Engineering Society Standard Std. 421.5, 2005.

- [35] "IEEE Standard Procedures for Obtaining Synchronous Machine Parameters by Standstill Frequency Response Testing," IEEE Standard Std 115, 1983.
- [36] H. W. Dommel and W. F. Tinney, "Optimal Power Flow Solutions," *IEEE*, Oct. 1968.
- [37] E. D. Tuglie, M. La Scala, and P. Scarpellini, "A Corrective Control for Angle and Voltage Stability," *Enhancement on the Transient Time-Scale*, Nov. 2000.
- [38] T. Martínez, "Voltage Stability Assessment of an Island Power System as a Function of Load Model," Master Thesis, University of Puerto Rico at Mayaguez Campus, Mayaguez, 2003.
- [39] L. M. Monge, "Effect Of Distributed Energy Storage Ssystems In The Voltage Stability Of An Island Power System," Master Thesis, University of Puerto Rico at Mayaguez Campus, Mayaguez, 2006.
- [40] A. Narang, "Impact Of Large-Scale Distributed Generation Penetration On Power System Stability," Canmet Energy Technology Center, 2006.
- [41] O. Alsac and B. Stott, "Optimal Load Flow With Steady-State Security," *IEEE*, Oct. 1973.
- [42] "The Potential Benefits of Distributed Generation And Rate-Related Issues That May Impede Their Expansion," U.S. Department of Energy, 2007.
- [43] "Model Distributed Generation Interconnection Procedures and Agreement," The National Association of Regulatory Utility Commissioners, 2002.
- [44] O. Barraza, "Optimización Dinámica," UMA, 2004.
- [45] N. Nimpitiwan, G. T. Heydt, R. Ayyanar, and S. Suryanarayanan, "Fault Current Contribution From Synchronous Machine and Inverter Based Distributed Generators," *IEEE*, 2007.
- [46] F. M. Bruck, F. A. Himmelstoss, "Modelling and Simulation of a Synchronous Machine,"

IEEE, 1998.

- [47] N. K. Poulsen, *Dynamic Optimization*. Denmark: The Technical University of Denmark, 2007.
- [48] A. H. Pablo Serra, "Optimización Dinámica y Cálculo de Variaciones," 2002.
- [49] J. Ma, B. W. Hogg, N. Zhiyuan, and Y. Yihan, "On-Line Decoupled Identification of Transient and Sub-Transient Generator Parameters," IEEE, 1994.
- [50] Y. Yuan, K. Qian, and C. Zhou, "The Optimal Location and Penetration Level of Distributed Generation," 2007.
- [51] R. Courant and F. John, *Integrating Improper Functions*, 1st ed. Springer, 2007.
- [52] M. Boozari, "State Estimation and Transient Stability Analysis in Power Systems Using Artificial Neural Networks," MS Thesis, Simon Fraser University, 2004.
- [53] F. Hamann. Método de Lagrange para la Solución de Problemas de Optimización Dinámica. [Online]. HYPERLINK "http://www.webpondo.org/fhamann/lagrange_slides.pdf"
http://www.webpondo.org/fhamann/lagrange_slides.pdf

Selected Bibliography

- [29] "Standard for Interconnecting Distributed Resources with Electric Power Systems," IEEE Standard 1547, 2003.
- [30] "Consideración de los Estándares del E pact 2005: Time-Based Metering and Communications Interconnection Standards for Distributed Resources ," AEE, 2007.
- [31] J. G. Slootweg and W. L. Kling, "Impacts of distributed generation on power system transient stability," IEEE, 2002.
- [32] L. Zhengyi, Z. Xiangjun, T. Shuntao, and G. Zigang, "A novel scheme of stability control for distributed generation systems," IEEE, 2004.
- [33] K. E. Brenan, S. L. Campbell, and L. Petzold, *Numerical Solution of Initial-Value Problems in Differential-Algebraic Equations*. Philadelphia: SIAM, 1995.
- [34] "IEEE Recommended Practice for Excitation System Models for Power System Stability Studies," IEEE Power Engineering Society Standart Std. 421.5, 2005.
- [35] "IEEE Standard Procedures for Obtaining Synchronous Machine Parameters by Standstill Frequency Response Testing," IEEE Standart Std 115, 1983.
- [36] H. W. Dommel and W. F. Tinney, "Optimal Power Flow Solutions," *IEEE*, Oct. 1968.
- [37] E. D. Tuglie, M. La Scala, and P. Scarpellini, "A Corrective Control for Angle and Voltage Stability," *Enhancement on the Transient Time-Scale*, Nov. 2000.
- [38] T. Martínez, "Voltage Stability Assessment of an Island Power System as a Function of Load Model," Master Thesis, University of Puerto Rico at Mayaguez Campus, Mayaguez, 2003.

- [39] L. M. Monge, "Effect Of Distributed Energy Storage Ssystems In The Voltage Stability Of An Island Power System," Master Thesis, University of Puerto Rico at Mayaguez Campus, Mayaguez, 2006.
- [40] A. Narang, "Impact Of Large-Scale Distributed Generation Penetration On Power System Stability," Canmet Energy Technology Center, 2006.
- [41] O. Alsac and B. Stott, "Optimal Load Flow With Steady-State Security," *IEEE*, Oct. 1973.
- [42] "The Potential Benefits of Distributed Generation And Rate-Related Issues That May Impede Their Expansion," U.S. Department of Energy, 2007.
- [43] "Model Distributed Generation Interconnection Procedures and Agreement," The National Association of Regulatory Utility Commissioners, 2002.
- [44] O. Barraza, "Optimización Dinámica," UMA, 2004.
- [45] N. Nimpitiwan, G. T. Heydt, R. Ayyanar, and S. Suryanarayanan, "Fault Current Contribution From Synchronous Machine and Inverter Based Distributed Generators," *IEEE*, 2007.
- [46] F. M. Bruck, F. A. Himmelstoss, "Modelling and Simulation of a Synchronous Machine," *IEEE*, 1998.
- [47] N. K. Poulsen, *Dynamic Optimization*. Denmark: The Technical Unversity of Denmark, 2007.
- [48] A. H. Pablo Serra, "Optimización Dinámica y Cálculo de Variaciones," 2002.
- [49] J. Ma, B. W. Hogg, N. Zhiyuan, and Y. Yihan, "On-Line Decoupled Identification of Transient and Sub-Transient Generator Parameters," *IEEE*, 1994.
- [50] Y. Yuan, K. Qian, and C. Zhou, "The Optimal Location and Penetration Level of Distributed Generation," 2007.

- [51] R. Courant and F. John, *Integrating Improper Functions*, 1st ed. Springer, 2007.
- [52] M. Boozari, "State Estimation and Transient Stability Analysis in Power Systems Using Artificial Neural Networks," MS Thesis, Simon Fraser University, 2004.
- [53] F. Hamann. Método de Lagrange para la Solución de Problemas de Optimización Dinámica. [Online]. HYPERLINK "http://www.webpondo.org/fhamann/lagrange_slides.pdf"
http://www.webpondo.org/fhamann/lagrange_slides.pdf

Appendix A: IEEE 14-Bus Test System Data

BUS DATA			
Bus Number	Voltage Base (kV)	V ₀ (PU)	θ ₀ (rad)
1	69	1	0
2	69	1	0
3	69	1	0
4	69	1	0
5	69	1	0
6	13.8	1	0
7	13.8	1	0
8	18	1	0
9	13.8	1	0
10	13.8	1	0
11	13.8	1	0
12	13.8	1	0
13	13.8	1	0
14	13.8	1	0

SLACK GENERATOR DATA								
Bus Number	Power rating (MVA)	Voltage rating (kV)	V ₀ (Pu)	θ ₀ (Pu)	Q max (Pu)	Q min (Pu)	V max (Pu)	V min (Pu)
1	100	69	1.06	0	9.9	-9.9	1.061	0.8

PV GENERATOR DATA								
Bus Number	Power Rating (MVA)	Voltage Rating (kV)	Active Power (Pu)	V ₀ (Pu)	Q max (Pu)	Q min (Pu)	V max (Pu)	V min (Pu)
2	100	69	0.4	1.045	0.5	-0.4	1.0451	0.8
6	100	13.8	0	1.07	0.24	-0.06	1.0701	0.6
3	100	69	0	1.01	0.4	0	1.0101	0.6
8	100	18	0	1.09	0.2517	-0.06	1.0901	0.6

TRANSFORMER DATA								
From Bus	To Bus	Power Rating (MVA)	Voltage Rating (kV)	Frequency Rating (Hz)	Voltage Ratio (kV/kV)	R (Pu)	X (Pu)	Fix Tap Ratio (Pu/Pu)
5	6	100	69	60	5	0	0.25202	0.932
4	9	100	69	60	5	0	0.55618	0.969
4	7	100	69	60	5	0	0.20912	0.978
8	7	100	18	60	1.304348	0	0.17615	0

BRANCH DATA							
From Bus	To Bus	Power Rating (MVA)	Voltage Rating (kV)	Frequency Rating (Hz)	R (Pu)	X (Pu)	B(Pu)
2	5	100	69	60	0.05695	0.17388	0.03400
6	12	100	13.8	60	0.12291	0.25581	0.00000
12	13	100	13.8	60	0.22092	0.19988	0.00000
6	13	100	13.8	60	0.06615	0.13027	0.00000
6	11	100	13.8	60	0.09498	0.19890	0.00000
11	10	100	13.8	60	0.08205	0.19207	0.00000
9	10	100	13.8	60	0.03181	0.08450	0.00000
9	14	100	13.8	60	0.12711	0.27038	0.00000
14	13	100	13.8	60	0.17093	0.34802	0.00000
7	9	100	13.8	60	0.00000	0.11001	0.00000
1	2	100	69	60	0.01938	0.05917	0.05280
3	2	100	69	60	0.04699	0.19797	0.04380
3	4	100	69	60	0.06701	0.17103	0.03460
1	5	100	69	60	0.05403	0.22304	0.04920
5	4	100	69	60	0.01335	0.04211	0.01280
2	4	100	69	60	0.05811	0.17632	0.03740
5	6	100	69	60	0.00000	0.25202	0.00000
4	9	100	69	60	0.00000	0.55618	0.00000
4	7	100	69	60	0.00000	0.20912	0.00000
8	7	100	18	60	0.00000	0.17615	0.00000

PQ LOAD DATA						
Bus Number	Power Rating (MVA)	Voltage rating (kv)	Active Power (Pu)	Reactive Power (Pu)	V max (Pu)	V min (Pu)
11	100	13.8	0.035	0.018	1.2	0.6
13	100	13.8	0.135	0.058	1.2	0.6
3	100	69	0.942	0.19	1.5	0.8
5	100	69	0.076	0.016	1.2	0.6
2	100	69	0.217	0.127	1.2	0.8
6	100	13.8	0.112	0.075	1.5	0.6
4	100	69	0.478	0.04	1.2	0.6
14	100	13.8	0.149	0.05	1.2	0.5
12	100	13.8	0.061	0.016	1.2	0.6
10	100	13.8	0.09	0.058	1.2	0.6
9	100	13.8	0.295	0.166	1.2	0.6

SYNCHRONOUS MACHINES DATA

Bus Number	Power Rating (MVA)	Voltage rating (kV)	Frequency rating (Hz)	Machine Model	XL (Pu)	ra (Pu)	Xd (Pu)	X'd (Pu)	X''d (Pu)	T'd0 (s)	T''d0 (s)	Xq (Pu)	X'q (Pu)	X''q (Pu)	T'q0 (s)	T''q0 (s)	M = 2H (kWs/kVA)	Damping coefficient
1	615	69	60	5.2	0.2396	0	0.8979	0.6	0.23	7.4	0.03	0.646	0.646	0.4	0	0.033	10.296	2
3	60	69	60	6	0	0.0031	1.05	0.185	0.13	6.1	0.04	0.98	0.36	0.13	0.3	0.099	13.08	2
2	60	69	60	6	0	0.0031	1.05	0.185	0.13	6.1	0.04	0.98	0.36	0.13	0.3	0.099	13.08	2
8	25	18	60	6	0.134	0.0014	1.25	0.232	0.12	4.75	0.06	1.22	0.715	0.12	1.5	0.21	10.12	2
6	25	13.8	60	6	0.134	0.0014	1.25	0.232	0.12	4.75	0.06	1.22	0.715	0.12	1.5	0.21	10.12	2

TURBINE GOVERNOR DATA

Generator number	Governor Type	ω_{ref0} (Pu)	R (Pu)	Tmax (Pu)	Tmin (Pu)	T2 (s)	T1 (s)
3	2	1	0.05	1.2	0.3	0.1	0.45
1	2	1	0.05	1.2	0.3	0.1	0.45

EXCITER SYSTEM DATA

Generator Number	Exciter Type	Vr Max (Pu)	Vr Min (Pu)	Ka (Pu/Pu)	Ta (s)	Kf (Pu/Pu)	Tf (s)	Te (s)	Tr (s)	Ae-1st Ceiling coefficient	Be-2nd Ceiling Coefficient
1	2	7.32	0	200	0.02	0.002	1	0.2	0.001	0.0006	0.9
3	2	4.38	0	20	0.02	0.001	1	1.98	0.001	0.0006	0.9
2	2	4.38	0	20	0.02	0.001	1	1.98	0.001	0.0006	0.9
4	2	6.81	1.395	20	0.02	0.001	1	0.7	0.001	0.0006	0.9
5	2	6.81	1.395	20	0.02	0.001	1	0.7	0.001	0.0006	0.9

Appendix B: Puerto Rico Electrical System Data

PV BUSES DATA			
Bus Number	Rated Capacity (MVA)	Rated Voltage (kV)	Rated Active Power (MW)
1, 2	448	22	380.8
3, 4	100	13.8	80
5, 6, 7, 8, 9, 10, 11, 12, 17, 18, 23, 24, 25, 26	51.2	13.8	40.96
13, 14, 21, 22, 27, 28, 29	75	13.8	60
15, 16	410	24	369
19, 20	233	20	198.05

PQ BUSES							
Bus Number	Voltage Rating (kV)	Active Power (MW)	Reactive Power (MVAR)	Bus Number	Voltage Rating (kV)	Active Power (MW)	Reactive Power (MVAR)
35	230	80.6	62.4	62	115	36.1	10.5
36	230	410.3	53.2	63	115	21.7	7.6
37	230	423.3	90.5	64	115	47.7	17.3
38	230	294.3	19.7	65	115	71.9	17.6
39	230	256.5	50.5	66	115	5	9
40	230	25.1	80.4	67	115	0.7	2.7
41	230	31	33.6	68	115	20.4	8.4
42	230	37.1	1.4	69	115	2.2	2.1
43	230	33.6	0.5	70	115	43.2	16.1
44	230	74	42.6	71	115	45	17.6
45	115	36	17.7	72	115	49	20.9
46	115	37.9	19.2	73	115	1.3	7.1
47	115	1.3	0.2	74	115	40.2	29.3
48	115	2.2	0.3	76	115	110	31.3
49	115	1.2	2.8	77	115	0.6	5.8
50	115	3.6	6.3	78	115	1.1	1.9
51	115	6	1.5	79	115	125.3	32.2
53	115	27.5	8.7	80	115	25.5	26.1
54	115	75.1	4.3	81	115	25.1	17.8
55	115	87.1	0.9	82	115	25.1	24.3
56	115	18.2	1.9	83	115	23.4	2.7
57	115	3.6	1.1	84	115	27.7	4.4
58	115	7.2	5.1	85	115	19.6	5.5
59	115	60.6	0.6	86	115	21.8	6.1
60	115	5	3.4	87	115	31.3	8
61	115	78.6	2.1	88	115	8.4	3.1

BRANCH DATA							
Line Name	From Bus	To Bus	Power Rating (MVA)	Voltage (kV)	Line length (km)	R (ohm/km)	X (ohm/km)
50300	35	36	462.11	230	49.18	0.05	0.48
37100	35	50	239	115	18.51	0.14	0.26
36900	35	57	231.1	115	11.73	0.05	0.44
37000	1	24	290.8	115	17.70	0.12	0.50
37300	35	53	137.4	115	43.13	0.13	0.27
50200	35	41	462.1	230	56.73	0.05	0.48
50400	35	44	462.1	230	60.35	0.05	0.48
50700	36	37	924.2	230	65.26	0.03	0.35
50900	36	39	924.2	230	42.66	0.03	0.35
51000	36	39	924.2	230	42.66	0.03	0.35
40300	36	60	231.1	115	17.98	0.05	0.44
40100	36	61	462.1	115	14.00	0.05	0.48
40200	36	61	462.1	115	14.00	0.05	0.48
50800	37	38	462.1	230	53.11	0.05	0.48
36300	37	63	231.1	115	7.53	0.05	0.44
41000	37	66	231.1	115	3.86	0.05	0.44
36300	37	66	231.1	115	4.44	0.05	0.44
51000	38	39	924.2	230	20.49	0.03	0.35
41200	38	72	145.4	115	12.25	0.12	0.47
36800	38	72	145.4	115	12.23	0.12	0.47
37900	38	80	145.4	115	18.07	0.12	0.47
38900-2	38	79	231.1	115	2.72	0.05	0.44
50900	39	40	924.2	230	17.27	0.03	0.35
39000	39	80	358.5	115	14.24	0.01	0.18
39000	39	65	239	115	8.05	0.14	0.26
39000-3	39	82	145.4	115	27.78	0.12	0.47
50200	40	41	462.1	230	59.71	0.05	0.48
37400	40	74	231.1	115	13.02	0.05	0.44
36100	40	89	121.5	115	10.46	0.13	0.30
36100	40	80	145.4	115	10.28	0.12	0.47
37500	40	80	145.4	115	9.17	0.12	0.47
37600	40	75	358.5	115	8.22	0.06	0.23
37700	40	75	462.1	115	8.22	0.05	0.48
38600	40	76	231.1	115	9.50	0.05	0.44
50100	41	42	462.1	230	32.52	0.05	0.48
37400	41	56	239	115	19.83	0.14	0.26
37400	41	73	231.1	115	10.91	0.05	0.44
50500	42	43	462.11	230	56.23	0.05	0.48

Line Name	From Bus	To Bus	Power Rating (MVA)	Voltage (kV)	Line length (km)	R (ohm/km)	X (ohm/km)
41300	42	55	462.1	115	2.41	0.05	0.48
50500	43	44	462.11	230	16.87	0.05	0.48
39100	43	45	462.1	115	17.70	0.05	0.48
36700	44	47	239	115	5.57	0.14	0.26
37200	44	47	145.4	115	5.57	0.12	0.47
36700	44	51	137.4	115	20.44	0.13	0.27
37200	44	46	145.4	115	6.50	0.12	0.47
37200	45	46	137.4	115	11.27	0.13	0.27
39800	47	48	145.4	115	24.14	0.12	0.47
37100	48	49	137.4	115	21.73	0.13	0.27
37100	49	50	137.4	115	20.28	0.13	0.27
36600	51	52	91.6	115	32.67	0.24	0.29
36600	52	53	91.6	115	5.63	0.24	0.29
37400	53	55	145.4	115	18.75	0.12	0.47
36400	53	90	83.7	115	18.43	0.24	0.31
36100	53	84	91.6	115	27.31	0.24	0.29
39100	54	55	231.1	115	17.70	0.05	0.44
37400	55	56	239	115	13.62	0.14	0.26
36900	57	58	231.1	115	4.97	0.05	0.44
39000-1	58	59	145.4	115	4.83	0.12	0.47
40300	58	60	231.1	115	24.62	0.05	0.44
36400	58	90	83.7	115	39.61	0.24	0.31
39000-7	59	81	145.4	115	16.87	0.12	0.47
36300	61	62	231.1	115	36.93	0.05	0.44
37800	61	64	231.1	115	24.66	0.05	0.44
36300	62	63	231.1	115	7.52	0.05	0.44
37800	64	65	145.4	115	19.71	0.12	0.47
37800-4	65	83	145.4	115	16.58	0.12	0.47
41400	66	67	145.4	115	17.06	0.12	0.47
36300	66	68	239	115	12.55	0.14	0.26
36200	68	69	145.4	115	26.14	0.12	0.47
36200	68	80	145.4	115	41.52	0.12	0.47
36200	69	70	145.4	115	5.23	0.12	0.47
36800	70	71	145.4	115	34.52	0.12	0.47
36800	71	72	145.4	115	2.41	0.12	0.47
37400	73	74	239	115	14.48	0.14	0.26
41500	74	88	231.1	115	11.80	0.05	0.44
38200	75	80	358.5	115	20.12	0.03	0.22
38400	76	77	231.1	115	5.63	0.05	0.44

Line Name	From Bus	To Bus	Power Rating (MVA)	Voltage (kV)	Line length (km)	R (ohm/km)	X (ohm/km)
38100	76	77	231.1	115	5.65	0.05	0.44
38500	76	78	231.1	115	5.39	0.05	0.44
38300	76	80	358.5	115	9.66	0.03	0.22
38800	77	78	290.8	115	5.63	0.12	0.50
38900	78	79	231.1	115	9.02	0.05	0.44
37800-4	80	83	145.4	115	16.09	0.12	0.47
39000-2	81	82	145.4	115	16.09	0.12	0.47
36100	84	85	91.6	115	6.23	0.24	0.29
36100	85	86	91.6	115	7.61	0.24	0.29
36100	86	87	121.5	115	5.95	0.13	0.30
36100	87	88	121.5	115	5.87	0.13	0.30
36100	88	89	121.5	115	4.83	0.13	0.30

SYNCHRONOUS MACHINES DATA

Power Rating (MVA)	Voltage Rating (kV)	Frequency Rating (Hz)	Machine Model	XL (Pu)	ra (Pu)	Xd (Pu)	X'd (Pu)	X''d (Pu)	T'd0 (s)	T''d0 (s)	Xq (Pu)	X'q (Pu)	X''q (Pu)	T'q0 (s)	T''q0 (s)	M = 2H (kWs/kVA)	Damping coefficient
448	22	60	4	0.1861	0	1.803	0.2802	0.2341	5.21	0.042	1.738	0.4479	0.215	0.578	0.068	6.08	0
100	13.8	60	4	0.1	0	1.98	0.208	0.165	12.9	0.05	1.81	0.3	0.145	3.9	0.05	11.2	0
51.2	13.8	60	4	0.1	0	1.36	0.199	0.158	5.99	0.037	1.312	0.312	0.116	0.425	0.057	5.42	0
75	13.8	60	4	0.063	0	1.26	0.17	0.107	8.1	0.05	1.21	0.315	0.135	1	0.05	8.08	0
410	24	60	4	0.14	0	1.55	0.245	0.19	3.8	0.032	1.48	0.438	0.215	0.46	0.061	5.58	2
233	20	60	4	0.2	0	1.694	0.317	0.23	5.36	0.0437	1.666	0.454	0.248	1.5	0.141	5.14	2

EXCITER SYSTEM DATA

Generator Number	Vr Max (Pu)	Vr Min (Pu)	Ka (Pu/Pu)	Ta (s)	Kf (Pu/Pu)	Tf (s)	Te (s)	Tr (s)	Ae-1st Ceiling coefficient	Be-2nd Ceiling Coefficient
1, 2	4.32	-4.32	50	0.06	0	1	0.52	0.001	0.0012	1.2639
3, 4, 23, 24, 25, 26	3.438	-3.438	25	0.2	0	0.35	0.6544	0.06	0.0015	1.5833
5, 6, 7, 8, 9, 10, 11, 12, 17, 18	4.13	-4.13	400	0.05	0	1	1.37	0.001	0.0137	0.6774
13, 14, 27, 28, 29	3.18	0	20	0.05	0	0.1	1.98	0.001	0.0016	1.7128
15, 16	3.29	0	400	0.02	0	1	0.92	0.001	0.1658	0.391
19, 20	3.48	0	250	0.06	0	0.33	0.613	0.001	0	3.7884
21, 22	4.38	0	20	0.05	0	0.1	1.98	0.001	0.0016	1.7128

TURBINE GOVERNOR DATA

Generator number	wref0 (Pu)	R (Pu)	Tmax (Pu)	Tmin (Pu)	T2 (s)	T1 (s)
1, 2	1	0.05	0.87	0	1	0.3
3, 4, 23, 24, 25, 26	1	0.05	1.05	0	0.9	0.3
5, 6, 7, 8, 9, 10, 11, 12, 17, 18	1	0.05	1.03	0	2	0.3
13, 14, 15, 16, 21, 22, 27, 28, 29	1	0.05	1	0	0.9	0.3
19, 20	1	0.05	0.9	0	1.5	0.3

Appendix C: Distributed Generation Data

DG 1 - SYNCHRONOUS MACHINES DATA [27]								
Power Rating (MVA)	Voltage Rating (kV)	Frequency Rating (Hz)	Machine Model	XL (Pu)	ra (Pu)	Xd (Pu)	X'd (Pu)	X''d (Pu)
7	4.16	60	4	0.1	0	1.654	0.3	0.2
T'd0 (s)	T''d0 (s)	Xq (Pu)	X'q (Pu)	X''q (Pu)	T'q0 (s)	T''q0 (s)	M = 2H (kWs/kVA)	Damping coefficient
1.94	0.033	0.99	0.2	0.243	0.4	0.033	7	0

DG 2 - SYNCHRONOUS MACHINES DATA [28]								
Power Rating (MVA)	Voltage Rating (kV)	Frequency Rating (Hz)	Machine Model	XL (Pu)	ra (Pu)	Xd (Pu)	X'd (Pu)	X''d (Pu)
12.5	11.4	60	4	0.217	0	2.4	0.34	0.23
T'd0 (s)	T''d0 (s)	Xq (Pu)	X'q (Pu)	X''q (Pu)	T'q0 (s)	T''q0 (s)	M = 2H (kWs/kVA)	Damping coefficient
3.8	0.044	1.32	0.715	0.12	1.5	0.089	6	1

TURBINE GOVERNOR DATA						
Governor Type	ω_{ref0} (Pu)	R (Pu)	Tmax (Pu)	Tmin (Pu)	T2 (s)	T1 (s)
2	1	0.05	1.2	0	0.2	0.3

EXCITER SYSTEM DATA					
Exciter Type	Vr Max (Pu)	Vr Min (Pu)	Ka (Pu/Pu)	Ta (s)	
2	4	-4	200	0.1	
Kf (Pu/Pu)	Tf (s)	Te (s)	Tr (s)	Ae-1st Ceiling coefficient	Be-2nd Ceiling Coefficient
0	1	1.37	0.05	0.0137	0.6774